ISSN: 2146-1414

MIRT

Molecular Imaging and Radionuclide Therapy

October 2019 Volume 28 Issue 3 www.tsnm.org

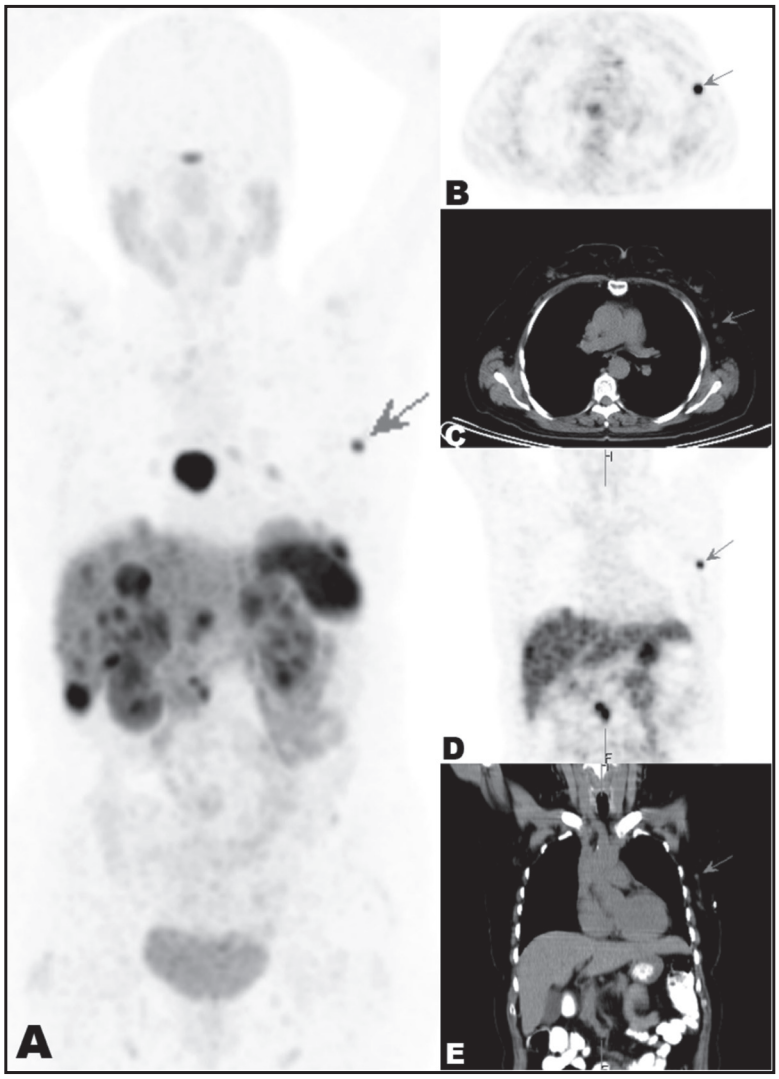

"Official Journal of the Turkish Society of Nuclear Medicine"

galenos yayinevi

TURKISH SOCIETY OF NUCLEAR MEDICINE 1975

MIRT

Molecular Imaging and Radionuclide Therapy

Scientific Advisory Board

MIRT

Molecular Imaging and Radionuclide Therapy

Turkish Society of Nuclear Medicine
Cinnah Caddesi Pilot Sokak No: 10/12 Çankaya 06650 Ankara, Turkey **Phone:** +90 312 441 00 45 **Fax:** +90 312 441 12 95 **Web:** www.tsnm.org **E-mail:** dernekmerkezi@tsnm.org
"Formerly Turkish Journal of Nuclear Medicine"

Reviewing the articles' conformity to the publishing standards of the Journal, typesetting, reviewing and editing the manuscripts and abstracts in English, creating links to source data, and publishing process are realized by Galenos.

Galenos Publishing House
Owner and Publisher
Erkan Mor

Publication Coordinator
Burak Sever

Web Coordinators
Turgay Akpınar

Graphics Department
Ayda Alaca
Çiğdem Birinci
Gülşah Özgül

Project Coordinators
Eda Kolukısa
Esra Semerci
Günay Selimoğlu
Hatice Balta
Zeynep Altındağ

Project Assistants
Duygu Yıldırım
Gamze Aksoy
Melike Eren
Saliha Tuğçe Güdücü

Research&Development
Mert Can Köse
Mevlüde Özlem Akgüney

Publisher Contact
Address: Molla Gürani Mah. Kaçamak Sk. No: 21/1
34093 İstanbul, Turkey
Phone: +90 (212) 621 99 25 **Fax:** +90 (212) 621 99 27
E-mail: info@galenos.com.tr/yayin@galenos.com.tr
Web: www.galenos.com.tr
Publisher Certificate Number: 14521

Publication Date: 30 August 2019
ISSN: 2146-1414 **E-ISSN:** 2147-1959
International scientific journal published quarterly.

MIRT

Molecular Imaging and Radionuclide Therapy

ABOUT US

Molecular Imaging and Radionuclide Therapy (formerly Turkish Journal of Nuclear Medicine) is the official publication of Turkish Society of Nuclear Medicine.

Focus and Scope

Molecular Imaging and Radionuclide Therapy (Mol Imaging Radionucl Ther, MIRT) is a double-blind peer-review journal published in English language. It publishes original research articles, invited reviews, editorials, short communications, letters, consensus statements, guidelines and case reports with a literature review on the topic, interesting images in the field of molecular imaging, multimodality imaging, nuclear medicine, radionuclide therapy, radiopharmacy, medical physics, dosimetry and radiobiology. MIRT is published three times a year (February, June, October). Audience: Nuclear medicine physicians, medical physicists, radiopharmaceutical scientists, radiobiologists.

The editorial policies are based on the "Recommendations for the Conduct, Reporting, Editing, and Publication of Scholarly Work in Medical Journals (ICMJE Recommendations)" by the International Committee of Medical Journal Editors (2016, archived at http://www.icmje.org/) rules.

Open Access Policy

This journal provides immediate open access to its content on the principle that making research freely available to the public supports a greater global exchange of knowledge.

Open Access Policy is based on rules of Budapest Open Access Initiative (BOAI) (http://www.budapestopenaccessinitiative.org/). By "open access" to [peer-reviewed research literature], we mean its free availability on the public internet, permitting any users to read, download, copy, distribute, print, search, or link to the full texts of these articles, crawl them for indexing, pass them as data to software, or use them for any other lawful purpose, without financial, legal, or technical barriers other than those inseparable from gaining access to the internet itself. The only constraint on reproduction and distribution, and the only role for copyright in this domain, should be to give authors control over the integrity of their work and the right to be properly acknowledged and cited.

Permission Requests

Instructions for Authors

Instructions for authors are published in the journal and on the website http://mirt.tsnmjournals.org

Manuscripts can only be submitted electronically through the Journal Agent website (http://www.journalagent.com/mirt/?plng=eng) after creating an account. This system allows online submission and review.

All published volumes in full text can be reached free of charge through the website http://mirt.tsnmjournals.org

Material Disclaimer

Scientific and legal responsibilities pertaining to the papers belong to the authors. Contents of the manuscripts and accuracy of references are also the author's responsibility. The Turkish Society of Nuclear Medicine, the Editor, the Editorial Board or the publisher do not accept any responsibility for opinions expressed in articles.

Financial expenses of the journal are covered by Turkish Society of Nuclear Medicine.

Correspondence Address

Editor-in-Chief, Prof. Zehra Özcan, MD,

Ege University, Medical School, Department of Nuclear Medicine, İzmir, Turkey

Phone: +90 312 441 00 45

Fax: +90 312 441 12 97

E-mail: editor@tsnmjournals.org

Web page: http://mirt.tsnmjournals.org

Publisher Corresponding Address

Galenos Yayınevi Tic. Ltd. Şti.

Address: Molla Gürani Mah. Kaçamak Sk. No: 21/1 34093

Fındıkzade, İstanbul, Turkey

Phone: +90 212 621 99 25

Fax: +90 212 621 99 27

E-mail: info@galenos.com.tr

MIRT

Molecular Imaging and Radionuclide Therapy

INSTRUCTIONS TO AUTHORS

Molecular Imaging and Radionuclide Therapy (Mol Imaging Radionucl Ther, MIRT) publishes original research articles, short communications, invited reviews, editorials, case reports with a literature review on the topic, interesting images, consensus statements, guidelines, letters in the field of molecular imaging, multimodality imaging, nuclear medicine, radionuclide therapy, radiopharmacy, medical physics, dosimetry and radiobiology. MIRT is published by the Turkish Society of Nuclear Medicine three times a year (February, June, October).

Molecular Imaging and Radionuclide Therapy does not charge any article submission or processing fees.

GENERAL INFORMATION

MIRT commits to rigorous peer review, and stipulates freedom from commercial influence, and promotion of the highest ethical and scientific standards in published articles. Neither the Editor(s) nor the publisher guarantees, warrants or endorses any product or service advertised in this publication. All articles are subject to review by the editors and peer reviewers. If the article is accepted for publication, it may be subjected to editorial revisions to aid clarity and understanding without changing the data presented.

Manuscripts must be written in English and must meet the requirements of the journal. The journal is in compliance with the uniform requirements for manuscripts submitted to biomedical journals published by the International Committee of Medical Journal Editors (NEJM 1997; 336:309-315, updated 2016). Manuscripts that do not meet these requirements will be returned to the author for necessary revision before the review. Authors of manuscripts requiring modifications have a maximum of two months to resubmit the revised text. Manuscripts returned after this deadline will be treated as new submissions.

It is the authors' responsibility to prepare a manuscript that meets ethical criteria. The Journal adheres to the principles set forth in the Helsinki Declaration October 2013 (https://www.wma.net/policies-post/wma-declaration-of-helsinki-ethical-principles-for-medical-research-involving-human-subjects/) and holds that all reported research involving "Human beings" conducted in accordance with such principles.

Reports describing data obtained from research conducted in human participants must contain a statement in the MATERIALS AND METHODS section indicating approval by the ethical review board (including the approval number) and affirmation that INFORMED CONSENT was obtained from each participant.

All manuscripts reporting experiments using animals must include a statement in the MATERIALS AND METHODS section giving assurance that all animals have received humane care in compliance with the Guide for the Care and Use of Laboratory Animals (www.nap.edu) and indicating approval by the ethical review board.

If the study should have ethical approval, authors asked to provide ethical approval in order to proceed the review process. If they provide approval, review of the manuscript will continue.

In case report(s) and interesting image(s) a statement regarding the informed consent of the patients should be included in the manuscript and the identity of the patient(s) should be hidden.

Subjects must be identified only by number or letter, not by initials or names. Photographs of patients' faces should be included only if scientifically relevant. Authors must obtain written consent from the patient for use of such photographs. In cases of image media usage that potentially expose patients' identity requires obtaining permission for publication from the patients or their parents/guardians.

If the proposed publication concerns any commercial product, the author must include in the cover letter a statement indicating that the author(s) has (have) no financial or other interest with the product or explaining the nature of any relations (including consultancies) between the author(s) and editor the manufacturer or distributor of the product.

All submissions will be screened by Crossref Smilarity Check powered by "iThenticate". Manuscripts with an overall similarity index of greater than 25%, or duplication rate at or higher than 5% with a single source will be returned back to authors.

MANUSCRIPT CATEGORIES

1. Original Articles

2. Short Communications are short descriptions of focused studies with important, but very straightforward results.

3. Reviews address important topics in the field. Authors considering the submission of uninvited reviews should contact the editor in advance to determine if the topic that they propose is of current potential interest to the Journal. Reviews will be considered for publication only if they are written by authors who have at least three published manuscripts in the international peer reviewed journals and these studies should be cited in the review. Otherwise only invited reviews will be considered for peer review from qualified experts in the area.

4. Editorials are usually written by invitation of the editor by the editors on current topics or by the reviewers involved in the evaluation of a submitted manuscript and published concurrently with that manuscript.

5. Case Report and Literature Reviews are descriptions of a case or small number of cases revealing a previously undocumented disease process, a unique unreported manifestation or treatment of a known disease process, unique unreported complications of treatment regimens or novel and important insights into a condition's pathogenesis, presentation, and/or management. The journal's policy is to accept case reports only if it is accompanied by a review of the literature on the related topic. They should include an adequate number of images and figures.

6. Interesting Image

One of the regular parts of Molecular Imaging and Radionuclide Therapy is a section devoted to interesting images. Interesting image(s) should describe case(s) which are unique and include interesting findings adding insights into the interpretation of patient images, a condition's pathogenesis, presentation, and/or management.

7. Consensus Statements or Guidelines may be submitted by professional societies. All such submissions will be subjected to peer review, must be modifiable in response to criticisms, and will be published only if they meet the Journal's usual editorial standards.

8. Letters to the Editor may be submitted in response to work that has been published in the Journal. Letters should be short commentaries related to specific points of agreement or disagreement with the published work.

Note on Prior Publication

Articles are accepted for publication on the condition that they are original, are not under consideration by another journal, or have not been previously published. Direct quotations, tables, or illustrations that have appeared in

MIRT

Molecular Imaging and Radionuclide Therapy

copyrighted material must be accompanied by written permission for their use from the copyright owner and authors. Materials previously published in whole or in part shall not be considered for publication. At the time of submission, authors must report that the manuscript has not been published elsewhere. Abstracts or posters displayed at scientific meetings need not be reported.

MANUSCRIPT SUBMISSION PROCEDURES

MIRT only accepts electronic manuscript submission at the web site http://www.journalagent.com/mirt/. After logging on to the website Click the 'online manuscript submission' icon. All corresponding authors should be provided with a password and a username after entering the information required. If you already have an account from a previous submission, enter your username and password to submit a new or revised manuscript. If you have forgotten your username and/or password, please send an e-mail to the editorial office for assistance. After logging on to the article submission system please read carefully the directions of the system to give all needed information and attach the manuscript, tables and figures and additional documents.

All Submissions Must Include:

1. Completed Copyright Assignment & Disclosure of Potential Conflict of Interest Form; This form should be downloaded from the website (provided in the author section), filled in thoroughly and uploaded to the website during the submission.
2. All manuscripts describing data obtained from research conducted in human participants must be accompanied with an approval document by the ethical review board.
3. All manuscripts reporting experiments using animals must include approval document by the animal ethical review board.
4. All submissions must include the authorship contribution form which is signed by all authors.

Authors must complete all online submission forms. If you are unable to successfully upload the files please contact the editorial office by e-mail.

MANUSCRIPT PREPARATION

General Format

The Journal requires that all submissions be submitted according to these guidelines:

- Text should be double spaced with 2.5 cm margins on both sides using 12-point type in Times Roman font.
- All tables and figures must be placed after the text and must be labeled.
- Each section (abstract, text, references, tables, figures) should start on a separate page.
- Manuscripts should be prepared as a word document (*.doc) or rich text format (*.rtf).
- Please make the tables using the table function in Word.
- Abbreviations should be defined in parenthesis where the word is first mentioned and used consistently thereafter.
- Results should be expressed in metric units. Statistical analysis should be done accurately and with precision. Please consult a statistician if necessary.
- Authors' names and institutions should not be included in the manuscript text and should be written only in the title page.

Title Page

The title page should be a separate form from the main text and should include the following:

- Full title (in English and in Turkish). Turkish title will be provided by the editorial office for the authors who are not Turkish speakers.
- Authors' names and institutions.
- Short title of not more than 40 characters for page headings.
- At least three and maximum eight keywords. (in English and in Turkish). Do not use abbreviations in the keywords. Turkish keywords will be provided by the editorial office for the authors who are not Turkish speakers. If you are not a native Turkish speaker, please reenter your English keywords to the area provided for the Turkish keywords. English keywords should be provided from http://www.nlm.nih.gov/mesh (Medical Subject Headings) while Turkish keywords should be provided from http://www.bilimterimleri.com.
- Word count (excluding abstract, figure legends and references).
- Corresponding author's e-mail and address, telephone and fax numbers.
- Name and address of person to whom reprint requests should be addressed.

Original Articles

Authors are required to state in their manuscripts that ethical approval from an appropriate committee and informed consents of the patients were obtained.

Original Articles should be submitted with a structured abstract of no more than 250 words. All information reported in the abstract must appear in the manuscript. The abstract should not include references. Please use complete sentences for all sections of the abstract. Structured abstract should include background, objective, methods, results and conclusions. Turkish abstract will be provided by the editorial office for the authors who are not Turkish speakers. If you are not a native Turkish speaker, please reenter your English abstract to the area provided for the Turkish abstract.

- Introduction
- Materials and Methods
- Results
- Discussion
- Study Limitations
- Conclusion

May be given for contributors who are not listed as authors, or for grant support of the research.

References should be cited in numerical order (in parentheses) in the text and listed in the same numerical order at the end of the manuscript on a separate page or pages. The author is responsible for the accuracy of references. Examples of the reference style are given below. Further examples will be found in the articles describing the Uniform Requirements for Manuscripts Submitted to Biomedical Journals (Ann Intern Med.1988; 208:258-265, Br Med J. 1988; 296:401-405). The titles of journals should be abbreviated according to the style used in the Index Medicus. Journal Articles and Abstracts: Surnames and initials of author's name, title of the article, journal name, date, volume number, and pages. All authors should be listed regardless of number. The citation of unpublished papers, observations or personal communications is not permitted. Citing an abstract is not recommended. Books: Surnames and initials of author's names, chapter title, editor's name, book title, edition, city, publisher, date and pages.

MIRT
Molecular Imaging and Radionuclide Therapy

INSTRUCTIONS TO AUTHORS

Sample References

Journal Article: Sayit E, Söylev M, Capa G, Durak I, Ada E, Yilmaz M. The role of technetium-99m-HMPAO-labeled WBC scintigraphy in the diagnosis of orbital cellulitis. Ann Nucl Med 2001;15:41-44.

Erselcan T, Hasbek Z, Tandogan I, Gumus C, Akkurt I. Modification of Diet in Renal Disease equation in the risk stratification of contrast induced acute kidney injury in hospital inpatients. Nefrologia 2009 doi: 10.3265/Nefrologia.2009.29.5.5449.en.full.

Article in a journal published ahead of print: Ludbrook J. Musculovenous pumps in the human lower limb. Am Heart J 2009;00:1-6. (accessed 20 February 2009).

Lang TF, Duryea J. Peripheral Bone Mineral Assessment of the Axial Skeleton: Technical Aspects. In: Orwoll ES, Bliziotes M (eds). Osteoporosis: Pathophsiology and Clinical Management. New Jersey, Humana Pres Inc, 2003;83-104.

Books: Greenspan A. Orthopaedic Radiology a Pratical Approach. 3th ed. Philadelphia, Lippincott Williams Wilkins 2000, 295-330.

Website: Smith JR. 'Choosing Your Reference Style', Online Referencing 2(3), http://orj.sagepub.com (2003, accessed October 2008).

- Tables

Tables must be constructed as simply as possible. Each table must have a concise heading and should be submitted on a separate page. Tables must not simply duplicate the text or figures. Number all tables in the order of their citation in the text. Include a title for each table (a brief phrase, preferably no longer than 10 to 15 words). Include all tables in a single file following the manuscript.

– Figure Legends

Figure legends should be submitted on a separate page and should be clear and informative.

– Figures

Number all figures (graphs, charts, photographs, and illustrations) in the order of their citation in the text. At submission, the following file formats are acceptable: AI, EMF, EPS, JPG, PDF, PPT, PSD, TIF. Figures may be embedded at the end of the manuscript text file or loaded as separate files for submission. All images MUST be at or above intended display size, with the following image resolutions: Line Art 800 dpi, Combination (Line Art + Halftone) 600 dpi, Halftone 300 dpi. Image files also must be cropped as close to the actual image as possible.

Short Communications:

Short communications should be submitted with a structured abstract of no more than 200 words. These manuscripts should be no longer than 2000 words, and include no more than two figures and tables and 20 references. Other rules which the authors are required to prepare and submit their manuscripts are the same as described above for the original articles.

Invited Review Articles:

- Title page (see above)
- Abstract: Maximum 250 words; without structural divisions; in English and in Turkish . Turkish abstract will be provided by the editorial office for the authors who are not Turkish speakers. If you are not a native Turkish speaker, please reenter your English abstract to the area provided for the Turkish abstract.
- Text
- Conclusion
- Acknowledgements (if any)
- References

Editorial:

- Title page (see above)
- Abstract: Maximum 250 words; without structural divisions; in English and in Turkish. Turkish abstract will be provided by the editorial office for the authors who are not Turkish speakers. If you are not a native Turkish speaker, please re enter your English abstract to the area provided for the Turkish abstract.
- Text
- References

Case Report and Literature Review

- Title page (see above)
- Abstract: Approximately 100-150 words; without structural divisions; in English and in Turkish. Turkish abstract will be provided by the editorial office for the authors who are not Turkish speakers. If you are not a native Turkish speaker, please re-enter your English abstract to the area provided for the Turkish abstract.
- Introduction
- Case report
- Literature Review and Discussion
- References

Interesting Image:

No manuscript text is required. Interesting Image submissions must include the following:

Title Page: (see Original article section)

Abstract: Approximately 100-150 words; without structural divisions; in English and in Turkish. Turkish abstract will be provided by the editorial office for the authors who are not Turkish speakers. If you are not a native Turkish speaker, please re-enter your English abstract to the area provided for the Turkish abstract.

Image(s): The number of images is left to the discretion of the author. (See Original article section)

Figure Legend: Reference citations should appear in the legends, not in the abstract. Since there is no manuscript text, the legends for illustrations should be prepared in considerable detail but should be no more than 500 words total. The case should be presented and discussed in the Figure legend section.

References: Maximum eight references (see original article section).

Letters to the Editor:

- Title page (see above)
- Short comment to a published work, no longer than 500 words, no figures or tables.
- References no more than five.

Consensus Statements or Guidelines: These manuscripts should typically be no longer than 4000 words and include no more than six figures and tables and 120 references.

Proofs and Reprints

Proofs and a reprint orders are sent to the corresponding author. The author should designate by footnote on the title page of the manuscript the name and

MIRT
Molecular Imaging and Radionuclide Therapy

address of the person to whom reprint requests should be directed. The manuscript when published will become the property of the journal.

Archiving

The editorial office will retain all manuscripts and related documentation (correspondence, reviews, etc.) for 12 months following the date of publication or rejection.

Submission Preparation Checklist

As part of the submission process, authors are required to check off their submission's compliance with all of the following items, and submissions may be returned to authors that do not adhere to these guidelines.

1. The submission has not been previously published, nor is it before another journal for consideration (or an explanation has been provided in Comments to the Editor).
2. The submission file is in Microsoft Word, RTF, or WordPerfect document file format. The text is double-spaced; uses a 12-point font; employs italics, rather than underlining (except with URL addresses); and the location for all illustrations, figures, and tables should be marked within the text at the appropriate points.
3. Where available, URLs for the references will be provided.
4. All authors should be listed in the references, regardless of the number.
5. The text adheres to the stylistic and bibliographic requirements outlined in the Author Guidelines, which is found in About the Journal.
6. English keywords should be provided from http://www.nlm.nih.gov/mesh(Medical Subject Headings), while Turkish keywords should be provided fromhttp://www.bilimterimleri.com
7. The title page should be a separate document from the main text and should be uploaded separately.
8. The "Affirmation of Originality and Assignment of Copyright/The Disclosure Form for Potential Conflicts of Interest Form" and Authorship Contribution Form should be downloaded from the website, filled thoroughly and uploaded during the submission of the manuscript.

TO AUTHORS

Copyright Notice

The author(s) hereby affirms that the manuscript submitted is original, that all statement asserted as facts are based on author(s) careful investigation and research for accuracy, that the manuscript does not, in whole or part, infringe any copyright, that it has not been published in total or in part and is not being submitted or considered for publication in total or in part elsewhere. Completed Copyright Assignment & Affirmation of Originality Form will be uploaded during submission. By signing this form;

1. Each author acknowledges that he/she participated in the work in a substantive way and is prepared to take public responsibility for the work.
2. Each author further affirms that he or she has read and understands the "Ethical Guidelines for Publication of Research".
3. The author(s), in consideration of the acceptance of the manuscript for publication, does hereby assign and transfer to the Molecular Imaging and Radionuclide Therapy all of the rights and interest in and the copyright of the work in its current form and in any form subsequently revised for publication and/or electronic dissemination.

Privacy Statement

The names and email addresses entered in this journal site will be used exclusively for the stated purposes of this journal and will not be made available for any other purpose or to any other party.

Peer Review Process

1. The manuscript is assigned to an editor, who reviews the manuscript and makes an initial decision based on manuscript quality and editorial priorities.
2. For those manuscripts sent for external peer review, the editor assigns at least two reviewers to the manuscript.
3. The reviewers review the manuscript.
4. The editor makes a final decision based on editorial priorities, manuscript quality, and reviewer recommendations.
5. The decision letter is sent to the author.

Contact Address

All correspondence should be directed to the Editorial Office:
Cinnah Caddesi Pilot Sokak No:10/12 06650 Çankaya / Ankara, Turkey
Phone: +90 312 441 00 45
Fax: +90 312 441 12 97
E-mail: info@tsnmjournals.org

MIRT
Molecular Imaging and Radionuclide Therapy

CONTENTS

Original Articles

Interesting Images

Index

Original Article
Mol Imaging Radionucl Ther 2019;28:89-95 DOI:10.4274/mirt.galenos.2019.20053

Diagnostic Value of Bone SPECT/CT in Patients with Suspected Osteomyelitis

Osteomiyelit Şüpheli Hastalarda Kemik SPECT/BT'nin Tanısal Değeri

Pelin Arıcan, Berna Okudan, Rıza Şefizade, Seniha Naldöken
University of Health Sciences, Ankara Numune Training and Research Hospital, Clinic of Nuclear Medicine, Ankara, Turkey

Abstract

Objectives: The aim of our retrospective study was to evaluate the contribution of single photon emission computed tomography/computed tomography (SPECT/CT) to three phase bone scintigraphy/SPECT for the assessment of osteomyelitis (OM) and patient's management.

Methods: Eighty-five patients who were suspected as having OM were included in this study. Tc-99m MDP three phase bone scintigraphy and SPECT/CT were performed to the region of suspected OM. SPECT/CT findings were compared with the findings of planar images/SPECT. Both planar bone scan/SPECT and SPECT/CT findings were divided into two groups: With OM and without OM. In all patients, scintigraphic diagnosis was confirmed by clinical follow up, laboratory findings, microscopic-bacteriological examinations, radiological, surgical, and pathological findings.

Results: SPECT/CT changed the diagnosis and treatment planning in 14/85 (16.5%) patients. SPECT/CT was significantly superior to planar scan/SPECT imaging for determining OM (kappa value was 0.626 for planar scan/SPECT, 0.929 for SPECT/CT). SPECT/CT was statistically more successful in detection of chronic OM, and useful in differentiating chronic OM from acute OM (kappa value was 0.541 for planar scan/SPECT, 0.944 for SPECT/CT).

Conclusion: SPECT/CT increases accuracy of the diagnosis in the evaluation of OM when it is compared to three phase bone scintigraphy/SPECT. SPECT/CT can change the diagnosis and management of the patients.

Keywords: Bone scintigraphy, osteomyelitis, infection, SPECT, SPECT/CT

Öz

Amaç: Retrospektif çalışmamızda osteomiyelitin (OM) değerlendirilmesinde ve hasta yönetiminde tek foton emisyon bilgisayarlı tomografi/bilgisayarlı tomografi (SPECT/BT) üç fazlı kemik sintigrafisi/SPECT'ye katkısı araştırıldı.

Yöntem: OM'den şüphelenilen 85 hasta çalışmaya dahil edildi. OM şüphesi bulunan bölgeye Tc-99m MDP üç fazlı kemik sintigrafisi ve SPECT/BT yapıldı. SPECT/BT bulguları planar görüntü/SPECT bulguları ile karşılaştırıldı. Planar kemik sintigrafisi/SPECT ve SPECT/BT bulguları iki gruba ayrıldı: OM olmayanlar ve OM olanlar. Tüm hastalarda sintigrafik tanı, klinik takip, laboratuvar, mikroskobik-bakteriyolojik inceleme, radyoloji, cerrahi ve patoloji ile doğrulanmıştır.

Bulgular: SPECT/BT, 14/85 (%16,5) hastada tanı ve tedavi planlamasını değiştirdi. SPECT/BT, OM'nin belirlenmesinde planar görüntüler/SPECT görüntülemeye göre anlamlı derecede üstün bulundu (kappa değeri planar tarama/SPECT için 0,626, SPECT/BT için 0,929). SPECT/BT, kronik OM'nin saptanmasında istatistiksel olarak daha başarılıydı ve akut OM'den kronik OM'nin ayırt edilmesinde faydalı idi (kappa değeri planar tarama/SPECT için 0,541, SPECT/BT için 0,944).

Sonuç: SPECT/BT, üç fazlı kemik sintigrafisi/SPECT ile karşılaştırıldığında OM değerlendirilmesinde tanı doğruluğunu arttırmaktadır. SPECT/BT hastaların teşhis ve yönetimini değiştirebilir.

Anahtar kelimeler: Kemik sintigrafisi, osteomyelit, enfeksiyon, SPECT, SPECT/BT

Address for Correspondence: Pelin Arıcan MD, University of Health Sciences, Ankara Numune Training and Research Hospital, Clinic of Nuclear Medicine, Ankara, Turkey **Phone:** +90 542 286 75 75 **E-mail:** psarican@yahoo.com ORCID ID: orcid.org/0000-0003-4278-9508
Received: 13.12.2017 **Accepted:** 28.06.2019

Introduction

Osteomyelitis (OM) is a bone infection. Early diagnosis of OM is essential for a successful therapy and management of the complications. Determining whether the OM is acute or chronic is very important for deciding an appropriate antimicrobial and surgical treatment. The diagnosis of bone infection is still challenging. Clinical and laboratory parameters such as erythrocyte sedimentation rate (ESR), C-reactive protein (CRP), microbiological examination are usually insufficient to make a correct diagnosis (1,2,3). The changes in plain radiography occur late and are non-specific. Computed tomography (CT) and magnetic resonance imaging (MRI) are able to show pathologic morphological changes in the bones and surrounding soft tissues. Although they are very sensitive, their specificity is moderate (3). Three-phase planar bone scintigraphy (3-phase PBS) is the first option among radionuclide techniques for detection of the OM since it is widely available, easy, and inexpensive. This technique has a high sensitivity, but its specificity is limited (1,2,3,4). PBS must be combined with single photon emission computed tomography (SPECT) to obtain high sensitivity and specificity however, their value is limited due to the poor accuracy in localizing the increased uptake (4,5). SPECT/CT can improve the prognostic value of planar radionuclide techniques since it evaluates morphologic and functional information together (4,5). Use of SPECT/CT significantly increases the diagnostic accuracy of skeletal scintigraphy (6). Nowadays, SPECT/CT has been used frequently in orthopedic diseases (7,8,9,10). In this retrospectively study, we aimed to evaluate the contribution and superiority of SPECT/CT to 3-phase PBS/SPECT for assessment of OM and management of patients.

Materials and Methods

Patients

We retrospectively analyzed 85 patients who were suspected as having OM with clinical and laboratory findings and we performed the 3-phase PBS-SPECT/CT. The mean age of the patients was 50±32 years (range 18-82 years). There was clinical suspicion of bone infection (pain, swelling, erythema, heat, fever, wound etc.), and abnormal laboratory findings (increased number of white blood cells and neutrophils, ESR and CRP) during 10-90 days in the selected patients. Patients without follow up, patients with prostheses or metallic instrumentation causing artifacts on CT, patients who had an operation within 3 months and using antibiotic therapy for more than 7 days were excluded. The study group was consisted of 34 females and 51 males. There were systemic diseases in 22 patients (diabetes mellitus n=16, tuberculosis n=2, ankylosing spondylitis n=2, others=2). All patients had X-rays before radionuclide imaging and clinical follow up for at least 6 months. The patients' characteristics are summarized in Table 1. All patients gave their written informed consents for the 3-phase PBS and SPECT/CT study. Local Ethics Committee approved the present retrospective study (3739/0.01.2014).

Three-phase PBS

After a bolus injection of the 740 MBq technetium-99m methylene diphosphonate (Tc-99m MDP) (Monrol, Eczacıbaşı, Turkey), perfusion images were obtained immediately by acquiring blood flow images, 1 frame for 60 sec, at 64x64 matrix. Blood pool images were acquired after perfusion (anterior-posterior position, 256x256 matrix, 500,000-750,000 counts). Whole body and static images were obtained 3 hours after the injection (whole body scan 8 cm/min, static images 500,000-750,000 counts). The images were acquired with a dual head gamma camera, equipped with a low energy, high resolution, large-field-of-view parallel-hole collimator (Millennium Hawkeye 4, GE Medical Systems, Milwaukee, WI).

SPECT/CT

After the 3-phase PBS, SPECT/CT was performed on the region of suspected OM in all patients, firstly, CT scan

Table 1. Patients' characteristics

Characteristics number of patients	
Total patients	85
Age (years) Mean age/range	 50±32/18-82
Sex Female/male	 34/51
Systemic disease DM/other	 16/6
Trauma Yes/no	 34/51
Operation Yes/no	 24/62
Antibiotic therapy (less than 7 days) Yes/no	39/46
Laboratory findings Increased ESR/normal ESR Increased CRP/normal CRP	 47/38 38/47
Localization Extremity Spine Skull Pelvis Other	 67 5 3 8 3

DM: Diabetes mellitus, ESR: Erythrocyte sedimentation rate, CRP: C-reactive protein

was obtained. Secondly, SPECT scan was taken at the same time in the supine position. Low dose CT scan acquisition parameters were 140 kV voltage, 2.5 mA tube current, 512x512 pixel matrix, 5 mm slice thickness, and 3 mm reconstruction. SPECT acquisition parameters were 128x128 pixel matrix, 360° acquisition, 6° steps and 25 sec per frame. SPECT data was reconstructed according to the ordered subset expectation maximization iterative technique.

Image interpretation

Images were interpreted by two qualified nuclear medicine specialists who were blinded to all clinical and radiological details of the patients ($p<0.005$). But they had information about the suspicious infection area due to the dynamic study. Each nuclear medicine specialist independently looked at the first 3-phase PBS and SPECT images together using a linear grey scale display. The uptake of perfusion, blood pool and delayed phase were compared with the opposite side. Then, SPECT/CT fusion images were read at the same time using color display. On the basis of the findings on the 3-phase PBS/SPECT and SPECT/CT, patients were divided into two groups: with OM, without OM (no OM).

Without OM: Normal radiotracer uptake on perfusion-blood pool phase, normal, slightly or mild increased radiotracer uptake in the delayed phase with no abnormal morphologic changes or detection of osteoarthritis-degenerative-traumatic-postoperative changes, osteonecrosis, heterotopic ossification on CT were described as no OM.

With OM: Intense or mild diffuse or focal increased radiotracer uptake at the lesion site in all three phases in 3-phase PBS was defined OM. Detection of periosteal reaction, small focus of gas or foreign bodies, soft tissue abscesses and edema on CT with scintigraphic findings were considered as acute OM (AOM). Bone destruction, sequestration, involucra, fistulous tract on CT associated with the radiotracer uptake were interpreted as chronic OM (COM).

Final Diagnosis

All patients were followed up in our hospital for 6 months. The final diagnosis was verified by microbiologic examination in 39 patients, by radiology and scintigraphic techniques in 31 patients (CT=8, MRI=17, gallium=6), and by surgery and histopathologic findings in 15 patients. We could not use the same gold standard, because there were not microbiologic-histopathologic results in all patients.

Statistical Analysis

Kappa test was used to compare 3-phase PBS/SPECT and SPECT/CT. Sensitivity, specificity, positive predictive value (PPV), negative predictive value (NPV), and accuracy of each method were calculated.

Results

Three-phase PBS/SPECT found OM in 48 (AOM=30, COM=18) (56.4%) patients. There was no OM in 37 (43.6%) patients. While OM was determined in 44 (AOM=16, COM=28) (51.7%) patients with SPECT/CT, it was not determined in 41 (48.3%) patients. In final diagnosis, OM was found in 49 (AOM=21, COM=28) (57.6%) patients. There was no OM in 36 patients. The results of 3-phase

Table 2. The results of planar scan/single photon emission computed tomography (SPECT), SPECT/CT, and final diagnosis in patients without osteomyelitis

AOM (n/N%)				COM (n/N%)		
	H	PT	PO	H	PT	PO
Planar/SPECT SPECT/CT	10/85 (11.7) 4/85 (4.7)	8/85 (9.4) 5/85 (5.8)	12/85 (14.1) 7/85 (8.2)	6/85 (7) 7/85 (8.2)	7/85 (8.2) 8/85 (9.4)	5/85 (5.8) 13/85 (15.2)
Final	7/85 (8.2)	6/85 (7)	8/85 (9.4)	7/85 (8.2)	7/85 (8.2)	14/85 (16.4)

AOM: Acute osteomyelitis, COM: Chronic osteomyelitis, H: Hematogenous, PT: Post-traumatic, PO: Post-operative, CT: Computed tomography

Table 3. The results of planar scan/single photon emission computed tomography (SPECT), SPECT/CT, and final diagnosis in patients without osteomyelitis

(n/N%)					
	N	OA-D	T-F	STI	M
Planar/SPECT	4/85 (4.7)	18/85 (21.1)	7/85 (8.2)	5/85 (5.8)	3/85 (3.5)
SPECT/CT	4/85 (4.7)	16/85 (18.8)	6/85 (7)	11/85 (12.9)	4/85 (4.7)
Final	4/85 (4.7)	14/85 (16.4)	5/85 (5.8)	10/85 (11.7)	3/85 (3.5)

N: Normal, OA-D: Osteoarthritis-degeneration, T-F: Trauma-fracture, STI: Soft tissue infection, M: Miscellaneous, CT: Computed tomography

PBS/SPECT, SPECT/CT and final diagnosis are given in detail in the Table 2 and 3.

When the findings of 3-phase PBS/SPECT and SPECT/CT were compared with the findings of the final diagnosis, it was observed that 3-phase PBS/SPECT predicted the correct diagnosis in 69 (82.1%) patients when SPECT/CT predicted the correct diagnosis in 83 (97.6%) patients. SPECT/CT changed the diagnosis and the treatment in 14 of 85 (16.5%) patients. Three-phase PBS/ SPECT showed false positive results in 11, and false negative results in 5 patients. SPECT/CT gave false positive results in 2 patients. There was no false negative result in SPECT/CT. The false positive and false negative results and the contribution of SPECT/CT are seen in the Table 4.

Sensitivity, specificity, PPV, NPV and accuracy of each method were calculated. The results are showed in the Table 5. When the kappa values of 3-phase PBS/SPECT and SPECT/CT were analyzed together, it was seen that SPECT/CT was significantly superior to PBS/SPECT in imaging for determining OM (kappa value was 0.626 for planar scan/SPECT, 0.929 for SPECT/CT). In addition, SPECT/CT was statistically more successful in detection of COM, and

Table 4. The contribution of single photon emission computed tomography (SPECT)/CT in the patients who had false negative and false positive results

Patient no	Side	Planar/SPECT	SPECT/CT	Contribution of SPECT/CT	Final diagnosis
12	Mandibula	FN (PO)	TP (COM)	Anatomic localization Morphologic changes	COM
19	Spine	FP (COM)	TN (STI)	Anatomic localization Morphologic changes	STI
28	Mandibula	FN (PO)	TP (AOM)	Anatomic localization	AOM
37	Foot	FP (AOM)	TN (STI)	Anatomic localization	STI
39	Hip	FP (COM)	TN (STI+fracture)	Morphologic changes	STI+fracture
44	Rib	FN (PO)	TP (COM)	Anatomic localization Morphologic changes	COM
48	**Knee**	**FP (AOM)**	**FP (COM)**	**No contribution**	**OA**
49	Spine	FN (fracture)	TP (COM)	Morphologic changes	COM
51	Foot	FP (AOM)	TN (fracture)	Morphologic changes	fracture
58	Hip	FP (COM)	TN (OA)	Anatomic localization Morphologic changes	OA
60	Foot	FP (AOM)	TN (bone tumor)	Morphologic changes	Ewing sarcoma
65	**Foot**	**FP (AOM)**	**FP (AOM)**	**No contribution**	**PO**
70	Hip	FP (AOM)	TN (HO)	Anatomic localization	HO
74	Tibia	FP (COM)	TN (OA)	Anatomic localization	OA
82	Mandibula	FN (PO)	TP (COM)	Anatomic localization	COM
84	Foot	FP (AOM)	TN (STI+fracture)	Anatomic localization morphologic changes	STI+fracture

AOM: Acute osteomyelitis, COM: Chronic osteomyelitis, STI: Soft tissue ınfection, OA: Osteoartritis, PO: Postoperative, HO: Heterotopic ossification, TN: True negative, TP: True positive, FN: False negative, FP: False positive, CT: Computed tomography

Table 5. Planar scan/single photon emission computed tomography (SPECT) and SPECT/CT assessment of osteomyelitis

	TN	TP	FN	FP	Sensitivity	Specificity	PPV	NPV	Acc
n/N (%)									
Planar/SPECT	31/85 (36.4)	38/85 (44.7)	5/85 (5.9)	11/85 (12.9)	38/43 (88.3)	31/41 (75.6)	38/48 (79.1)	31/36 (86.1)	69/85 (81.1)
SPECT/CT	42/85 (49.4)	41/85 (48.2)	0	2/85 (2.4)	41/41 (100)	42/44 (95.4)	41/43 (95.3)	42/42 (100)	83/85 (97.6)

TN: True negative, TP: True positive, FN: False negative, FP: False positive, PPV: Positive predictive value, NPV: Negative predictive value, Acc: Accuracy, CT: Computed tomography

useful in differentiating COM from AOM (kappa value was 0.541 for PBS/SPECT, 0.944 for SPECT/CT).

Discussion

The diagnosis of OM is challenging. The localization of the infection site and determination of acute or COM are important for planning the treatment. The treatment of OM is multidisciplinary. It is very important to take the appropriate antimicrobial treatment and to choose the patients for surgery. Untreated or insufficiently treated bone infection leads to destruction and recurrence of diseases. Three-phase PBS is widely used for evaluation of the suspected OM (1,2,3,4). SPECT/CT has become an increasingly important diagnostic modality in addition to 3-phase PBS in orthopedic diseases (7,8,9,10). In this study, we investigated the contribution and superiority of SPECT/CT to 3-phase PBS/SPECT in the patients who were suspected as having OM and underwent 3-phase PBS.

Three-phase PBS in the diagnosis of OM has high sensitivity, but its specificity is limited (1,2,3). SPECT/CT increases sensitivity and specificity in diagnosis of OM (4,5,7,8). We found that SPECT/CT was a more sensitive and specific method in comparison to PBS/SPECT for diagnosing OM (sensitivity 88.3% versus 100%; specificity 75.6% versus 95.4%). SPECT/CT improved specificity rather than sensitivity. Analysis of the kappa values showed that SPECT/CT was significantly better than PBS/SPECT in the diagnosis of OM. Horger et al. (7) found that sensitivity was 78% for PBS/SPECT and SPECT/CT. But specificity of SPECT/CT was higher than PBS/SPECT. It was 50% for PBS/SPECT and 86% for SPECT/CT. In our experiment, sensitivity was similar with this study, but specificity was significantly higher for both techniques. In our study, the number of patients who had a history of fracture and several bone surgery was more than in the study of Horger et al. (7).

In our study, SPECT/CT showed actual anatomical localization of radiotracer uptake and allowed true localization, extension, and activation of infection. Actual anatomic localization was particularly useful for differentiating soft tissue and bone infection. Morphologic changes on CT also helped to make a correct diagnosis. While soft tissue infection was detected in only 5 patients with 3-phase PBS/SPECT, 11 patients were interpreted with soft tissue infection with SPECT/CT in our study. The most important contribution of SPECT/CT was the change of the diagnosis and treatment in 14 of 85 (16.5%) patients. SPECT/CT changed the diagnosis as true positive in five patients who had false negative results with PBS/SPECT. In 9 of 11 patients who had false positive results with PBS/SPECT, accurate diagnosis was provided by SPECT/CT. It had no contribution to diagnosis in two patients. Osteoarthritis was found with CT in one patient who was reported to have COM with SPECT/CT. She was suffering from active rheumatoid arthritis and had chronic morphologic changes on CT. Therefore, the findings of bone scan and SPECT/CT should be interpreted with clinical information. In the other patient who was reported to have AOM with SPECT/CT,

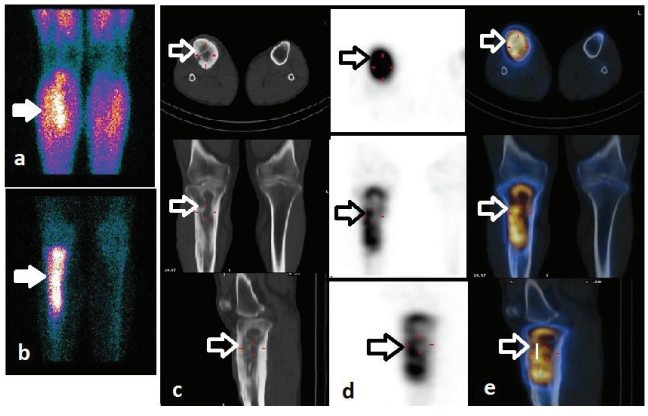

Figure 1. Three-phase planar bone scintigraphy of a 41-year-old man with right leg pain and erythema. (A) Blood pool (B) late static images show hyperemia and increased osteoblastic activity in right upper half tibia (arrows). (C) Axial, (D) coronal (E) sagittal computed tomography (CT), single photon emission computed tomography (SPECT) and SPECT/CT images. The heterogeneous increased uptake and chronic morphological changes are seen in the fusion images (arrows). The planar images suggest acute osteomyelitis without SPECT/CT. But chronic osteomyelitis is described with the morphological changes in the CT images. Chronic osteomyelitis is confirmed by pathology

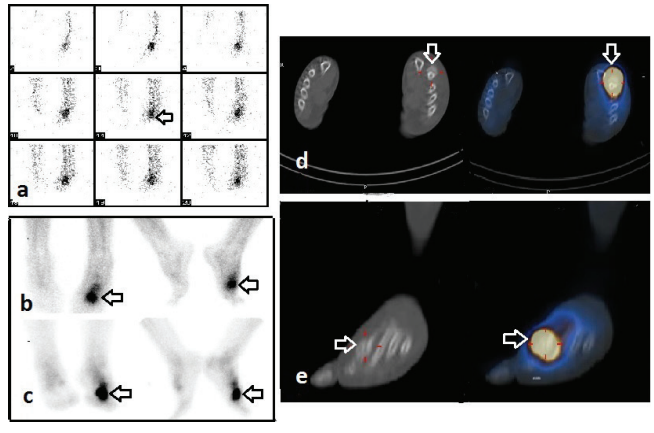

Figure 2. Three-phase PBS of a 56-year-old woman with left foot swelling, pain, and trauma history for 2 years. (A) Perfusion (B) blood pool (C) late static images show slightly increased perfusion, blood pool and osteoblastic activity in left metatarsophalangeal region (arrows). The planar images suggest acute osteomyelitis without single photon emission computed tomography (SPECT)/computed tomography (CT). (D) Axial (E) sagittal CT, and fusion images show fracture site and callus in the distal of second metatarsal bone associated with focal intense increased uptake (arrows). Fracture and callus are confirmed by diagnostic CT

the final diagnosis was postoperative changes which was supported with clinic follow up and microbiologic results. This patient had had surgery five months before the scan. Both techniques failed to differentiate postoperative changes from infection. Three-phase PBS could be interpreted as false positive in this period, because bone surgery leads to increase in bone turnover and osteoblastic activity. Accurate differentiation of AOM from COM is very important for patient management. Increased radiotracer uptake is found on all three phases of 3-phase PBS in both AOM and reactive COM. As AOM is treated with antimicrobial therapy, surgery with antimicrobial therapy may be needed in COM (11). SPECT/CT is important in differentiating AOM from reactive COM. In our experience, SPECT/CT correctly classified COM in 8 of 36 patients who were interpreted as AOM on 3-phase PBS (Figure 1). We saw that SPECT/CT was particularly useful for the diagnosis of post-traumatic and post-operative OM in the patients with reactive COM.

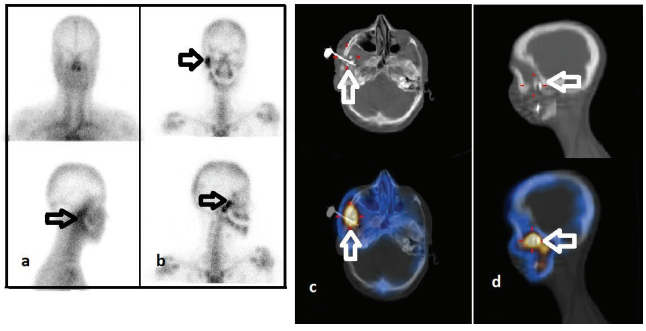

Figure 3. A 18-year-old woman who was operated due to hemifacial atrophy and was being suspected as having osteomyelitis in right mandibula five months after the operation. (A) There is mild hyperemia on the right temporomandibular region in blood pool (B) delayed anterior and right lateral static images show intense focal increased radiotracer uptake in the same area with hyperemia (arrows). (C) Axial and (D) sagittal single photon emission computed tomography/computed tomography, images show intense focal increased radiotracer uptake around the metal implant on the zygomatic bone (arrows). These findings are interpreted as acute osteomyelitis. The result of microbiological examination is reported as infection

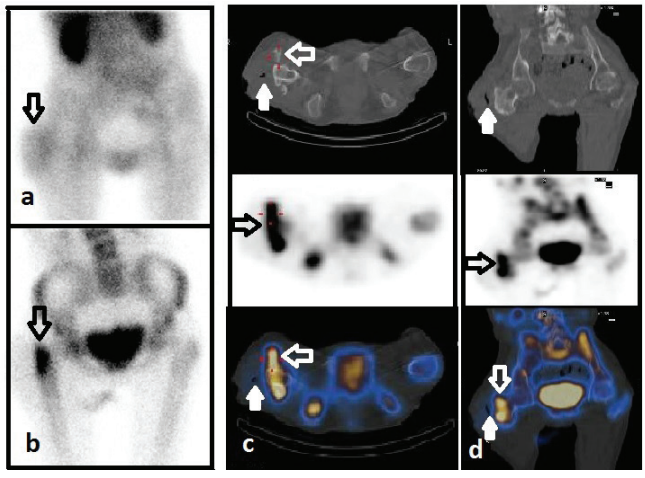

Figure 4. A 22-year-old woman who had right hemiplegia and was suspected as having osteomyelitis in the right upper femur. (A) Blood pool anterior image shows heterogeneous hyperemia in the soft tissues just lateral to the trochanter major (arrows). (B) The intense osteoblastic uptake is seen on trochanteric regions in the anterior late static image. (C) Axial, (D) coronal single photon emission computed tomography (SPECT)/CT images show fistula tract in the soft tissue (white arrows). Fusion images show that radiotracer uptake around the trochanter major is associated with the bone structures within soft tissue (arrows). The findings of SPECT/computed tomography (CT) are described as heterotopic ossification and soft tissue infection. This diagnosis is confirmed by CT and pathology

SPECT/CT improved the image quality, resolution and identified minimal increased activity. SPECT/CT might easily evaluate the small multiple osseous structure in hand-wrist, and foot-ankle (12,13). SPECT/CT confirmed final diagnosis in 40 out of 41 patients with suspected lesions in their hands and feet (Figure 2). It is sometimes difficult to identify an infection focus in the appendicular skeleton such as skull, vertebra or pelvis with 3-phase PBS, because of compact bone structure and superposition of bones (14). In our study, there were three patients with suspected OM of skull after operation. OM sites could be diagnosed accurately in these patients by SPECT/CT (Figure 3). Bolouri et al. (15) performed bone SPECT/CT to evaluate patients who were suspected as having OM on the jaw. They found that SPECT/CT slightly improved the specificity of 3-phase PBS. Damle et al. (16) reported a case with skull base OM. Planar image was equivocal, but SPECT/CT was helpful in the detection of OM. Spinal OM and spondylodiscitis are localized in vertebral body and intervertebral disc. Soft tissue abscesses often accompany spinal infection (1). Since detailed anatomic localization is possible, SPECT/CT is helpful in differentiating OM from spondylodiscitis. Additionally, fracture and degenerative changes can be differentiated from infection with CT component. SPECT/CT confirmed the final diagnosis in 5 patients with spine lesions in our study. We found COM in 1 patient, soft tissue infection in 1 patient, fracture in 1 patient, degenerative change in 2 patients. Distinguishing insufficiency or traumatic fractures from infection in pelvic region is very important. In this study, there were 2 patients who were suspected as having OM in pelvis. SPECT/CT correctly diagnosed soft tissue infection in one patient and revealed heterotopic ossification and soft tissue infection in the other patient who was suspected as having OM (Figure

4). The therapy of those patients completely changed. Linke et al. (8) reported that bone SPECT/CT findings led to change in the diagnosis of one third of patients with pain in the extremities (17). The highest rate of diagnostic alteration was found 60% among patients who were suspected as having OM (8).

Study Limitations

There were three limitations in our study. The main limitation was the retrospective design of the study. Despite the fact that the nuclear medicine specialists did not know the clinical and radiological results of the patients, they had information about the region of suspected OM due to perfusion and blood pool images.

The second limitation was that there was lack of standard gold reference for the final diagnosis of OM. All patients did not have microbiologic and histopathologic examinations. We had to compare the 3-phase PBS and SPECT/CT results with different references. Because of this reason, there was no standardization in the final diagnosis.

The third limitation in our study was that poor image quality due to low dose CT. Even though low dose CT was enough for anatomic localization of radiotracer uptake; the morphologic evaluation of particularly small and compact bone structures in the foot, hand, mandibula, and spine was difficult.

Conclusion

Three-phase PBS combined with SPECT/CT is an useful tool in diagnosis of OM. We think that SPECT/CT has more diagnostic accuracy than 3-phase PBS/SPECT in differentiation of reactive COM and AOM. Especially SPECT/CT is superior in postoperative and posttraumatic OM. SPECT/CT is very successful in the evaluation of skull, vertebra, pelvis, spine, hand, and foot than PBS. We recommend that SPECT/CT should be used in selected patients.

Ethics

Ethics Committee Approval: This retrospective study was approved by the Ethics Committee of the Ankara Numune Training and Research Hospital (3739/0.01.2014).

Informed Consent: All patients gave their written informed consents.

Peer-review: Externally peer-reviewed.

Authorship Contributions

Concept: P.A., B.O., Design: P.A., B.O., Data Collection or Processing: P.A., R.Ş., S.N., Analysis or Interpretation: P.A., B.O., Literature Search: P.A., Writing: P.A.

Conflict of Interest: No conflict of interest was declared by the authors.

Financial Disclosure: The authors declared that this study received no financial support.

References

1. Palestro CJ. Radionuclide imaging of osteomyelitis. Semin Nucl Med 2015;45:32-46.
2. Bruggen van der W, Bleeker-Rovers CP, Boerman OC, Gotthardt M, Oyen WJ. PET and SPECT in osteomyelitis and prosthetic bone and joint infections: a systematic review. Semin Nucl Med 2010;40:3-15.
3. Gotthardt M, Bleeker-Rovers CP, Boerman OC, Oyen WJ. Imaging of inflammation by PET, conventional scintigraphy, and other imaging techniques. J Nucl Med 2010;51:1937-1949.
4. Huellner MW, Strobel K. Clinical applications of SPECT/CT in imaging the extremities. Eur J Nucl Med Mol Imaging 2014;41(Suppl 1):50-58.
5. O'Connor MK, Kemp BJ. Single photon emission computed tomography/computed tomography: basic instrumentation and innovations. Semin Nucl Med 2006;36:258-266.
6. Mariani G, Bruselli L, Kuwert T, Kim EE, Flotats A, Israel O, Dondi M, Watanabe N. A rewiew on the clinical uses of SPECT/CT. Eur J Nucl Med Mol Imaging 2010;37:1959-1985.
7. Horger M, Eschmann SM, Pfannenberg C, Storek D, Vonthein R, Claussen CD, Bares R. Added value of SPECT/CT in patients suspected of having bone infection: preliminary results. Arch Orthop Trauma Surg 2007;127:211-221.
8. Linke R, Kuwert T, Uder M, Forst R, Wuest W. W. Skeletal SPECT/CT of the peripheral extremities. AJR Am J Roentgenol 2010;194:329-335.
9. Even-Sapir E, Flusser G, Lerman H, Lievshitz G, Metser U. SPECT/multislice low-dose CT: a clinically relevant constituent in the imaging algoritm of nononcologic patients referred for bone scintigraphy. J Nucl Med 2007;48:319-324.
10. Arıcan P, OkudanTekin B, Şefizade R, Naldöken S, Bastuğ A, Özkurt B. The role of bone SPECT/CT in the evaluation of painful joint prostheses. Nucl Med Commun 2015;36:931-930.
11. Wing VW, Jeffrey RB Jr, Federle MP, Helms CA, Traton P. Chronic osteomyelitis examined by CT. Radiology 1985;154:171-174.
12. Schleich FS, Schürch M, Huellner MW, Hug U, von Wartburg U, Strobel K, Veit-Haibachn P. Diagnostic and therapeutic impact of SPECT/CT in patients with unspecific pain of the hand and wrist. EJNMMI Res 2012;2:53.
13. Singh VK, Javed S, Parthipun A, Sott AH. The diagnostic value of single photon-emission computed tomography bone scans combined with CT (SPECT-CT) in diseases of the foot and ankle. Foot Ankle Surg 2013;19:80-83.
14. Younis JA. Additive value of 99mTechnetium methylene diphosphonate hybrid single-photon emission computed tomography/computed tomography in the diagnosis of skull base osteomyelitis in otitis externa patients compared to planar bone scintigraphy. World J Nucl Med 2018;17:286-292.
15. Bolouri C, Merwald M, Huellner MW, Velt-Haibach P, Kuttenberger J, Perez-Lago M, Seifert B, Strobel K. Performance of orthopantomography planar scintigraphy, CT alone, and SPECT/CT in patients with suspected osteomyelitis of the jaw. Eur J Nucl Med Mol Imaging 2013;40:411-417.
16. Damle NA, Kumar R, Kumar P, Jaganathan S, Patnecha M, Bal C, Bandopadhyaya G, Malhotra A. SPECT/CT in the diagnosis of skull base osteomyelitis. Nucl Med Mol Imaging 2011;45:212-216.
17. Govaert GA, IJpma FF, McNally M, McNally E, Reininga IH, Glaudemans AW. Accuracy of diagnostic imaging modalities for peripheral post-traumatic osteomyelitis - a systematic review of the recent literature. Eur J Nucl Med Mol Imaging 2017;44:1393-1407.

Original Article
Mol Imaging Radionucl Ther 2019;28:96-103 DOI:10.4274/mirt.galenos.2019.83723

Effects of the Use of Automatic Tube Current Modulation on Patient Dose and Image Quality in Computed Tomography

Bilgisayarlı Tomografide Otomatik Tüp Akımı Modülasyonu Kullanımının Hasta Dozu ve Görüntü Kalitesi Üzerine Etkileri

Ayşegül Yurt[1], *İsmail Özsoykal*[1], *Funda Obuz*[2]
[1]*Dokuz Eylül University Faculty of Medicine, Department of Medical Physics, İzmir, Turkey*
[2]*Dokuz Eylül University Faculty of Medicine, Department of Radiology, İzmir, Turkey*

Abstract

Objectives: The frequency of abdominal computed tomography examinations is increasing, leading to a significant level of patient dose. This study aims to quantify and evaluate the effects of automatic tube current modulation (ATCM) technique on patient dose and image quality in contrast-enhanced biphasic abdominal examinations.

Methods: Two different scan protocols, based on constant tube current and ATCM technique, were used on 64 patients who visited our radiology department periodically. For three patient groups with different patient size, results from two protocols were compared with respect to patient dose and image quality. Dosimetric evaluations were based on the Computed Tomography Dose Index, dose length product, and effective dose. For the comparison of image qualities between two protocols, Noise Index (NI) and Contrast to Noise Ratio (CNR) values were determined for each image. Additionally, the quality of each image was evaluated subjectively by an experienced radiologist, and the results were compared between the two protocols.

Results: Dose reductions of 31% and 21% were achieved by the ATCM protocol in the arterial and portal phases, respectively. On the other hand, NI exhibited an increase between 9% and 46% for liver, fat and aorta. CNR values were observed to decrease between 5% and 19%. All images were evaluated by a radiologist, and no obstacle limiting a reliable diagnostic evaluation was found in any image obtained by either technique.

Conclusion: These results showed that the ATCM technique reduces patient dose significantly while maintaining a certain level of image quality.

Keywords: Tomography, radiation protection, abdomen

Öz

Amaç: Abdominal bilgisayarlı tomografi incelemelerinin sıklığı artmakta ve önemli miktarda hasta dozuna yol açmaktadır. Bu çalışma, kontrastlı, çift fazlı abdomen incelemelerinde otomatik tüp akım modülasyon tekniğinin hasta dozu ve görüntü kalitesi üzerine etkilerini ölçmeyi ve değerlendirmeyi amaçlamaktadır.

Yöntem: Radyoloji anabilim dalını periyodik olarak ziyaret eden 64 hastaya sabit tüp akımı ve otomatik tüp akımı modülasyonu tekniğine dayanan iki farklı tarama protokolü uygulandı. Farklı hasta boyutlarına sahip üç hasta grubu için, iki protokolden elde edilen sonuçlar hasta dozu ve görüntü kalitesi açısından karşılaştırıldı. Dozimetrik değerlendirmeler, Bilgisayarlı Tomografi Doz İndeksi, doz uzunluk çarpımı ve etkin doza dayandırıldı. İki protokol arasındaki görüntü kalitesinin karşılaştırılması amacıyla her görüntü için Gürültü İndeksi (NI) ve Kontrast Gürültü Oranı (CNR) değerleri belirlendi. Ek olarak, her görüntü deneyimli bir radyolog tarafından öznel olarak değerlendirildi ve sonuçlar iki protokol arasında karşılaştırıldı.

Bulgular: Otomatik tüp akım modülasyon protokolü ile arteriyel ve portal fazlarda sırasıyla %31 ve %21 doz düşüşleri sağlandı. Öte yandan, NI karaciğer, yağ ve aort için %9 ile %46 arasında bir artış gösterdi. CNR değerlerinin ise %5 ile %19 arasında azaldığı gözlendi. Tüm görüntüler

Address for Correspondence: Ayşegül Yurt MD, Dokuz Eylül University Faculty of Medicine, Department of Medical Physics, İzmir, Turkey
Phone: +90 537 338 86 82 **E-mail:** aysegul.yurt@gmail.com ORCID ID: orcid.org/0000-0001-9898-2329
Received: 21.03.2019 **Accepted:** 01.07.2019

bir radyolog tarafından değerlendirildi ve herhangi bir teknikle elde edilen görüntülerde güvenilir bir tanısal değerlendirmeyi sınırlayan bir engel bulunmadı.

Sonuç: Bu sonuçlar, otomatik tüp akım modülasyon tekniğinin, belirli bir görüntü kalitesi seviyesini korurken hastanın dozunu önemli ölçüde azalttığını göstermiştir.

Anahtar kelimeler: Tomografi, radyasyondan korunma, abdomen

Introduction

In the early 1990s, helical computed tomography (CT) devices were introduced for medical imaging. Shortened examination times, improved visibility of vascular structures and potential reduction in the use of contrast material enabled intensive use of this technology. However, the clinical use of CT increased mainly after multislice helical CT scanners became available towards the end of the decade. Today, images from 64 to 320 slices can be acquired in a single rotation of the X-ray tube within one-third of a second. These advances led to a further increase in the use of CT for cardiovascular examinations, perfusion imaging, brain, heart, breast, colon, and whole body studies (1).

Radiation exposure of patients having CT scans has increased as a consequence of more frequent use of CT. Recent studies on major medical centers in the UK showed that only 11% of all applications in the radiology departments are CT applications, whereas the effective radiation dose of patients due to CT applications was reported as 40% in 1998 and 68% in 2008 (2). Although offering shorter image acquisition time and higher spatial resolution, multislice CT technology has some dosimetric handicaps to be considered. In MSCT, over-beaming and end effect terms refer to the necessity of beam and scan widths extending beyond detector area and imaged region, respectively. These conditions that arise due to image reconstruction purposes lead to increase in radiation dose to the patient, when compared to single slice CT scanners. On the other hand, smaller gantry designs for MSCT devices led to a shorter patient-tube distance which obviously affects patient dose (3). These conditions have forced CT manufacturers to develop dose optimization strategies either based on image processing or the prevention of unnecessary radiation. The most common strategy among these is the use of Automatic Exposure Control (AEC), where the tube current is adjusted by the scanner according to the patient size. Since the beginning of the 2000s, AEC systems have been developed by the manufacturers based on different operating mechanisms; however, offering similar opportunities on patient dose control, image quality, and tube life (4,5).

In CT, AEC is applied based on two main techniques: Automatic Current Setting (ACS) and Automatic Tube Current Modulation (ATCM), which can be activated separately or combined. In ACS technique, scanner generates an optimized constant tube current to be applied along the scanned region for which ATCM offers a modulated tube current. This modulation may be achieved either for every single longitudinal slice along the z-axis or at different angular projections of the tube on x-y plane. These techniques are known as longitudinal ATCM and angular ATCM, respectively.

Longitudinal ATCM, a commonly used ACS technique, is available under different names among different manufacturers. Z-DOM, a longitudinal ATCM named by Philips, makes use of a pre-scan radiograph, named as a topogram, to compute the attenuation properties of the patient as a function of scan length and modulate tube current based on this information. This dose modulation mechanism works in accordance with a reference image quality selected and standardized by the user, in terms of a Noise Index (NI) (6). In CT exams that include both head&neck and abdominal regions, for example, Z-DOM technique achieves both radiation protection in thyroids and good image quality in abdominal region by locally decreasing and increasing tube current. However, scan protocols applying constant tube current usually fail to meet these goals at the same time. These scans end up with either overexposure of thyroids or underexposure of abdominal region depending on the amount of tube current.

In the literature, studies carried on the abdominal CT examinations of adults report commonly that the use of AEC techniques leads to a considerable decrease in patient dose while keeping a reasonable image quality (6,7,8,9,10,11,12,13,14). This study aims to focus on the use of Z-DOM in contrast-enhanced biphasic abdominal examinations and to make evaluations on image quality and patient dose. The results will be examined with respect to different patient groups in different size.

Materials and Methods

Patient Profile and Scan Protocol

This retrospective study was conducted in accordance with ethical standards under the responsibility of the

Institutional Review Board that approved the study (decision no: 2015/05-19). Sixty four patients undergoing contrast-enhanced biphasic abdominal CT examination were involved in the study. The scans were performed with a 64-slice CT scanner (Brilliance, Philips medical systems, Netherlands) which is located in the radiology department of our university hospital. All data regarding both image quality and dosimetric quantities were classified under three patient groups with respect to patient size for a better evaluation of the results. This classification was carried out based on CT images, according to the effective diameter measurements of the patients taken from the abdominal region. Effective diameter, D_{eff}, was determined using lateral and anterioposterior sizes of the patient as shown in Equation 1.

$$D_{eff} = (D_{LAT} + D_{AP})/2 \quad (1)$$

Patients with effective diameters in the range of 21-26 cm were included in the first group, patients with effective diameters in the range of 26-31 cm were included in the second group, and patients with effective diameters in the range of 31-36 cm were included in the third group.

Cohort of the study involved the patients who underwent biphasic abdominal examinations periodically. In these examinations, the arterial phase scan involved thorax and abdomen while portal phase scan involved abdominopelvic region (Figure 1). Scan parameters regarding weight based routine protocol and ATCM protocol are given in Table 1. All parameters were kept constant except effective tube current.

Patient Dosimetry

Computed Tomography Dose Index ($CTDI_{vol}$) and Dose Length Product (DLP) values are two main dosimetric quantities reported by the scanner following each exam. $CTDI_{vol}$ refers to the dose output of the CT scanner measured in a cylindrical PMMA phantom with an ionization chamber. It represents absorbed dose, in mGy, in the central slice of the scan range. Therefore, it is not a direct measure of patient dose, however, it offers the opportunity for dosimetric comparison between different scanning protocols and it is commonly used for quality control purposes. DLP, on the other hand, represents the total radiation output of a scanner along the axis of scan and it is determined by multiplying $CTDI_{vol}$ with the scan length. These two quantities were obtained from examination specific dose reports given by the scanner which has been objected to a dosimetric quality control test prior to the collection of data. Besides $CTDI_{vol}$ and DLP, effective dose (E) was calculated for each scan using E per DLP (E/DLP) value recommended by the European Commission's Guidelines, as shown in Equation 2.

$$E = E_{DLP} \times DLP \quad (2)$$

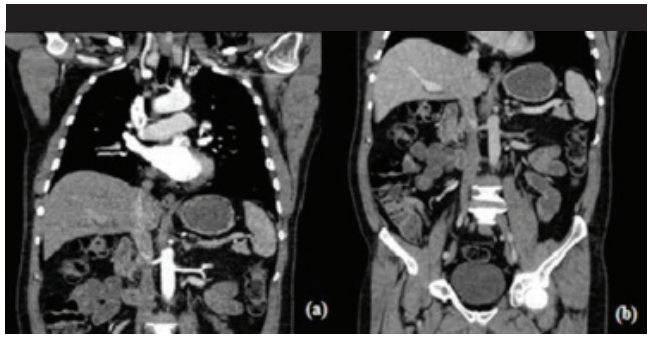

Figure 1. Scan regions for arterial phase (A) and portal phase (B)

Table 1. Contrast-enhanced biphasic abdominal scan protocols

		Routine scan protocol		Z-DOM scan protocol	
Effective tube current (mAs/slice)	**Patient weight (kg)**	**Arterial phase**	**Portal phase**	**Arterial phase**	**Portal phase**
	40-80	200	200	Z-DOM	Z-DOM
	80<	250	250	Z-DOM	Z-DOM
Tube voltage (kVp)		120	120	120	120
Slice thickness (mm)		0.9	2	0.9	2
Pitch		1.172	1.172	1.172	1.172
Increment (mm)		0.45	1	0.45	1
Scan length (mm)		500	500	500	500
Collimation (mm)		64 x 0.625	64 x 0.625	64 x 0.625	64 x 0.625
Field of view (mm)		350	350	350	350
Gantry rotation time (s)		0.75	0.75	0.75	0.75
Image matrix size		512 x 512	512 x 512	512 x 512	512 x 512
Reconstruction filter		Standard (B)	Standard (B)	Standard (B)	Standard (B)

Here, E stands for the E (mSv) to the patient due to CT scan. E_{DLP} represents the E per DLP, and it is given as 0.015 mSv/mGy.cm specific to abdominal scans (15). Two scan protocols were compared based on $CTDI_{vol}$, DLP and E.

Image Quality

In this part of the study, following the dosimetric comparison, NI and Contrast to Noise Ratio (CNR) of the images obtained via both protocols were compared, and the image quality was examined objectively based on these parameters as recommended by the international authorities. In addition to this, subjective evaluation made by a clinician was another method in which image quality was considered.

Objective Approach

Objective analysis of the image quality was based on NI which is defined as the standard deviation in the pixel values (i.e., Hounsfield Units, HU) for a homogeneous object being scanned. Circular region of ınterest (ROI) was drawn to measure NI in three regions: The subcutaneous fat in the anterior region of the abdomen, liver, and aorta. Figure 2 shows three ROIs with identical areas that were cared to be located at the same regions for each patient. For each image, an average NI calculation was made based on the NI measurements taken in three consecutive slices. Apart from NI, average CNR values were determined to compare the images by means of contrast resolution. CNR value of two tissues A and B was determined as shown in Equation 3 (16):

$$CNR = (S_A - S_B) / [(SD_A)^2 + (SD_B)^2]^{1/2} \quad (3)$$

Where S_A and S_B denote mean HU values within the ROIs while SD_A and SD_B denote the standard deviation, or NI, measured for tissues A and B, respectively. CNR values were obtained for liver-fat and aorta-fat and compared between two scan protocols (Figure 2).

Subjective Approach

In addition to the objective analysis of image quality, subjective evaluations were made on images by a radiologist who rated the overall image quality and the visibility of anatomic details. This evaluation was done by grading the diagnostic quality of the image examined without any information known about the scan protocol. The grading scale is given in Table 2. Minimum grade required for an image to be regarded as acceptable in terms of diagnostic quality was determined as 2, referring to a study carried out by Mulkens et al. (14).

Presentation and Statistical Analysis of Data

Among all data obtained for patient dose and image quality, arithmetic mean values were calculated and presented for different patient groups (1, 2 and 3) as well as all patients (overall). Besides, data obtained for dosimetric and objective image quality purposes were analyzed statistically using Mann-Whitney U and t-test, respectively.

Results

In this study, 30 female and 34 male patients were examined. The mean age of the patients was 57.4±12.7 years. On the other hand, mean D_{eff} values were found to be 23.8±2 cm, 28.9±1.4 cm, and 33.1±1.5 cm for group 1, group 2 and group 3, respectively. In Table 3 and Table 4 are given the dosimetric results obtained for each biphasic scan protocol for different patient sizes. ATCM protocol was observed to lead 31% and 21% reductions in E for arterial and portal phases, respectively, according to the results obtained from all patient groups, as given in Table 5 which also represents the results based on different patient groups.

Statistical Analysis

Statistical analysis on dosimetric data mostly gave significantly different ($p<0.05$) results across patient

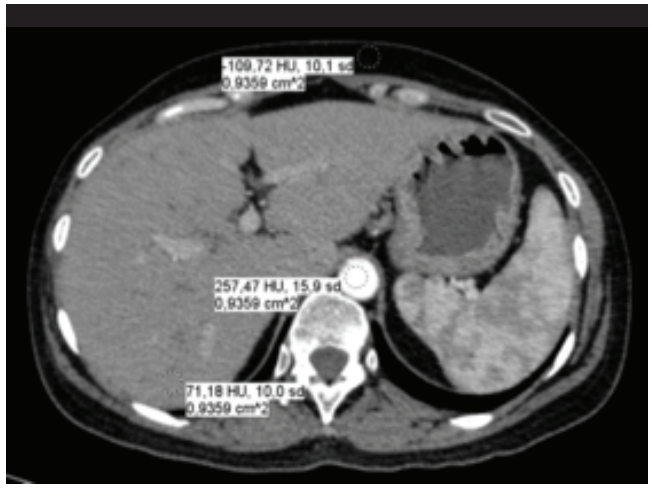

Figure 2. Objective analysis of image quality

Table 2. Grading scale for subjective evaluation	
4	There is no handicap due to noise, and the image quality is very high.
3	A low level of noise is observed in the image, but a reliable diagnostic quality has been maintained.
2	The noise observed in the image is moderate but suitable for a successful diagnostic evaluation.
1	High level of noise observed in the image prevents a reliable diagnostic evaluation.
0	Noise level totally prevents any diagnostic evaluation.

groups for routine and Z-DOM scanning protocols. The only exception was the portal phase examination of patients in group 3 for which the dosimetric results were not observed to be significantly different for two scan protocols ($p>0.05$).

Findings based on NI and CNR obtained for the objective image quality comparison of two protocols are given in Table 6. As observed, images obtained from the ATCM protocol had higher NI and lower CNR values compared to the routine protocol. However, statistical analysis showed that, for patients in group 3, there was no significant difference between two protocols based on NI and CNR values ($p>0.05$), unlike the findings obtained from group 1 and group 2 ($p<0.05$).

Results from subjective image quality evaluations made by a radiologist are given in Table 7. Findings indicated that all images met an acceptable level of diagnostic quality, regardless of which scan protocol was used.

Discussion

Patient size, institution-specific scan protocols and the use of multiphase scanning are three main factors that affect patient dose in CT examinations (17). In this study, a new scan protocol that used Z-DOM was evaluated against routinely used constant tube current protocol for biphasic abdominal CT exams. The two quantities of evaluation were patient dose and image quality.

Z-DOM protocol was observed to lead significant reductions in $CTDI_{vol}$, DLP and E values across all patient groups (Table 3 and Table 4). The percentage reductions are presented in Table 5 indicating that the use of Z-DOM decreased the radiation exposure of the patients between 19% and 37% for the arterial phase and between 2% and 34% for the portal phase. The reason for difference in dose reduction rates observed for the two phases is based on the differences in the anatomic regions scanned. In the arterial phase, the scan area involves thorax and abdomen, while the portal phase includes abdominal and pelvic regions. Since the pelvic region with a bony structure has a higher radiation attenuation compared to the thoracic region filled with air, higher amounts of tube current are needed in this region. This explains why a lower dose reduction rate was observed in the portal phase compared to the arterial phase, especially for patients in group 2 and group 3.

Table 3. $CTDI_{vol}$, DLP and E values of scan protocols for arterial phase

	Routine scan protocol				Z-DOM scan protocol			
	1 (n=16)	2 (n=36)	3 (n=12)	Overall (n=64)	1 (n=16)	2 (n=36)	3 (n=12)	Overall (n=64)
$CTDI_{vol}$ (mGy)	13.2	13.9	14.4	**13.8**	8.2	9.6	11.3	**9.6**
DLP (mGy.cm)	660	697	722	**692**	413	475	585	**480**
E (mSv)	9.9	10.5	10.8	**10.4**	6.2	7.2	8.8	**7.3**

DLP: Dose Length Product, $CTDI_{vol}$: Computed Tomography Dose Index, E: Effective dose

Table 4. $CTDI_{vol}$, DLP and E values of scan protocols for portal phase

	Routine scan protocol				Z-DOM scan protocol			
	1 (n=16)	2 (n=36)	3 (n=12)	Overall (n=64)	1 (n=16)	2 (n=36)	3 (n=12)	Overall (n=64)
$CTDI_{vol}$ (mGy)	12.8	13.9	15.5	**13.9**	8.5	10.9	14.3	**10.9**
DLP (mGy.cm)	639	694	773	**695**	422	543	758	**553**
E (mSv)	9.6	10.4	11.6	**10.4**	6.3	8.1	11.4	**8.3**

DLP: Dose Length Product, $CTDI_{vol}$: Computed Tomography Dose Index, E: Effective dose

Table 5. Dose reductions for patients in group 3

Dose reduction	Arterial phase				Portal phase			
	1 (n=16)	2 (n=36)	3 (n=12)	Overall (n=64)	1 (n=16)	2 (n=36)	3 (n=12)	Overall (n=64)
$CTDI_{vol}$ (%)	38	31	21	**31**	33	21	7	**21**
DLP (%)	37	32	19	**31**	34	22	2	**21**
E (%)	37	32	19	**31**	34	22	2	**21**

DLP: Dose Length Product, $CTDI_{vol}$: Computed Tomography Dose Index, E: Effective dose

On the other hand, Table 5 shows different rates of decreases observed in $CTDI_{vol}$, DLP and E values across 3 groups of patients. Based on Table 5, it could be concluded that the rate of dose reduction was inversely proportional with the patient size. Dosimetric differences between the scan protocols were supported by statistical analysis, where all group based and phase based comparisons yielded significantly different results, except for the portal phase scan of patients in group 3. This was due to the high radiation attenuation property of the pelvic region in patients in group 3, so that, the tube current applied by Z-DOM was not much different from the routine protocol.

In a study that Lee et al. (18) conducted on abdominal CT scans, dose reduction up to 45% was reported and it was shown that higher dose reduction rates were achieved with lower body mass index. These results were parallel to the results obtained from our study. In another study carried out by S. Livingstone et al. (7) on contrast-enhanced biphasic abdominal examinations, dose reductions between 16% and 28% were achieved with the protocol using ATCM compared to fixed current protocols based on patient weight. According to the results of our study, dose reduction rates were observed approximately between 10% (group 3) and 35% (group 1) among the 3 groups when both phases were considered together (Table 5). The results of a comprehensive study in which dosimetric data from 12 centers in the USA were collected showed that the third quartile of the biphasic abdominal CT doses was 32 mSv (19). This value represented the exam specific reference dose level for these medical centers. In this study, the total E due to biphasic abdominal examination was reported as 20.8 mSv and 15.6 mSv, for routine protocol and ATCM protocol, respectively. These values showed that using ATCM techniques, Z-DOM in this case, provided CT scans with lower radiation doses.

In the second part of the study, the diagnostic quality of the images obtained by both protocols was compared using objective and subjective approaches. NI and CNR measurements and calculations were conducted as part of the objective image quality assessment. Table 6 shows the increase in NI values across all patient groups for the protocol using the Z-DOM technique. This increase was observed to become lower as the patient size increased. This is because the Z-DOM technique uses higher tube currents in overweight patients to maintain image quality at a certain level. Comparison of two protocols based on CNR values is given in Table 6. According to this table, CNR values regarding liver-fat and aorta-fat decreased between 5% and 19% in all patient groups for both arterial and portal phases. The conclusion reached with these two tables was that the use of Z-DOM technique leaded to lower objective image quality when compared to routine examination protocol. However, increased noise in the image and therefore decreased contrast between the tissues do not always mean that the image does not meet diagnostic standards required for a successful evaluation. Subjective image quality assessment performed in the last part of the study had an important role in this context. According to the results obtained from the subjective assessment which was made by a radiologist based on the scale given in Table 2, all images were concluded to have the criterion of acceptable diagnostic quality (Table 7).

It is of great importance that the patient dose is brought to the lowest possible level so as to present adequate diagnostic information to the clinician. In order to achieve this goal, it is necessary for the clinical staff to review all parameters of the examination protocols. On the other hand, further advances should follow in the present techniques of image reconstruction developed by the manufacturers which recently play a very important role in

Table 6. Group-specific and overall changing in Noise Index and Contrast to Noise Ratio due to the use of automatic tube current modulation protocol

	Arterial phase				Portal phase			
	1 (n=16)	2 (n=36)	3 (n=12)	Overall (n=64)	1 (n=16)	2 (n=36)	3 (n=12)	Overall (n=64)
NI Increase in tissues								
LIVER (%)	28	21	18	**22**	32	22	14	**23**
FAT (%)	26	25	20	**24**	15	14	9	**13**
AORTA (%)	46	28	18	**31**	41	26	21	**29**
Decrease in CNR for tissues								
LIVER/FAT(%)	17	15	13	**15**	16	12	5	**12**
AORTA/FAT (%)	18	16	10	**15**	19	15	8	**15**

CNR: Contrast to Noise Ratio, NI: Noise Index

Table 7. Mean values of subjective grading scores				
	Arterial phase		Portal phase	
	Routine protocol	Z-DOM protocol	Routine protocol	Z-DOM protocol
1 (n=16)	4	3.3	4	3.5
2 (n=36)	4	3.1	4	3.2
3 (n=12)	3.6	2.6	3.6	2.9
Overall (n=64)	**3.9**	**3.1**	**3.9**	**3.2**

the dose reduction strategies. In addition, clinical physicists, technicians, and radiologists should have more detailed knowledge of the use of AEC techniques that are available for different scanners with different working principles.

Study Limitations

The main limitation of our study was the lack of multiple subjective evaluations made on image quality. There was only one reader for image grading. Increasing the number of readers could help for less bias and more reliable results.

Conclusion

In conclusion, when Z-DOM technique was used instead of weight-based fixed current protocol in contrast-enhanced biphasic abdominal examinations, it was observed that patient doses decreased inversely proportional to the patient size while keeping a sufficient image quality.

Acknowledgements

The authors would like to offer their special thanks to Handan Güleryüz, head of Dokuz Eylül University Hospital Radiology Department, who made this study possible. The authors also would like to thank to Gizem Şişman, Rukiye Çakır Haliloğlu and the department staff for their assistance with the collection of data.

Ethics

Ethics Committee Approval: This retrospective study was conducted in accordance with ethical standards under the responsibility of the Institutional Review Board that approved the study (decision no: 2015/05-19).

Informed Consent: Retrospective study.

Peer-review: Externally peer-reviewed.

Authorship Contributions

Surgical and Medical Practices: A.Y., İ.Ö., Concept: A.Y., İ.Ö., Design: A.Y., İ.Ö., F.O., Data Collection or Processing: A.Y., İ.Ö., F.O., Analysis or Interpretation: A.Y., İ.Ö., F.O., Literature Search: A.Y., İ.Ö., Writing: A.Y., İ.Ö., F.O.

Conflict of Interest: No conflict of interest was declared by the authors.

Financial Disclosure: The authors declared that this study received no financial support.

References

1. AAPM Report No. 96: The Measurement, Reporting and Management of Radiation Dose in CT;2007.
2. Hart D, Wall B, Hillier M, Shrimpton P. Frequency and Collective Dose for Medical and Dental X-Ray Examinations in the UK, 2008:2010. Available from: http://scholar.google.com/scholar?hl=en&btnG=Search&q=intitle:Frequency+and+Collective+Dose+for+Medical+and+Dental+X-ray+Examinations+in+the+UK+,+2008#0
3. Heggie JCP, Kay JK, Lee WK. Importance in optimization of the multi-slice computed tomography scan protocols. Australas Radiol 2006;50:278-285.
4. Lee CH, Goo JM, Ye HJ, Ye SJ, Park CM, Chun EJ, Im JG. Radiation Dose Modulation Techniques in the Multidetector CT Era: From Basics to Practice. Radiographics 2008;28:1451-1459.
5. Kalra MK, Maher MM, Toth TL, Schmidt B, Westerman BL, Morgan HT, Saini S. Techniques and applications of automatic tube current modulation for CT. Radiology 2004;233:649-657.
6. Supawitoo Sookpeng. Investigation of CT Dosimetry Techniques for Use in Optimisation of Automatic Tube Current Modulation (ATCM) Performance Supawitoo Sookpeng BSc (Hons), MSc (Radiation Science). 2014.
7. Livingstone RS, Dinakaran PM, Cherian RS, Eapen A. Comparison of radiation doses using weight-based protocol and dose modulation techniques for patients undergoing biphasic abdominal computed tomography examinations. J Med Phys 2009;34:217-222.
8. Papadakis AE, Perisinakis K, Damilakis J. Automatic exposure control in pediatric and adult multidetector CT examinations: A phantom study on dose reduction and image quality. Med Phys 2008;35:4567-4576.
9. Kalra MK, Naz N, Rizzo SM, Blake MA. Computed tomography radiation dose optimization: scanning protocols and clinical applications of automatic exposure control. Curr Probl Diagn Radiol 2005;34:171-181.
10. Kalender WA, Wolf H, Suess C. Dose reduction in CT by anatomically adapted tube current modulation. II. Phantom measurements. Med Phys 1999;26:2248-2253.
11. Funama Y, Awai K, Hatemura M, Shimamura M, Yanaga Y, Oda S, Yamashita Y. Automatic tube current modulation technique for multidetector CT: is it effective with a 64-detector CT? Radiol Phys Technol 2008;1:33-37.
12. Spampinato S, Gueli AM, Milone P, Raffaele LA. Dosimetric changes with computed tomography automatic tube-current modulation techniques. Radiol Phys Technol 2018;11:184-191.
13. Imai K, Ikeda M, Enchi Y, Niimi T. Quantitative assessment of image noise and streak artifact on CT image: comparison of z-axis automatic tube current modulation technique with fixed tube current technique. Comput Med Imaging Graph 2009;33:353-358.
14. Mulkens TH, Bellinck P, Baeyaert M, Ghysen D, Van Dijck X, Mussen E, Venstermans C, Termote JL. Radiology Use of an Automatic Exposure Control Mechanism for Dose Optimization in Multi-Detector Row CT Examinations : Clinical Evaluation. Radiology 2005;237:213-223.

15. Bongartz G, Golding SJ, Jurik AG, Leonardi M, van Persijn E, van Meerten R, Rodríguez, Schneider K, Calzado A, Geleijns J, Jessen KA, Panzer PC W, Shrimpton GT. European Guidelines for Multislice Computed Tomography. 2004.
16. Tapiovaara MJ, Wagner RF. SNR and noise measurements for medical imaging: I. A practical approach based on statistical decision theory. Phys Med Biol 1993;38:71-92.
17. Smith-Bindman R, Wang Y, Yellen-Nelson TR, Moghadassi M, Wilson N, Gould R, Seibert A, Boone JM, Krishnam M, Lamba R, Hall DJ, Miglioretti DL. Predictors of CT Radiation Dose and Their Effect on Patient Care: A Comprehensive Analysis Using Automated Data. Radiology 2016;282:182-193.
18. Lee S, Yoon SW, Yoo SM, Ji YG, Kim KA, Kim SH, Lee JT. Comparison of image quality and radiation dose between combined automatic tube current modulation and fixed tube current technique in CT of abdomen and pelvis. Acta Radiol 2011;52:1101-1106.
19. Smith-Bindman R, Moghadassi M, Wilson N, Nelson TR, Boone JM, Cagnon CH, Gould R, Hall DJ, Krishnam M, Lamba R, McNitt-Gray M, Seibert A, Miglioretti DL. Radiation Doses in Consecutive CT Examinations from Five University of California Medical Centers. Radiology 2015;277:134-141.

Original Article
Mol Imaging Radionucl Ther 2019;28:104-111 DOI:10.4274/mirt.galenos.2019.63825

Correlation of SUV_{max} and Apparent Diffusion Coefficient Values Detected by Ga-68 PSMA PET/MRI in Primary Prostate Lesions and Their Significance in Lymph Node Metastasis: Preliminary Results of an On-going Study

Ga-68 PSMA PET/MRG ile Tespit Edilen Primer Prostat Lezyonlarında SUV_{maks} ve Görünür Difüzyon Katsayısı Değerlerinin Korelasyonu ve Lenf Nodu Metastazlarında Önemi: Devam Eden Klinik Çalışmanın Ön Bulguları

Lebriz Uslu-Beşli[1], Barış Bakır[2], Sertaç Asa[1], Ekrem Güner[3], Çetin Demirdağ[4], Onur Erdem Şahin[1], Emre Karayel[1], Muhammet Sait Sağer[1], Haluk Burçak Sayman[1], Kerim Sönmezoğlu[1]

[1]*Istanbul University-Cerrahpasa Faculty of Medicine, Department of Nuclear Medicine, İstanbul, Turkey*
[2]*Istanbul University İstanbul Faculty of Medicine, Department of Radiology, İstanbul, Turkey*
[3]*University of Health Sciences, Bakırköy Dr. Sadi Konuk Training and Research Hospital, Clinic of Urology, İstanbul, Turkey*
[4]*İstanbul University-Cerrahpasa Faculty of Medicine, Department of Urology, İstanbul, Turkey*

Abstract

Objectives: Gallium-68 (Ga-68) prostate specific membrane antigen (PSMA) positron emission tomography (PET) has been shown to be more accurate than multiparametric prostate magnetic resonance imaging (MRI) in detection of primary prostate lesions. Using hybrid PET/MRI we aim to detect the correlation between SUV_{max} and apparent diffusion coefficient (ADC) in primary prostate lesions and to assess their prognostic value in detection of lymph node (LN) metastasis.

Methods: Twenty-six patients, who were diagnosed as having prostate cancer with biopsy and underwent Ga-68 PSMA PET/MRI together with biparametric prostate MRI (bpMRI) were included. SUV_{max}, SUV_{mean} and ADC were recorded for index lesions drawing a region of interest (ROI) of 1 cm^2 around the pixel with the highest SUV_{max} (ROI-1) and another ROI following borders of prostate tumor detected by bpMRI (ROI-2). Presence of LN metastasis was recorded according to PSMA PET/MRI.

Results: SUV_{max} was inversely correlated with ADC (ROI-1: p=0.010; ROI-2: p=0.017 for b=800). SUV_{max} and SUV_{means} were both higher in patients with LN metastasis and ADC was lower in patients with LN metastasis for ROI-1. SUV_{max} cut-off value of 19.8 for ROI-1 and 20.9 for ROI-2 had sensitivity and specificity of 77.8% and 76.5%, respectively for detection of LN metastasis, whereas ADC (b=800) cut-off value of $0.92x10^{-3}$ mm^2/s had sensitivity and specificity of 87.5% and 76.5%, respectively. SUV_{max}/ADC (b=800) ratio increased the sensitivity and specificity to 100% and 82.4%, respectively.

Conclusion: SUV and ADC values are inversely correlated in primary prostate lesions and the combined use of both values increases the diagnostic accuracy of hybrid PET/MRI in the detection of primary prostate lesions.

Keywords: Gallium-68, prostate specific membrane antigen, positron emission tomography/magnetic resonance imaging, multiparametric prostate magnetic resonance imaging, prostate cancer, lymph node metastasis

Address for Correspondence: Lebriz Uslu-Beşli MD, Istanbul University-Cerrahpasa Faculty of Medicine, Department of Nuclear Medicine, İstanbul, Turkey
Phone: +90 212 414 30 00/22189 **E-mail:** lebriz.uslu@istanbul.edu.tr ORCID ID: orcid.org/0000-0003-1868-3957
Received: 23.04.2019 **Accepted:** 30.05.2019

Öz

Amaç: Galyum-68 (Ga-68) prostat spesifik membran antijeni (PSMA) pozitron emisyon tomografinin (PET) primer prostat lezyonunu saptamada multiparametrik prostat manyetik rezonans görüntülemeden (MRG) daha doğru olduğu gösterilmiştir. Hibrit PET/MRG kullanarak primer prostat lezyonlarında SUV_{maks} ve görünür difüzyon katsayısı (ADC) arasındaki korelasyonu tespit etmeyi ve lenf nodu (LN) metastazı tespitinde prognostik değerlerini saptamayı amaçlıyoruz.

Yöntem: Biyopsi ile prostat kanseri tanısı almış, biparametrik prostat MRG (bpMRG) ile birlikte Ga-68 PSMA PET/MRG yapılmış 26 hasta çalışmaya alındı. İndeks lezyonların SUV_{maks}, $SUV_{ortalama}$ ve ADC değerleri, hem en yüksek SUV_{maks} olan piksel etrafında 1 cm^2 çapında ilgi alanı (ROI) çizerek (ROI-1) hem de bpMRI tarafından tespit edilen prostat tümörünün sınırlarını takip eden bir başka ROI çizerek (ROI-2) kaydedildi. LN metastazı varlığı PSMA PET/MRG'ye göre belirlendi.

Bulgular: SUV_{maks} ve ADC arasında ters korelasyon saptandı (b=800 için ROI-1: p=0,010; ROI-2: p=0,017). SUV_{maks} ve $SUV_{ortalama}$ değerleri LN metastazlı hastalarda daha yüksek bulundu ve ADC değeri ROI-1 için LN metastazlı hastalarda daha düşüktü. SUV_{maks} sınır değeri ROI-1 için 19,8 ve ROI-2 için 20,9 alındığında LN metastazının saptanmasında duyarlılık ve özgüllük sırasıyla %77,8 ve %76,5 olarak bulundu. Buna karşılık ADC (b=800) sınır değeri $0,92x10^{-3}$ mm^2/s alındığında duyarlılık ve özgüllük sırasıyla %87,5 ve %76,5 olarak saptandı. SUV_{maks}/ADC (b=800) oranı, duyarlılığı ve özgüllüğü sırasıyla %100 ve %82,4'e yükseltti.

Sonuç: SUV ve ADC değerleri primer prostat lezyonlarında ters korelasyon gösterir ve her iki değerin birlikte kullanımı primer prostat lezyonlarının tespitinde hibrit PET/MRG'nin tanısal doğruluğunu arttırır.

Anahtar kelimeler: Galyum-68, prostat spesifik membran antijeni, pozitron emisyon tomografi/manyetik rezonans görüntüleme, multiparametrik prostat manyetik rezonans görüntüleme, prostat kanseri, lenf nodu metastazı

Introduction

Prostate cancer is the second most common diagnosed cancer in men and the fifth leading cause of cancer-related death worldwide (1). Death rates are lower in developed countries, due to early detection of the disease and improved treatment methods (1). Prostate specific antigen (PSA) is a glycoprotein produced by prostate cells and though not specific for prostate cancer, elevated PSA values detected by PSA screening was shown to aid in early diagnosis of prostate cancer, thus decrease prostate cancer-related death rates (2,3,4).

The screening for prostate cancer is generally made by serum PSA level measurement together with digital rectal examination (DRE). Prostate 12-core needle biopsy under transrectal ultrasonography guidance (TRUS-biopsy) is the most common method used for diagnosis of prostate cancer (5). Multiparametric prostate magnetic resonance imaging (mpMRI) has been introduced as a novel imaging approach for diagnosis and localization of primary prostate lesions (6). MpMRI guided prostate biopsy was shown to be more accurate than conventional TRUS-biopsy (7). Therefore, although mpMRI is not routinely recommended as a screening tool for detection of prostate cancer, it is recommended for patients with elevated PSA values despite negative TRUS-biopsy (8,9,10).

The most common sites for metastasis in prostate cancer are bones (84%), distant lymph nodes (LN) (10.6%), liver (10.2%) and thorax (9.1%) (11). However, magnetic resonance imaging (MRI) alone has limited value in detection of LN and distant organ metastasis.

Prostate specific membrane antigen (PSMA), which functions on cell membrane as glutamate carboxypeptidase-2 or folate hydrolase, was shown to be over-expressed in prostate cancer cells (12), which led to the introduction of Ga-68 labeled urea-based PSMA inhibitor (Ga-68-PSMA-HBED-CC) as a novel positron emission tomography (PET) tracer used for staging of patients with prostate cancer with high accuracy, for detection of LN and organ metastasis, as well as for detection of residual or recurrent local disease (13). PSMA overexpression in prostate cancer cells was shown to be associated with higher prostate cancer grade, resulting in higher incidence of metastasis and castration resistance (14). Similarly, apparent diffusion coefficient (ADC) value obtained from diffusion-weighted imaging (DWI) component of mpMRI was shown to be inversely correlated with Gleason score and was reported to provide quantitative information on tumor characteristics and aggressiveness (15). Hybrid PET/MRI systems have also been shown to be more accurate than mpMRI in terms of detecting primary prostate lesions (16,17).

The aim of our study is to detect the correlation between maximum and mean standardized uptake value (SUV_{max} and SUV_{mean}) and ADC values of primary prostate lesions and to assess the prognostic value of SUV_{max} and ADC in terms of detecting LN metastasis.

Materials and Methods

This retrospective study was approved by İstanbul University Clinical Research Ethics Committee (14/01/2019-6927) and conducted between May 2017 and April 2018. All procedures performed in this study involving human participants were in accordance with the ethical standards of the Institutional and/or National Research Committee

and with the 1964 Helsinki Declaration and its later amendments or comparable ethical standards.

Study Population

Twenty-six patients, with a mean age of 67.5±7.0 years (median age: 67.5, range: 50-83 years), who were diagnosed as having prostate cancer using TRUS-biopsy and underwent whole body Ga-68 PSMA PET/computerized tomography (PET/CT) or PET/MRI together with prostate PET/MRI including biparametric-MRI (bpMRI) sequences were included in our retrospective analysis. The patients had elevated serum PSA values (mean: 65.2±199.6 ng/mL, median: 21.4 ng/mL, range: 5.4-934 ng/mL) and they did not receive any previous treatment or did not undergo any operation related with prostate cancer or with benign prostate hyperplasia previously. Patient characteristics are given in Table 1.

Imaging

For Ga-68 PSMA PET imaging, all patients were injected Ga-68-PSMA-HBED-CC with a mean activity of 255.3±77.7 MBq (6.9±2.1 mCi), intravenously. Radiolabeling procedure was performed using a fully automated radiopharmaceutical synthesis device based on a modular concept (Eckert & Ziegler Eurotope, Berlin, Germany) as described previously by Kabasakal et al. (18).

All PET/MRI images were acquired using an integrated 3 Tesla - PET/MRI scanner (GE Signa PET/MRI, GE Healthcare, Waukesha, Wisconsin, USA). Prostate PET/MRI including bpMRI was acquired at mean 104.9±43.6 minutes post-injection including an initial localizer scan, a 3D dual-echo fast spoiled gradient recalled echo liver-accelerated volume acquisition sequence (LAVA-FLEX) for MRI based attenuation correction (MRAC), followed by a high-resolution axial T1-weighted (T1W) 3D LAVA-FLEX sequence, T2-weighted (T2W) periodically rotated overlapping parallel lines with enhanced reconstruction (PROPELLER) technique at 3-planes (axial, sagittal and coronal) and field of view optimized and constrained undistorted single shot (FOCUS) DWI (b values: 50-400-800 and 50-1400) and ADC mapping. PET emission scan was recorded together with MRI sequences and acquisition time per bed position was 3.5 min. PET attenuation correction was performed using vendor-based algorithm including MRAC data and atlas-based attenuation correction map.

A total of 10 patients had a whole-body PET/MRI at mean 87.5±20.3 minutes post-injection in the caudo-cranial direction from mid-thigh to vertex, including an initial localizer scan, 3D LAVA-FLEX for MRAC, high-resolution axial T1W 3D LAVA-FLEX sequence, coronal T2W short-tau inversion recovery (STIR), axial DWI (b values: 50-1000) and ADC mapping.

A total of 16 patients had whole-body Ga-68 PSMA PET/CT images acquired prior prostate PET/MRI using an integrated PET/CT scanner (Siemens Biograph 6, Knoxville, TN, USA or GE Discovery 710, Waukesha, WI, USA) at 71.6±14.4 minutes post-injection. An initial CT topogram was followed by a CT transmission scan and an emission PET scan in the caudo-cranial direction from mid-thigh to vertex. Imaging parameters for transmission CT scan were as follows: Low tube current (130 kVp 48-76 mAs), slice thickness of 4.0 mm, gantry rotation time of 0.6 s and collimator width of 6x3 mm. PET emission scan was acquired at 2-4 min per bed position (GE Discovery PET/CT: 2 min/bed, Siemens Biography 6 PET/CT: 4 min/bed) at caudo-cranial direction. Iterative image reconstruction method using CT transmission images were utilized for attenuation correction. All patients were asked to empty bladder before initiation of whole-body PET/CT or PET/MRI as well as prostate PET/MRI acquisition to minimize bladder activity.

Image Analysis

All whole-body PET images (PET/CT and PET/MRI) were reviewed and analyzed by two nuclear medicine physicians (LUB and SA) together and all prostate PET/MRI images including bpMRI sequences were reviewed together with a radiologist (BB) and a nuclear medicine physician (LUB) together using vendor-based work station (GE AW Volume

Table 1. Patient characteristics

Age (mean±SD)	67.9±7.0 years
Gleason scores (n)	
3+4	12
4+3	5
4+4	5
4+5	2
5+4	1
5+5	1
Mean serum PSA value (mean±SD)	65.2±199.6 ng/mL
Presence of lymph node metastasis (n)	9
Presence of bone metastasis (n)	3
Presence of visceral organ metastasis (n)	0
Whole body PET/CT (n)	16
Whole body PET/MRI (n)	10
Mean Ga-68 PSMA activity (mean±SD)	255.3±77.7 MBq (6.9±2.1 mCi)

SD: Standard deviation, PSA: Prostate specific antigen, PET/CT: Positron emission tomography/computed tomography, MRI: Magnetic resonance imaging, PSMA: Prostate specific membrane antigen, Ga-68: Gallium-68

Share 7, GE Medical Systems, Buc, France). Localization and extension of the primary tumor in the prostate gland was recorded on a prostate scheme for both PET and MRI data separately. SUV_{max} and mean ADC (ADC) were measured drawing region of interest (ROI) 1 cm^2 around the pixel with the highest SUVmax in the prostate tumor (ROI-1) and another ROI following the borders of prostate tumor (ROI-2) detected by bpMRI. Whole-body PET images were used to detect presence of LN and organ metastasis.

Statistical Analysis

Statistical analysis was performed using SPSS software version 21.0 (IBM Corp., Armonk, New York, USA) and the level of significance was taken as p value less than 0.05. Pearson correlation analysis was performed to observe the relationship between SUV and ADC values. Mann-Whitney U test was performed to analyze the relationship between LN metastasis status and SUV and ADC values. Receiver operating characteristic (ROC) curve analysis was calculated to assess the ability to discriminate the LN metastasis status based on SUV and ADC values.

Results

SUV_{max}, SUV_{mean} and ADC values (for both b=1400 and b=800) obtained from ROI-1 and ROI-2 of the prostate lesion were given in Table 2.

For both ROI-1 and ROI-2, SUV_{max} value was inversely correlated with both ADC (b=1400) value (ROI-1: p=0.026, r=-0.444; ROI-2: p=0.032, r=-0.429) and ADC (b=800) value (ROI-1: p=0.010, r=-0.506; ROI-2: p=0.017, r=-0.473) (Table 3). Also, SUV_{mean} value was inversely correlated with both ADC (b=1400) value (ROI-1: p=0.013, r=-0.488; ROI-2: p=0.018, r=-0.468) and ADC (b=800) value (ROI-1: p=0.004, r=-0.553; ROI-2: p=0.009, r=-0.508) for both ROI-1 and ROI-2 (Figure 1A, 1B).

SUV_{max} and SUV_{mean} were significantly higher in patients with LN metastasis for both ROI-1 and ROI-2 (ROI-1: p=0.01 and p=0.01; ROI-2: p=0.02 and p=0.01, respectively) (Table 4) (Figures 2, 3). Although ADC values were significantly lower in patients with LN metastasis for ROI-1 (p=0.04 for b=1400 and p=0.02 for b=800), there was no significant difference in terms of ADC values in patients with LN metastasis for ROI-2. The ratios of SUV_{max}/ADC and

Table 2. Mean maximum and mean standardized uptake values and apparent diffusion coefficient values of prostate lesions obtained from drawing 2 different region of interests

ROI-1	**Mean±SD**	**Range**
SUV_{max}	23.3±25.5	2.9-122.5
SUV_{mean}	16.7±16.1	2.3-71.7
ADC (b=1400) (x 10^{-3} mm^2/s)	0.87±0.19	0.41-1.39
ADC (b=800) (x 10^{-3} mm^2/s)	0.97±0.21	0.56-1.39
ROI-2		
SUV_{max}	21.2±22.9	2.7-117.9
SUV_{mean}	14.5±14.1	2.0-70.4
ADC (b=1400) (x 10^{-3} mm^2/s)	0.78±0.16	0.42-1.19
ADC (b=800) (x10^{-3} mm^2/s)	0.98±0.22	0.55-1.53

ROI: Region of interest, ADC: Apparent diffusion coefficient, SD: Standard deviation

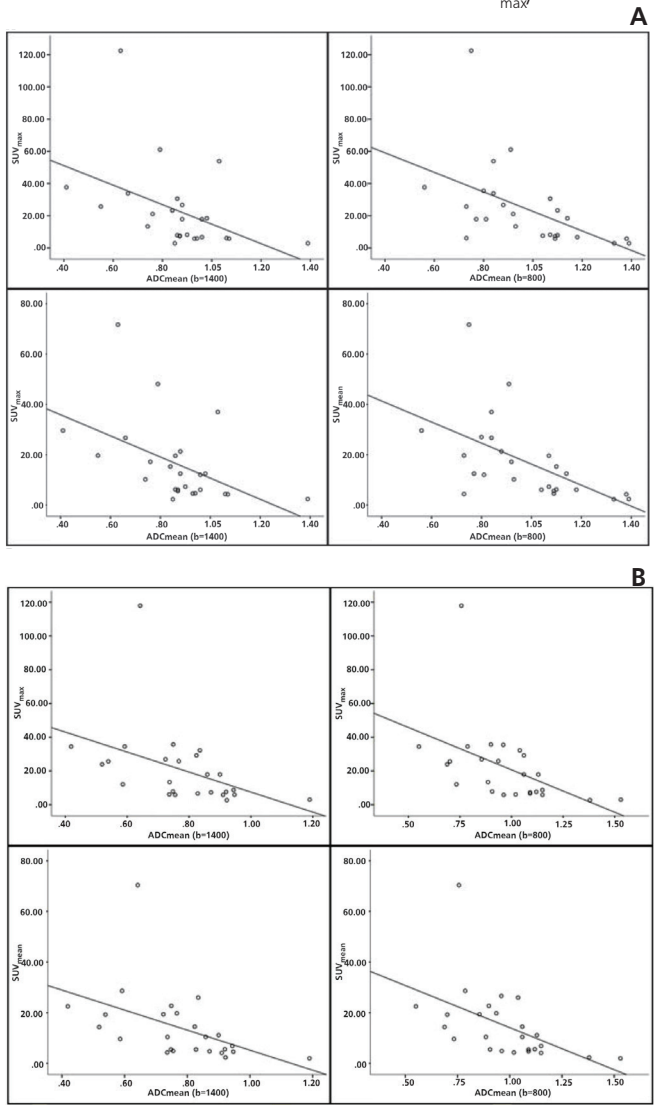

Figure 1. Both SUV_{max} and SUV_{mean} values were found to be inversely correlated with ADC values (both for b=1400 and b=800) for ROI-1 (A) and ROI-2 (B)

SUV_{max}: Maximum standardized uptake value, SUV_{mean}: Mean standardized uptake value, ADC_{mean}: Mean apparent diffusion coefficient value, ROI: Region of interest

SUV_{mean}/ADC for both b values (b=1400 and b=800) were significantly higher in patients with LN metastasis for both ROI-1 and ROI-2 (Table 4).

ROC analysis revealed that SUV_{max} cut-off level of 19.8 for ROI-1 and 20.9 for ROI-2 predicted the presence of LN metastasis with sensitivity of 77.8% and specificity of 76.5% (Table 5). For SUV_{mean}, cut-off level of 16.3 for ROI-1 and 10.8 for ROI-2 had sensitivity of 77.8% and 88.9% and specificity of 82.4% and 76.5%, respectively. For ADC (b=800) and ADC (b=1400) cut-off levels of $0.92x10^{-3}$ mm^2/s and $0.82x10^{-3}$ mm^2/s had sensitivities of 87.5% and 50% and specificities of 76.5% and 82.4%, respectively in prediction of LN metastasis. When SUV/ADC ratios were taken for both SUV_{max} and SUV_{mean} values as well as for both ADC values; sensitivity and specificity increased to 100% and 82.4%, respectively for ROI-1 and to 87.5% and 82.4%, respectively for ROI-2 (Table 5).

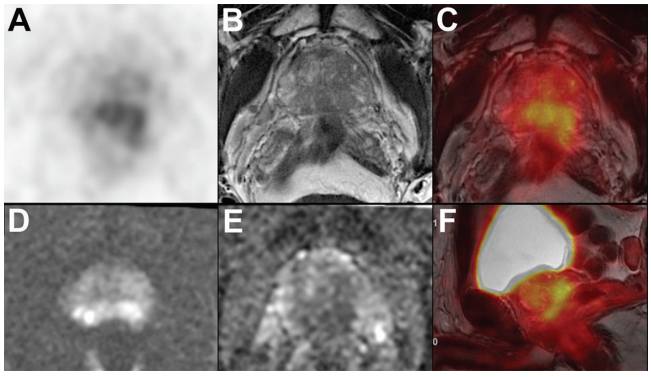

Figure 2. Sixty-nine-year-old patient with Gleason score 4+3 prostate cancer detected by prostate 12-core needle biopsy under transrectal ultrasonography guidance. His serum prostate specific antigen level was 27.0 ng/mL at the time of diagnosis. Axial Ga-68 prostate specific membrane antigen (PSMA) positron emission tomography (PET) (A), axial T2-weighted magnetic resonance imaging (MRI) (B), fused PET/MRI (C), FOCUS diffusion weighted imaging for b=1400 s/mm^2 (D), apparent diffusion coefficient (ADC) map for b=800 s/mm^2 (E) and sagittal fused PET/MRI (F) images exhibited PSMA-positive tumor located at bilateral peripheral zone of the prostate gland (SUV_{max}: 6.7, SUV_{mean}: 6.1, ADC: 1.18 s/mm^2 for region of interest (ROI)-1 and SUV_{max}: 6.6, SUV_{mean}: 5.5, ADC: 1.09 s/mm^2 for ROI-2). The patient did not have any lymph node or organ metastasis according to the PSMA PET images

Table 3. Correlation analysis between maximum and mean standardized uptake value and apparent diffusion coefficient

ROI-1	**p**	**r**
SUV_{max} - ADC (b=1400)	0.026	-0.444
SUV_{max} - ADC (b=800)	0.010	-0.506
SUV_{mean} - ADC (b=1400)	0.013	-0.488
SUV_{mean} - ADC (b=800)	0.004	-0.553
ROI-2		
SUV_{max} - ADC (b=1400)	0.032	-0.429
SUV_{max} - ADC (b=800)	0.017	-0.473
SUV_{mean} - ADC (b=1400)	0.018	-0.468
SUV_{mean} - ADC (b=800)	0.009	-0.508

ROI: Region of interest, ADC: Apparent diffusion coefficient

Discussion

MpMRI has been introduced as a novel imaging approach for diagnosis, localization and characterization of primary prostate lesions and has been shown to have a good sensitivity for detecting clinically significant prostate cancer and guiding prostate biopsy (19,20). However, despite its several advantages, mpMRI has also some limitations, including poor detection of low-grade disease, low inter-observer agreement, poor quality images within six weeks after TRUS-biopsy due to residual hemorrhage and inflammation, limited patient cooperation, especially in

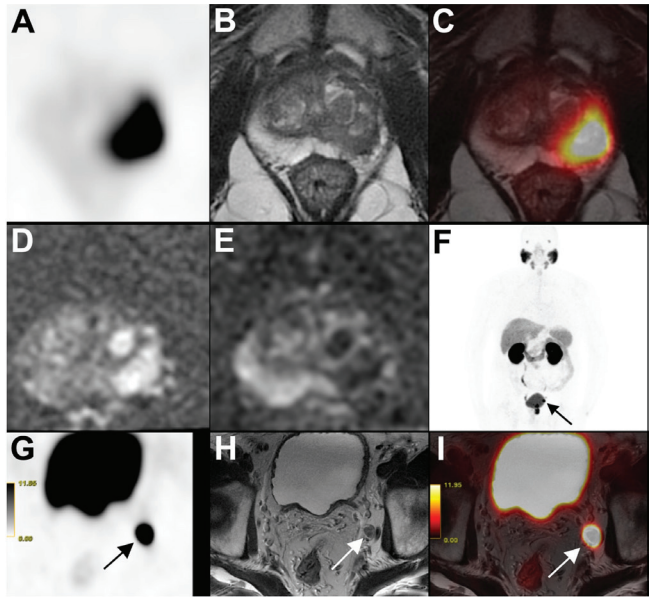

Figure 3. Eighty-three-year-old patient with Gleason score 4+4 prostate cancer detected by prostate 12-core needle biopsy with serum prostate specific antigen level of 5.8 ng/mL at the time of diagnosis. Axial Ga-68 prostate specific membrane antigen (PSMA) positron emission tomography (PET) (A), axial T2-weighted (T2W) magnetic resonance imaging (MRI) (B), fused PET/MRI (C), FOCUS diffusion weighted imaging for b=1400 s/mm^2 (D) and apparent diffusion coefficient (ADC) map for b=800 s/mm^2 (E) images showed intense PSMA uptake at the prostate tumor located at left peripheral zone (SUV_{max}: 53.9, SUV_{mean}: 37.0, ADC: 0.84 s/mm^2 for region of interest (ROI)-1 and SUV_{max}: 32.2, SUV_{mean}: 26.0, ADC: 1.04 s/mm^2 for ROI-2). Metastatic pelvic lymph node with intense PSMA uptake can be seen on maximum intensity projection (F) image, axial PSMA PET (G), axial T2W MRI (H) and fused PET/MRI (I) images (arrows)

claustrophobic patients and lower sensitivity in transitional zone tumors (19,21). Ga-68 PSMA PET/CT and PET/MRI, on the other hand were shown to have better sensitivity and higher diagnostic accuracy than mpMRI in the detection of primary prostate cancer, both in index lesions and in cases of multifocal disease (17,22,23,24).

Ga-68 PSMA uptake was shown to be correlated with tumor Gleason score, serum PSA levels, PI-RADS category and DRE findings (25). ADC value obtained by mpMRI was also found to be correlated with Gleason scores (26,27), serum PSA levels (28), molecular markers (29) and was introduced to be a promising tool to monitor therapy

Table 4. Comparison of standardized uptake value parameters and apparent diffusion coefficient values according to presence of lymph node metastasis

	Lymph node metastasis (+)		Lymph node metastasis (-)		p
ROI-1	**Mean±SD**	**Median (range)**	**Mean±SD**	**Median (range)**	
SUV_{max}	42.1±34.7	33.9 (5.9-122.5)	13.4±10.4	7.9 (2.9-37.7)	**0.01**
SUV_{mean}	29.6±20.4	26.7 (4.7-71.7)	9.9±7.5	6.2 (2.3-29.6)	**0.01**
ADC (b=1400) ($x10^{-3}$ mm^2/s)	0.82±0.14	0.84 (0.63-1.03)	0.89±0.21	0.87 (0.41-1.39)	**0.04**
ADC (b=800) ($x10^{-3}$ mm^2/s)	0.84±0.06	0.84 (0.75-0.92)	1.04±0.23	1.10 (0.56-1.39)	**0.02**
SUV_{max}/ADC (b=1400)	57.5±59.6	40.9 (6.3-194.4)	19.0±22.4	9.1 (2.1-92.0)	**0.01**
SUV_{max}/ADC (b=800)	57.0±46.1	42.4 (22.9-163.3)	15.4±16.5	7.7 (2.1-67.3)	**0.01**
SUV_{mean}/ADC (b=1400)	39.6±34.5	30.1 (5.0-113.8)	14.2±17.3	7.2 (1.7-72.2)	**0.01**
SUV_{mean}/ADC (b=800)	39.6±25.8	32.8 (16.2-95.6)	11.4±12.6	6.0 (1.7-52.9)	**0.01**
ROI-2					
SUV_{max}	35.6±32.2	26.9 (5.9-117.9)	13.5±11.0	7.8 (2.7-35.7)	**0.02**
SUV_{mean}	24.5±18.9	19.8 (4.6-70.4)	9.1±6.7	5.6 (2.0-22.7)	**0.01**
ADC (b=1400) ($x10^{-3}$ mm^2/s)	0.74±0.15	0.75 (0.52-0.95)	0.80±0.18	0.82 (0.42-1.19)	0.49
ADC (b=800) ($x10^{-3}$ mm^2/s)	0.89±0.15	0.90 (0.69-1.13)	1.01±0.24	1.06 (0.55-1.53)	0.15
SUV_{max}/ADC (b=1400)	53.0±55.1	37.9 (6.2-183.6)	20.3±21.4	9.2 (2.5-82.2)	**0.01**
SUV_{max}/ADC (b=800)	47.2±44.6	33.1 (15.8-155.8)	16.0±16.6	7.6 (2.0-62.5)	**0.01**
SUV_{mean}/ADC (b=1400)	35.8±32.5	27.2 (4.9-109.6)	13.8±13.9	7.2 (1.7-53.7)	**0.02**
SUV_{mean}/ADC (b=800)	32.1±25.7	23.8 (9.9-93.0)	10.8±10.8	5.9 (1.3-40.9)	**0.01**

ROI: Region of interest, SD: Standard deviation, ADC: Apparent diffusion coefficient

Table 5. Sensitivity of specificity of different standardized uptake value parameters and apparent diffusion coefficient values in terms of prediction of lymph node metastasis

ROI-1	**Cut-off level**	**Sensitivity**	**Specificity**
SUV_{max}	19.8	77.8%	76.5%
SUV_{mean}	16.3	77.8%	82.4%
ADC (b=1400) ($x10^{-3}$ mm^2/s)	0.82	50%	82.4%
ADC (b=800) ($x10^{-3}$ mm^2/s)	0.92	87.5%	76.5%
SUV_{max}/ADC (b=800)	22.5	100%	82.4%
SUV_{mean}/ADC (b=800)	15.5	100%	82.4%
ROI-2			
SUV_{max}	20.9	77.8%	76.5%
SUV_{mean}	10.8	88.9%	76.5%
SUV_{max}/ADC (b=800)	27.6	87.5%	82.4%
SUV_{mean}/ADC (b=800)	17.2	87.5%	82.4%

ROI: Region of interest, ADC: Apparent diffusion coefficient

response (30,31). To our knowledge, PSMA uptake and ADC values were not compared before using hybrid PET/MRI or PET/CT systems. However, an inverse correlation between PSMA uptake and ADC values in primary prostate tumor is an expected finding according to the current literature.

Hybrid PET/MRI systems provide better anatomical delineation of prostate gland compared to hybrid PET/CT systems due to better soft-tissue resolution of the MRI component, and enable one-stop-shop imaging for prostate cancer patients, including Ga-68 PSMA PET and mpMRI in a single session. Therefore, PET/MRI has more potential to aside misdiagnosis due to physiological or false-positive PSMA uptake in the prostate gland (32,33). Also, simultaneous acquisition of PET and MRI images could provide additional advantages, which are not provided by PET/CT systems. However, to date, there are still limited number of studies on Ga-68 PSMA PET/MRI in evaluation of primary prostate tumor and in its diagnostic accuracy compared to PET/CT or mpMRI.

We found higher SUV_{max} and SUV_{mean} values and lower ADC values in patients with LN metastasis, which may be due to the presence of more aggressive tumor with higher Gleason scores, that were documented to have both higher PSMA uptake and lower ADC values in the literature (26,27,34). Concomitant usage of SUV and ADC parameters by using the ratio of SUV/ADC further increased the sensitivity and specificity of PET/MRI imaging in predicting LN metastasis.

Study Limitations

The main limitation in our study was the lack of post-operative histopathological result in our cohort and the small sample size. Therefore, we could not compare PSMA uptake with Gleason scores and we had to evaluate the status of LN metastasis only by Ga-68 PSMA PET imaging.

Conclusion

SUV and ADC values are inversely correlated in primary prostate lesions and the combined use of both values increases the diagnostic accuracy of hybrid PET/MRI in the detection of primary prostate lesions. SUV_{max}, SUV_{mean} and ADC detected by Ga-68 PSMA PET/MRI are future promising new prognostic values for detecting LN metastasis in prostate cancer patients.

Ethics

Ethics Committee Approval: This retrospective study was approved by İstanbul University Clinical Research Ethics Committee (14/01/2019-6927).

Informed Consent: Retrospective study.

Peer-review: Externally peer-reviewed.

Authorship Contributions

Surgical and Medical Practices: L.U.B., B.B., E.G.., Ç.D., E.K., Concept: L.U.B., B.B., H.B.S., K.S., Design: L.U.B., B.B., Data Collection or Processing: L.U.B., S.A., E.G., O.E.Ş., Analysis or Interpretation: L.U.B., B.B., S.S., H.B.S., K.S., Literature Search: L.U.B., M.S.S., Writing: L.U.B., B.B., S.A., O.E.Ş., S.S.

Conflict of Interest: No conflict of interest was declared by the authors.

Financial Disclosure: The authors declared that this study received no financial support.

References

1. Torre LA, Bray F, Siegel RL, Ferlay J, Lortet-Tieulent J, Jemal A. Globan cancer statistics, 2012. CA Cancer J Clin 2015;65:87-108.
2. Schröder FH, Hugosson J, Roobol MJ, Tammela TL, Ciatto S, Nelen V, Kwiatkowski M, Lujan M, Lilja H, Zappa M, Denis LJ, Recker F, Páez A, Määttänen L, Bangma CH, Aus G, Carlsson S, Villers A, Rebillard X, van der Kwast T, Kujala PM, Blijenberg BG, Stenman UH, Huber A, Taari K, Hakama M, Moss SM, de Koning HJ, Auvinen A; ERSPC Investigators. Prostate-Cancer Mortality at 11 Years of Follow-up. N Engl J Med 2012;366:981-990.
3. Schröder FH, Hugosson J, Roobol MJ, Tammela TL, Zappa M, Nelen V, Kwiatkowski M, Lujan M, Määttänen L, Lilja H, Denis LJ, Recker F, Paez A, Bangma CH, Carlsson S, Puliti D, Villers A, Rebillard X, Hakama M, Stenman UH, Kujala P, Taari K, Aus G, Huber A, van der Kwast TH, van Schaik RH, de Koning HJ, Moss SM, Auvinen A; ERSPC Investigators. Screening and prostate cancer mortality: Results of the European Randomised Study of Screening for Prostate Cancer (ERSPC) at 13 years of follow-up. Lancet 2014;384:2027-2035.
4. Tsodikov A, Gulati R, Etzioni R. Reconciling the effects of screening on prostate cancer mortality in the ERSPC and PLCO trials. Ann Intern Med 2018;168:608-609.
5. Cuzick J, Thorat MA, Andriole G, Brawley OW, Brown PH, Culig Z, Eeles RA, Ford LG, Hamdy FC, Holmberg L, Ilic D, Key TJ, La Vecchia C, Lilja H, Marberger M, Meyskens FL, Minasian LM, Parker C, Parnes HL, Perner S, Rittenhouse H, Schalken J, Schmid HP, Schmitz-Dräger BJ, Schröder FH, Stenzl A, Tombal B, Wilt TJ, Wolk A. Prevention and early detection of prostate cancer. Lancet Oncol 2014;15:484-492.
6. Marberger M, Barentsz J, Emberton M, Hugosson J, Loeb S, Klotz L, Koch M, Shariat SF, Vickers A. Novel approaches to improve prostate cancer diagnosis and management in early-stage disease. BJU Int 2012;109(Suppl 2):1-7.
7. Sonn GA, Natarajan S, Margolis DJ, MacAiran M, Lieu P, Huang J, Dorey FJ, Marks LS. Targeted Biopsy in the Detection of Prostate Cancer Using an Office Based Magnetic Resonance Ultrasound Fusion Device. J Urol 2013;189:86-91.
8. Carroll PR, Parsons JK, Andriole G, Bahnson RR, Barocas DA, Castle EP, Catalona WJ, Dahl DM, Davis JW, Epstein JI, Etzioni RB, Farrington T, Hemstreet GP 3rd, Kawachi MH, Lange PH, Loughlin KR, Lowrance W, Maroni P, Mohler J, Morgan TM, Nadler RB, Poch M, Scales C, Shaneyfelt TM, Smaldone MC, Sonn G, Sprenke P, Vickers AJ, Wake R, Shead DA, Freedman-Cass D. NCCN Clinical Practice Guidelines Prostate Cancer Early Detection, Version 2.2015. J Natl Compr Canc Netw 2015;13:1534-1561.
9. Heidenreich A, Bastian PJ, Bellmunt J, Bolla M, Joniau S, van der Kwast T, Mason M, Matveev V, Wiegel T, Zattoni F, Mottet N; European

Association of Urology. EAU guidelines on prostate cancer. part 1: screening, diagnosis, and local treatment with curative intent-update 2013. Eur Urol 2014;65:124-137.

10. Rosenkrantz AB, Verma S, Choyke P, Eberhardt SC, Eggener SE, Gaitonde K, Haider MA, Margolis DJ, Marks LS, Pinto P, Sonn GA, Taneja SS. Prostate Magnetic Resonance Imaging and Magnetic Resonance Imaging Targeted Biopsy in Patients with a Prior Negative Biopsy: A Consensus Statement by AUA and SAR. J Urol 2016;196:1613-1618.
11. Gandaglia G, Abdollah F, Schiffmann J, Trudeau V, Shariat SF, Kim SP, Perrotte P, Montorsi F, Briganti A, Trinh QD, Karakiewicz PI, Sun M. Distribution of metastatic sites in patients with prostate cancer: A population-based analysis. Prostate 2014;74:210-216.
12. Barinka C, Rojas C, Slusher B, Pomper M. Glutamate Carboxypeptidase II in Diagnosis and Treatment of Neurologic Disorders and Prostate Cancer. Curr Med Chem 2012;19:856-870.
13. Li Q, Xiang P, Lin X, Grajo JR, Yang L, Xu Y, Duan Y, Vyas U, Harisinghani M, Mahmood U, Samir AE. The Role of Imaging in Prostate Cancer Care Pathway: Novel Approaches to Urologic Management Challenges Along 10 Imaging Touch Points. Urology 2018;119:23-31.
14. Bravaccini S, Puccetti M, Bocchini M, Ravaioli S, Celli M, Scarpi E, De Giorgi U, Tumedei MM, Raulli G, Cardinale L, Paganelli G. PSMA expression: A potential ally for the pathologist in prostate cancer diagnosis. Sci Rep 2018;8:4254.
15. Park SY, Kim CK, Park BK, Lee HM, Lee KS. Prediction of biochemical recurrence following radical prostatectomy in men with prostate cancer by diffusion-weighted magnetic resonance imaging: Initial results. Eur Radiol 2011;21:1111-1118.
16. Eiber M, Weirich G, Holzapfel K, Souvatzoglou M, Haller B, Rauscher I, Beer AJ, Wester HJ, Gschwend J, Schwaiger M, Maurer T. Simultaneous 68Ga-PSMA HBED-CC PET/MRI Improves the Localization of Primary Prostate Cancer. Eur Urol 2016;70:829-836.
17. Hicks RM, Simko JP, Westphalen AC, Nguyen HG, Greene KL, Zhang L, Carroll PR, Hope TA. Diagnostic Accuracy of 68 Ga-PSMA-11 PET/MRI Compared with Multiparametric MRI in the Detection of Prostate Cancer. Radiology 2018;289:730-737.
18. Kabasakal L, Demirci E, Ocak M, Akyel R, Nematyazar J, Aygun A, Halac M, Talat Z, Araman A. Evaluation of PSMA PET/CT imaging using a 68Ga-HBED-CC ligand in patients with prostate cancer and the value of early pelvic imaging. Nucl Med Commun 2015;36:582-587.
19. Greer MD, Choyke PL, Turkbey B. PI-RADSv2: How we do it. J Magn Reson Imaging 2017;46:11-23.
20. Kasivisvanathan V, Rannikko AS, Borghi M, Panebianco V, Mynderse LA, Vaarala MH, Briganti A, Budäus L, Hellawell G, Hindley RG, Roobol MJ, Eggener S, Ghei M, Villers A, Bladou F, Villeirs GM, Virdi J, Boxler S, Robert G, Singh PB, Venderink W, Hadaschik BA, Ruffion A, Hu JC, Margolis D, Crouzet S, Klotz L, Taneja SS, Pinto P, Gill I, Allen C, Giganti F, Freeman A, Morris S, Punwani S, Williams NR, Brew-Graves C, Deeks J, Takwoingi Y, Emberton M, Moore CM; PRECISION Study Group Collaborators. MRI-Targeted or Standard Biopsy for Prostate-Cancer Diagnosis. N Engl J Med 2018;378:1767-1777.
21. Wang X, Bao J, Ping X, Hu C, Hou J, Dong F, Guo L. The diagnostic value of PI-RADS V1 and V2 using multiparametric MRI in transition zone prostate clinical cancer. Oncol Lett 2018;16:3201-3206.
22. Berger I, Annabattula C, Lewis J, Shetty DV, Kam J, Maclean F, Arianayagam M, Canagasingham B, Ferguson R, Khadra M, Ko R, Winter M, Loh H, Varol C. 68Ga-PSMA PET/CT vs. mpMRI for locoregional prostate cancer staging: correlation with final histopathology. Prostate Cancer Prostatic Dis 2018;21:204-211.
23. Donato P, Roberts MJ, Morton A, Kyle S, Coughlin G, Esler R, Dunglison N, Gardiner RA, Yaxley J. Improved specificity with 68Ga PSMA PET/CT to detect clinically significant lesions "invisible" on multiparametric MRI of the prostate: a single institution comparative analysis with radical prostatectomy histology. Eur J Nucl Med Mol Imaging 2019;46:20-30.
24. Al-Bayati M, Grueneisen J, Lütje S, Sawicki LM, Suntharalingam S, Tschirdewahn S, Forsting M, Rübben H, Herrmann K, Umutlu L, Wetter A. Integrated 68Gallium Labelled Prostate-Specific Membrane Antigen-11 Positron Emission Tomography/Magnetic Resonance Imaging Enhances Discriminatory Power of Multi-Parametric Prostate Magnetic Resonance Imaging. Urol Int 2018;100:164-171.
25. Jena A, Taneja R, Taneja S, Singh A, Kumar V, Agarwal A, Subramanian N. Improving diagnosis of primary prostate cancer with combined 68Ga-prostate-specific membrane antigen-HBED-CC simultaneous PET and multiparametric MRI and clinical parameters. AJR Am J Roentgenol 2018;211:1246-1253.
26. Jyoti R, Jain TP, Haxhimolla H, Liddell H, Barrett SE. Correlation of apparent diffusion coefficient ratio on 3.0 T MRI with prostate cancer Gleason score. Eur J Radiol Open 2018;5:58-63.
27. Sokmen BK, Sokmen D, Ucar N, Ozkurt H, Simsek A. The correlation between biological activity and diffusion-weighted MR imaging and ADC value in cases with prostate cancer. Arch Ital Urol Androl 2017;89:277-281.
28. Iraha Y, Murayama S, Kamiya A, Iraha S, Ogawa K. Diffusion-weighted MRI and PSA correlations in patients with prostate cancer treated with radiation and hormonal therapy. Anticancer Res 2012;32:4467-4471.
29. Ma T, Yang S, Jing H, Cong L, Cao Z, Liu Z, Huang Z. Apparent diffusion coefficients in prostate cancer: correlation with molecular markers Ki-67, HIF-1α and VEGF. NMR Biomed 2018:31.
30. Kim AY, Kim CK, Park SY, Park BK. Diffusion-Weighted Imaging to Evaluate for Changes From Androgen Deprivation Therapy in Prostate Cancer. Am J Roentgenol 2014;203:645-650.
31. Qi WX, Zhang Q, Li P, Zhang XM, Zhang GY, Wu B, Lu JJ, Jiang GL, Fu S. The predictive role of ADC values in prostate cancer patients treated with carbon-ion radiotherapy: initial clinical experience at Shanghai Proton and Heavy Ion Center (SPHIC). J Cancer Res Clin Oncol 2016;142:1361-1367.
32. Ferraro DA, Rupp NJ, Donati OF, Messerli M, Eberli D, Burger IA. 68Ga-PSMA-11 PET/MR Can Be False Positive in Normal Prostatic Tissue. Clin Nucl Med 2019;44:291-293.
33. Pizzuto DA, Müller J, Mühlematter U, Rupp NJ, Töpfer A, Mortezavi A, Nagel H, Kranzbühler B, Eberli D, Burger IA. The central zone has increased 68Ga-PSMA-11 uptake: "Mickey Mouse ears" can be hot on 68Ga-PSMA-11 PET. Eur J Nucl Med Mol Imaging 2018;45:1335-1343.
34. Jena A, Taneja R, Taneja S, Singh A, Kumar V, Agarwal A, Subramanian N. Improving Diagnosis of Primary Prostate Cancer With Combined 68 Ga-Prostate-Specific Membrane Antigen–HBED-CC Simultaneous PET and Multiparametric MRI and Clinical Parameters. AJR Am J Roentgenol 2018;211:1246-1253.

Original Article
Mol Imaging Radionucl Ther 2019;28:112-119 DOI:10.4274/mirt.galenos.2019.65707

Solitary Pulmonary Nodule: Morphological Effects on Metabolic Activity Assessment

Soliter Pulmoner Nodül: Metabolik Aktivite Değerlendirmesinde Morfolojik Etkiler

Mehmet Erdoğan[1], Şehnaz Evrimler[2], Hüseyin Aydın[2], Adnan Karaibrahimoğlu[3], Sevim Süreyya Şengül[1]
[1]*Süleyman Demirel University Faculty of Medicine, Department of Nuclear Medicine, Isparta, Turkey*
[2]*Süleyman Demirel University Faculty of Medicine, Department of Radiology, Isparta, Turkey*
[3]*Süleyman Demirel University Faculty of Medicine, Department of Biostatistics and Medical Informatics, Isparta, Turkey*

Abstract

Objectives: We aimed to evaluate the effects of morphological characteristics of the solitary pulmonary nodules (SPN) on metabolic activity assessment. To the best of our knowledge, this is the first study to compare the volumetric metabolic activity parameters according to the morphologic parameters of the nodules.

Methods: In this retrospective study, ^{18}F-FDG positron emission tomography and computed tomography scans performed between 2011 and 2018 were evaluated by a nuclear and diagnostic radiologist. One hundred thirteen patients with SPNs with biopsy-proven diagnosis were included. SPNs were classified as solid, partially solid (PS), and ground glass opacity (GGO).

Results: SPN diameter, SUV_{max}, metabolic tumor volume (MTV), total lesion glycolysis (TLG), and density were significantly higher in the malignant group. SUV_{max}, MTV, TLG increased in direct proportion to the diameter. There was no a significant difference between GGO, PS, and solid nodules in terms of SUV_{max} values. MTV and TLG values increased in parallel with the density of the nodules, but this increase was only significant in the malignant group. There was a significant difference between SPNs <2 cm and SPNs ≥2 cm in terms of MTV, while there was no difference in terms of SUV_{max}. The cut-off value determined by the ROC curve was found to be 4.39 for SUV_{max}, 7.33 mL for MTV and 31.88 g for TLG. The cut-off values for SUV_{max} of solid and subsolid nodules were close to each other, but cut-off values for MTV and TLG were higher in solid nodules.

Conclusion: SUV_{max}, MTV, and TLG are affected by diameter and attenuation. We suggest using different MTV and TLG cut-off values for solid and subsolid nodules, but we suggest using same SUV_{max} values. MTV can be a more reliable parameter than SUV_{max} in prediction of malignancy in smaller nodules.

Keywords: Positron emission tomography, solitary pulmonary nodule, metabolic tumor volume, total lesion glycolysis

Öz

Amaç: Soliter pulmoner nodüllerin (SPN) morfolojik özelliklerinin metabolik aktivite değerlendirmesi üzerindeki etkilerini değerlendirmeyi amaçladık. Bildiğimiz kadarıyla, volümetrik metabolik aktivite parametrelerini nodüllerin morfolojik parametrelerine göre karşılaştıran ilk çalışma budur.

Yöntem: 2011 ve 2018 yılları arasında yapılan ^{18}F-FDG pozitron emisyon tomografisi ve bilgisayarlı tomografi taramaları, bir nükleer tıp uzmanı ve radyoloji uzmanı tarafından retrospektif olarak değerlendirildi. Biyopsi ile kanıtlanmış tanısı olan 113 SPN hastası dahil edildi. SPN'ler solid, kısmi solid (PS) ve buzlu cam opasitesi (GGO) olarak sınıflandırıldı.

Bulgular: SPN çapı, SUV_{maks}, metabolik tümör hacmi (MTV), toplam lezyon glikoliz (TLG) ve dansite malign grupta anlamlı olarak yüksek bulundu. SUV_{maks}, MTV ve TLG değerleri çap ile doğru orantılı olarak arttı. GGO, PS ve solid nodüller arasında SUV_{maks} değerleri arasında anlamlı bir fark yoktu. MTV, TLG değerleri nodüllerin yoğunluğu ile paralel olarak arttı; ancak sadece malign grupta anlamlı fark bulundu. 2 cm'den küçük grupta MTV için anlamlı fark varken SUV_{maks} için yoktu. ROC eğrisi ile belirlenen kesme değerinin SUV_{maks} için 4,39, MTV için 7,33 mL, TLG için 31,88 g olduğu bulundu. Solid ve subsolid nodüllerin SUV_{maks} için cut-off değeri birbirine yakındı, ancak MTV, TLG için cut-off değer solid nodüllerde daha yüksekti.

Address for Correspondence: Mehmet Erdoğan MD, Süleyman Demirel University Faculty of Medicine, Department of Nuclear Medicine, Isparta, Turkey
Phone: +90 530 925 75 30 **E-mail:** mdr_erdogan@yahoo.com ORCID ID: orcid.org/0000-0001-7724-778X
Received: 17.05.2019 **Accepted:** 05.08.2019

Sonuç: SUV_{maks}, MTV ve TLG çap ve atenüasyondan etkilenmektedir. Solid ve subsolid nodüller için farklı MTV ve TLG cut-off değerlerinin kullanılmasının gerektiğini; ancak SUV_{maks} için gerekli olmadığını düşünmekteyiz. MTV, küçük nodüller için malignite tahmininde SUV_{maks}'tan daha güvenilir bir parametre olabilir.

Anahtar kelimeler: Pozitron emisyon tomografi, soliter pulmoner nodül, metabolik tümör volümü, total lezyon glikolizis

Introduction

A solitary pulmonary nodule (SPN) is a well-defined, round or oval lesion with a diameter less than 3 cm, surrounded by normal parenchyma, not associated with atelectasis, lymphadenopathy, pneumonia and pleural effusion (1,2). SPNs are detected in 0.9-2% of chest X-rays and 90% of them are seen incidentally (3). Multidetector computed tomography (MDCT) allows detection of nodules with smaller sizes, even with diameter of 1-5 mm, which results in increase in detection rates of SPNs ranging between 8-51% (4,5). SPNs are classified as solid and subsolid nodules. Subsolid nodules can be either pure ground glass opacity (GGO) or semisolid (SS). The etiology of SPNs can be benign or malignant. If MDCT and follow-up imaging findings are indeterminate, ^{18}F-FDG positron emission tomography (PET)/CT or biopsy is needed for precise diagnosis (6,7). ^{18}F-FDG PET/CT is a non-invasive technique that demonstrates the amount of glucose metabolism used by metabolically active cells, gives morphological information and provides differentiation between malignant and benign lesions (8). A standardized uptake value (SUV) is a semiquantitative method for evaluation of ^{18}F-FDG uptake besides qualitative interpretation with the PET scans. The maximum SUV (SUV_{max}) >2.5 is accepted as a threshold value for malignant lesions, although there can be some variations in the literature (8,9,10,11). On the other hand, ^{18}F-FDG avidity can also be observed in benign conditions such as inflammation, infection; or malignant diseases can be less avid secondary to volumetric effects such as nodule size (12,13,14,15,16,17,18,19). Kim et al. (20) has mentioned that, SUV_{max} values of half of the bronchoalveolar carcinoma and carcinoid tumors, which constitute 2% of all lung cancers, cause false negative PET results.

Metabolic activity of the lesions can be measured with volumetric parameters, metabolic tumor volume (MTV) and total lesion glycolysis (TLG). The MTV is a volumetric measurement of tumor cells measured by semi-automatic delineation tools using a specific threshold of SUV. TLG is defined as the product of the mean SUV and the MTV. SUV_{mean} is the mean value of SUV in a chosen region (21).

The aim of this study was to evaluate morphological and metabolic activity parameters for SPNs and the effects of morphological characteristics of the nodule on metabolic activity assessment. To the best of our knowledge, this is the first study to compare the volumetric metabolic activity parameters according to the morphologic parameters of the nodules.

Materials and Methods

^{18}F-FDG PET/CT scans were performed in a Lutetium-Yttrium Oxyorthosilicate (LYSO) PET/64-slice CT scanner (Philips Gemini TF) for pulmonary nodule assessment between 2011 and 2018. PET/CT images were evaluated retrospectively by a nuclear radiologist with 8 years of experience (M.E.). Approval from the local research ethics committee was granted. One hundred thirteen SPNs with biopsy-proven diagnosis were included in the study. Histopathological findings were accepted as the gold standard method. Patients with multiple nodules, and calcified nodules were excluded.

Non-contrast Thorax CT scans were performed with Siemens Somatom Definition AS, 128 slice CT machine. Imaging parameters were as follows; automatic effective mA, 120 kVp, gantry rotation speed 0.5 sec, slice thickness 1 mm. Images were retrospectively evaluated by a diagnostic radiologist with 15 years of experience (H.A). The radiologist was blinded to the histopathology and PET findings. Nodule size, location, margins, density, vascular sign, and pleural tag were evaluated individually. SPNs were classified as solid, SS, GGO nodules according to their densities. Besides, their densities were calculated by region of interest (ROI) replacement in Hounsfield unit (HU).

^{18}F-FDG PET/CT scans were performed after 6-hours fastening. Three point seven MBq/kg (0.1 mCi/kg) ^{18}F-FDG was given by intravenous injection. PET and CT images (non-corrected and attenuation-corrected) were obtained using maximum intensity projection and cross-sectional methods. SUV_{max}, metabolic activity volumetric parameters such as MTV, and TLG were calculated. MTV was calculated by ROI replacement in metabolically active area in each slice. TLG was calculated as the product of SUV_{mean} and MTV (SUV_{max}) >2.5 was accepted as a threshold value for malignant lesions (Figure 1, 2).

Both of the diagnostic radiologist and the nuclear radiologist made a final assessment for prediction of benignity or malignancy, independently from each other.

Statistical Analysis

Statistical analyses of the study were performed by SPSS 20.0 (IBM Inc., Chicago, IL, USA). Descriptive statistics were presented as mean±standard deviation for continuous variables and as frequency (percentage) for categorical variables with tables. Normality of continuous variables were checked by the Kolmogorov-Smirnov test. Mann-Whitney U for two independent groups and Kruskal-Wallis tests for multiple groups were used to compare continuous numerical data since there was no normal distribution. ROC analysis was performed for SUV_{max} and MTV values according to malignancy status and cut-off values were determined. Differential diagnosis rates such as specificity, sensitivity, accuracy and Kappa coefficients were calculated by comparing histopathological, radiological and nuclear medical evaluations. Monte Carlo corrected chi-square analysis was performed to determine the relationship between histopathological tumor subtypes and other categorical variables. P<0.05 was considered as statistically significant result by assuming a type 1 error value of 5% in all analyses.

Results

The vast majority (79.6%) of patients were male and the average age was 67.88±10.75 years (median=68). According to the histopathological diagnosis, 16.8% (n=19) of SPNs were benign, and 83.2% (n=94) were malignant (Table 1). Malignancy subtypes were adenocarcinoma (37.2%), squamous cell carcinoma (SCC) (25.7%), small cell carcinoma (15.9%), carcinoid tumor (2.7%) and bronchoalveolar carcinoma. Metastasis was detected in one patient. The distribution of SPNs according to attenuation was; solid (77.9%), SS (15.9%) and GGO (6.2%), respectively.

Spiculated margin, vascular sign, and pleural tag presence were predominantly observed in the malignant group (Table 1). The attenuation distribution of nodules was; solid, SS, and GGO, respectively (Table 1). SPN diameter, SUV_{max}, MTV, TLG, and density values were significantly different between the malignant and benign SPNs according to the histopathologic results. Those parameters were significantly higher in the malignant group (Table 1, 2). However, no significant difference was found amongst the malignant subtypes.

SUV_{max}, MTV, and TLG increased in direct proportion to the SPN diameter (R values were 0.53, 0.70 and 0.75 respectively, p<0.001). When we separated SPNs in two groups according to diameter, such as <2 cm and ≥2 cm, there was a significant difference between groups in terms of MTV (p<0.001), while there was no difference in terms of SUV_{max} (p=0.096) (Table 3). According to margin classification, most of the well-defined ones were SCC, lobulated ones were adenocarcinoma, and spiculated ones were small cell carcinoma and SCC (p=0.036).

According to threshold value of 2.5; the sensitivity, specificity, accuracy, positive predictive value (PPV), and negative predictive value (NPV) of SUV_{max} were found as 98.9%, 52.6%, 91.1%, 91.1%, and 90.9%, respectively (Kappa=0.620). On the other hand, sensitivity, specificity, accuracy, PPV, and NPV of final diagnosis of CT evaluation were calculated as 90.4%, 63.1%, 85.8%, 92.3%, and 57.1%, respectively (Kappa=0.514).

The cut-off value calculated by the ROC curve analysis for SUV_{max}, based on the likelihood of malignancy, was found to be 4.39 (sensitivity 93.6%, specificity 89.5% and accuracy 92.9%), (AUC=0.950±0.027; p<0.001) (Figure 3). Similarly,

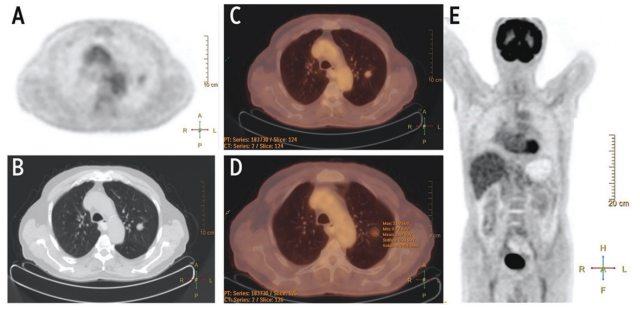

Figure 1. A well-defined and solid solitary pulmonary nodules was detected in left upper lobe in positron emission tomography (PET) image. (A) Axial non-contrast Thorax computed tomography (CT) at parenchyma window (B), and PET/CT image (C). Measurement of activity parameters were consistent with benign lesions on PET/CT image (D). MIP image of total body PET showed no significant activity (E)

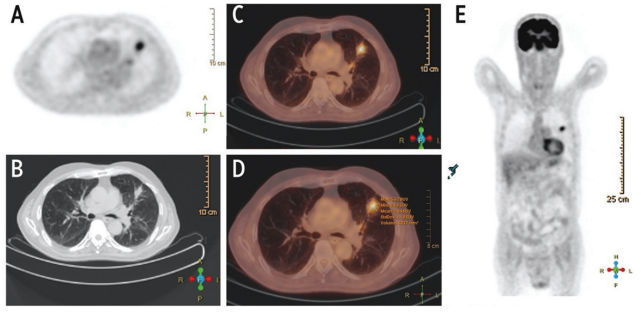

Figure 2. A spiculated and solid solitary pulmonary nodules was detected in left upper lobe in positron emission tomography (PET) image. (A) Axial non-contrast Thorax computed tomography (CT) at parenchyma window (B), and PET/CT image (C). Measurement of activity parameters were consistent with malignancy on PET/CT image (D). MIP image of total body PET showed significant activity in left upper lobe (E)

ROC analysis for MTV measurements calculated the cut-off value as 7.33 (AUC=0.774±0.066; p<0.001) (sensitivity 79.8%, specificity 68.4%, accuracy 77.9%) (Figure 3). The cut-off value calculated for TLG measurements was 31.88 g (AUC=0.891±0.039; p<0.001) (sensitivity 76.6%, specificity 89.5%, accuracy 78.8%) (Figure 3). The cut-off value calculated for the density was 2.5 HU, while the ROC curve was found to be significant (AUC=0.694±0.080; p=0.008) (Figure 3).

In both benign and malignant groups, there was no significant difference between SUV_{max} values amongst GGO, SS and solid nodules. In benign group MTV and TLG values increased in parallel with the density of the nodules, but no significant difference was found. On the other hand, in malignant group, both MTV and TLG values increased in direct proportion to the density of the nodules, significantly (Table 4). Cut-off values of SUV_{max}, MTV, TLG for subsolid SPNs were 4.41, 5.22 and 14.06, respectively. Cut-off values of SUV_{max}, MTV, and TLG for solid SPNs were 4.39, 17.53 and 73.38, respectively (Table 5).

Table 1. Demographic findings of patients and computed tomography findings of benign-malignant solitary pulmonary nodules

		Benign (n=19)	Malignant (n=94)	p
		Mean±SD		
Age		66.00±14.95	68.39±9.74	0.605
Gender	Male	13 (68.4)	77 (81.9)	0.185
	Female	6 (31.6)	17 (18.1)	
SPN diameter	mm	18.73±8.10	27.02±6.47	**0.002**
Density (HU)		4.78±42.37	20.38±32.75	**0.008**
		n (%)	n (%)	
Attenuation	GGO	3 (15.8)	4 (4.3)	**0.001**
	PS	7 (36.8)[a]	11 (11.7)[b]	
	Solid	9 (47.4)[a]	79 (84.0)[b]	
Margins	Well-defined	10 (52.6)[a]	7 (7.4)[b]	**<0.001**
	Lobulated	5 (26.3)	30 (31.9)	
	Spiculated	4 (21.1)[a]	57 (60.6)[b]	
Vascular sign	(-)	13 (68.4)	38 (40.4)	**0.026**
	(+)	6 (31.6)	56 (59.6)	
Pleural tag	(-)	13 (68.4)	38 (40.4)	**0.026**
	(+)	6 (31.6)	56 (59.6)	
Localization	Central	3 (14.8)[a]	42 (44.7)[b]	**0.048**
	Peripheral	16 (84.2)[a]	52(55.3)[b]	

Mann-Whitney U test and chi-square test.
[a, b]: Significantly different categories.
GGO: Ground glass opacity, PS: Partially solid, SD: Standard deviation, HU: Hounsfield unit, SPN: Solitary pulmonary nodule

Discussion

We investigated the morphological and metabolic activity parameters for SPNs and the effect of morphological characteristics of the nodule on metabolic activity assessment (SUV_{max} and volumetric parameters such as MTV and TLG). In this study, we compared the ^{18}F-FDG PET and CT findings of SPNs with histopathological diagnosis of 113 patients. Ninety four of them (83.2%) were malignant and 19 of them (16.8%) were benign.

We accepted SUV_{max}>2.5 as a threshold value for malignant nodules and ≤2.5 for benign nodules in ^{18}F-FDG PET evaluation, similarly with most of the studies in literature (8,9,10,11). However, ^{18}F-FDG avidity can also be observed in benign conditions such as inflammation, infection;

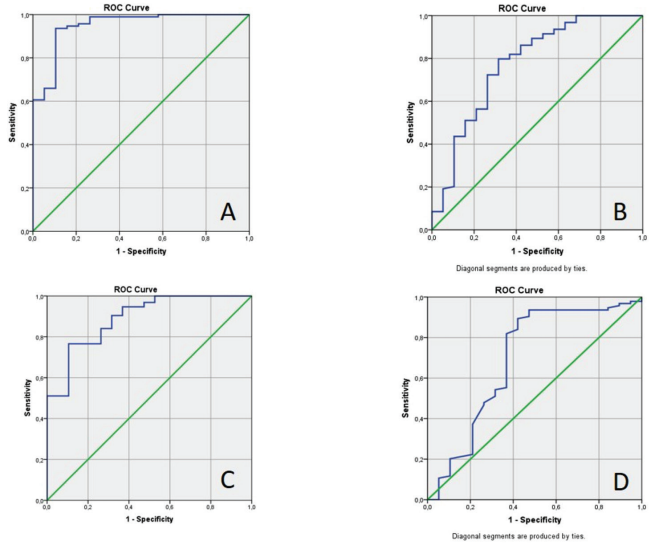

Figure 3. ROC analysis of SUV_{max} (A), metabolic tumor volume (B), total lesion glycolysis (C), and density (D) for malignancy

Table 2. Positron emission tomography/computed tomography findings of benign and malignant solitary pulmonary nodules

	Benign (n=19)	Malignant (n=94)	p
	Mean±SD		
SUV_{max}	2.98±2.11	11.94±19.17	**<0.001**
MTV (mL)	8.88±10.91	19.17±14.34	**<0.001**
TLG (g)	17.79±20.57	103.11±90.68	**<0.001**

Mann-Whitney U test & chi-square test.
[a, b]: Significantly different categories.
SD: Standard deviation, MTV: Metabolic tumor volume, TLG: Total lesion glycolysis

or malignant diseases can be less avid secondary to volumetric effects such as nodule size, ROI placement, etc. (12,13,14,15,16,17,18,19). SUV_{max} values of half of the bronchoalveolar carcinoma and carcinoid tumors which constitute 2% of all lung cancers, may cause false negative PET results (20).

Table 3. Relationship between ^{18}F-FDG positron emission tomography/computed tomography SUV_{max} and volumetric parameters and diameter

Diameter		SUV_{max}	MTV	TLG
(n=113)	**R**	0.526	0.695	0.752
	p	<0.001*	<0.001*	<0.001*
Benign				
(n=19)	**R**	0.306	0.822	0.794
	p	0.203	<0.001*	<0.001
Malignant				
(n=94)	**R**	0.389	0.554	0.604
	p	<0.001*	<0.001*	<0.001
<20 mm				
(n=31)	**R**	0.304	0.582	0.352
	p	0.096	0.001*	0.052
≥20 mm				
(n=82)	**R**	0.195	0.463	0.482
	p	0.078	<0.001*	<0.001

Spearman's Rho test.
*Statistically significant at p<0.05 level.
MTV: Metabolic tumor volume, TLG: Total lesion glycolysis

Table 4. ^{18}F-FDG positron emission tomography/computed tomography SUV_{max} and volumetric parameters according to attenuation classification

Benign	GGO (n=3)	PS (n=7)	Solid (n=9)	p
	Mean±SD			
SUV_{max}	1.86±1.01	3.14±2.31	3.22±2.28	0.653
MTV (mL)	1.27±1.29	5.33±2.34	14.18±14.11	0.060
TLG (g)	2.26±2.99	10.86±9.92	28.35±24.86	0.071
Dansite	-56.67±45.09[a]	-0.28±13.03	29.22±35.97[b]	**0.011**
Malign	**(n=4)**	**(n=11)**	**(n=79)**	
SUV_{max}	7.60±4.23	9.38±6.62	12.52±20.72	0.191
MTV (mL)	13.05±10.04	8.59±7.09[a]	20.95±14.62[b]	**0.002**
TLG (g)	62.94±63.91	41.78±53.11[a]	113.69±92.52[b]	**0.002**
Density (HU)	-60.0±64.42[a]	-12.81±46.82[c]	29.08±16.57[b,d]	**<0.001**

Kruskal-Wallis test.
[a,b] and [c,d]: Significantly different categories.
GGO: Ground glass opacity, PS: Partially solid, MTV: Metabolic tumor volume, TLG: Total lesion glycolysis, HU: Hounsfield unit

In our study, sensitivity, specificity, accuracy, PPV and NPV were 98.9%, 52.6%, 91.1%, 91.1%, and 90.9%, respectively (Kappa=0,620) in comparison with histopathological findings. In a study by Orlacchio et al. (22), the sensitivity, specificity and accuracy were calculated as 76.9%, 100%, and 89.2% according to SUV_{max} threshold of 2.5 in benign (46.4%) and malign (53.6%) SPNs. Opoka et al. (23) calculated 95% sensitivity, 88% specificity, 91.5% accuracy in their study using SUV_{max} threshold value of 2.5 in 40 malignant and 42 benign SPNs. Although we found higher sensitivity, the specificity was lower, and the accuracy was similar in comparison with Orlacchio et al's. (22) study. We think that, this may result from small patient population in benign group in our study. In addition, 9 of the 19 benign SPNs had infectious etiology in our study. SPNs with infectious, inflammatory, granulomatous etiology can cause higher ^{18}F-FDG avidity (11). Deppen et al. (24) found similar sensitivity (92%) and specificity (40%) in their study performed in a region of endemic granulomatous diseases.

Grgic et al. (10) evaluated malignancy ratios of 140 patients with using different SUV_{max} threshold value and found that more than 90% of nodules with SUV_{max}<2 were benign. Sensitivity, specificity and NPV were 96%, 55%, and 92%, respectively. The highest diagnostic accuracy was found with SUV_{max} threshold of 4 (sensitivity, specificity and accuracy of 85%). ROC analysis in a study with 88 SPNs by Hou et al. (25) showed SUV_{max}>3.635 as the best threshold value for SPNs (sensitivity 83.3%, sensitivity 62.5%, accuracy 79.2%). In our study, ROC analysis demonstrated

Table 5. Cut-off values of SUV_{max}, metabolic tumor volume, total lesion glycolysis for subsolid and solid solitary pulmonary nodules

		SUV_{max}	MTV	TLG
Subsolid	n=25	6.44±5.64	7.52±6.85	31.77±46.42
Solid	n=88	9.63±4.96	20.26±14.64	104.96±91.69
	p	0.001	<0.001*	<0.001*
Subsolid	AUC	0.900	0.760	0.913
	Cut-off	4.41	5.215	14.065
		Sens=93.6% Spec=89.4% Accu=92.9%	73.33% 70.0% 72.0%	86.67% 90.0% 880%
Solid	AUC	0.954	0.652**	0.850
	Cut-off	4.39	17.53	73.38
		Sens=93.6% Spec=89.4% Accu=92.9%		96.2% 22.2% 88.6%

*Statistically significant at p<0.05 level.
**Not significant.
MTV: Metabolic tumor volume, TLG: Total lesion glycolysis

(AUC=0.950±0.027; p<0.001) SUV_{max} cut-off value as 4.39 for malignant nodules, similar with the study by Grgic et al. (10) and higher than the study by Hou et al. (25) (sensitivity 93.6%, specificity 89.5% and accuracy 92.9%). Sensitivity, specificity and accuracy values for threshold value of 4.39 were also higher than both two studies.

We observed that, SUV_{max} was significantly higher in the malignant group. However, no significant difference was found amongst the malignant histopathologic subtypes. Also, Divisi et al. (12) found no significant correlation between histopathological findings and SUV_{max} (p=0.586). Davidson et al. (26) showed that SCC was more ^{18}F-FDG avid than adenocarcinoma.

Volumetric parameters developed for measuring metabolic activity are MTV, and TLG in PET scans. In our study, there was a significant difference between malignant and benign nodules in terms of MTV and TLG values. All of the measurements were significantly higher in malignant group. However, there was no significant difference amongst the malignant histopathologic subtypes. ROC analysis showed cut-off value of 7.33 mL for MTV (AUC=0.774±0.066; p<0.001) (sensitivity 79.8%, specificity 68.4%, accuracy 77.9%) and 31.88 g for TLG (AUC=0.891±0.039; p<0.001) (sensitivity 76.6%, specificity 89.5%, accuracy 78.8%). There has been a few studies in literature researching the relationship between volumetric parameters and prognosis in small cell lung cancer, mesothelioma, non-small cell lung cancers (27,28,29). However, according to our literature search, this is the first study to evaluate the volumetric parameters in SPNs.

Winer-Muram (30) has declared that the probability of malignancy increases with the size. Kim et al. (31) observed that SUV_{max} was directly proportional to the lesion size, but inversely proportional to the GGO percentage. Divisi et al. (12) and Khalaf et al. (32) found consistent results with the study by Kim et al. (31) in terms of relation between nodule size and SUV_{max}.

We also observed that SPN diameter was significantly larger in the malignant group. In addition, SUV_{max}, MTV, TLG increased in direct proportion to the SPN diameter (R values were 0.53, 0.70 and 0.75, respectively, p<0.001). When we separated SPNs according to diameter into two groups, such as <2 cm and ≥2 cm, there was a significant difference between groups in terms of MTV (p<0.001), while there was no difference between groups in terms of SUV_{max} (p=0.096). Therefore, MTV can be a more reliable parameter than SUV_{max} in prediction of malignancy in smaller nodules (p<0.001).

Zhou et al. (33) and Nakamura et al. (34) mentioned that solid component predominancy increases by the invasiveness of adenomatous lung lesions in SS nodules. Our study showed that malignancy rates were directly proportional to the density. On the contrary, there was no significant difference in density measurements of subsolid nodules between benign and malignant group (p=0.70).

Chun et al. (35) revealed that SUV_{max} of SS nodules was higher in benign inflammatory group than in malignant group, but there was no significant difference between groups in terms of GGO nodules. They concluded that follow-up was recommended instead of immediate biopsy for such cases. Nomori et al. (17) evaluated 15 GGO and 101 solid nodules in their study and concluded that ^{18}F-FDG PET was not a feasible method for GGO nodules because of having lower sensitivity (10%) and specificity (20%), unlike it was a feasible method for solid nodules because of having higher sensitivity (90%) and specificity (71%). We observed no significant difference amongst GGO, SS and solid nodules neither in benign nor malignant group in terms of SUV_{max} values. In both benign and malignant groups, MTV and TLG values increased in parallel with the density of the nodules, but significant difference was only found in malignant group. SUV_{max} cut-off value of solid and subsolid nodules were considerably close to each other, but MTV and TLG were higher in solid nodules than the other groups. Thus, we think that there is a need for using different cut-off levels of MTV and TLG for solid and subsolid nodules, but there is no need for using different cut-off level of SUV_{max}.

Study Limitations

The limitations of our study can be listed as follows; (1) the histopathological findings were results of tru-cut biopsy, not lobectomy, (2) biopsies were performed for only malignancy suspected nodules, others were followed-up radiologically. That was the reason why we had a smaller patient group in the benign group.

Conclusion

MDCT or ^{18}F-FDG PET findings can be indeterminate for malignancy prediction of SPNs on their own, and should be interpreted together. Metabolic activity assessment can be done by measurements of SUV_{max} and volumetric parameters such as MTV and TLG on PET scans. They are all expected to be found higher in malignancy. However, these parameters are affected by morphological characteristics, such as diameter and attenuation of the nodule. According to these differences, it is controversial which parameter is more reliable. We think that, there is a need for using different cut-off levels of MTV and TLG for solid and subsolid nodules, but there is no need for using different cut-off level of SUV_{max}. MTV can be a more

reliable parameter than SUV_{max} in prediction of malignancy in smaller nodules (<2 cm). We suggest that, further studies are needed for evaluation of volumetric parameters in SPNs.

Ethics

Ethics Committee Approval: Approval from the Süleyman Demirel University Local Research Ethics Committee was granted (desicion no: 138, 04.07.2018).

Informed Consent: Retrospective study.

Peer-review: Externally peer-reviewed.

Authorship Contributions

Surgical and Medical Practices: M.E., S.S.Ş., Concept: M.E., Design: Ş.E., Data Collection or Processing: H.A., Analysis or Interpretation: A.K., Literature Search: M.E., Ş.E., Writing: M.E., Ş.E..

Conflict of Interest: No conflict of interest was declared by the authors.

Financial Disclosure: The authors declared that this study received no financial support.

References

1. Tuddenham WJ. Glossary of terms for thoracic radiology: recommendations of the Nomenclature Committee of the Fleischner Society. AJR Am J Roentgenol 1984;143:509-517.
2. Ost D, Fein AM, Feinsilver SH. Clinical practice. The solitary pulmonary nodule. N Engl J Med 2003;348:2535-2542.
3. Midthun DE, Swensen SJj, Jett JR, editors. Approach to the solitary pulmonary nodule. Mayo Clin Proc 1993;68:378-385.
4. Gohagan J, Marcus P, Fagerstrom R, Pinsky P, Kramer B, Prorok P; Writing Committee, Lung Screening Study Research Group. Baseline findings of a randomized feasibility trial of lung cancer screening with spiral CT scan vs chest radiograph: the Lung Screening Study of the National Cancer Institute. Chest 2004;126:114-121.
5. Swensen SJ, Jett JR, Hartman TE, Midthun DE, Sloan JA, Sykes AM, Aughenbaugh GL, Clemens MA. Lung cancer screening with CT: Mayo Clinic experience. Radiology 2003;226:756-761.
6. Lee HY, Lee KS. Ground-glass opacity nodules: histopathology, imaging evaluation, and clinical implications. J Thorac Imaging 2011;26:106-118.
7. Naidich DP, Bankier AA, MacMahon H, Schaefer-Prokop CM, Pistolesi M, Goo JM, Macchiarini P, Crapo JD, Herold CJ, Austin JH, Travis WD. Recommendations for the management of subsolid pulmonary nodules detected at CT: a statement from the Fleischner Society. Radiology 2013;266:304-317.
8. Sim YT, Poon FW. Imaging of solitary pulmonary nodule-a clinical review. Quant Imaging Med Surg 2013;3:316-326.
9. Herder GJ, van Tinteren H, Golding RP, Kostense PJ, Comans EF, Smit EF, Hoekstra OS. Clinical prediction model to characterize pulmonary nodules: validation and added value of 18 F-fluorodeoxyglucose positron emission tomography. Chest 2005;128:2490-2496.
10. Grgic A, Yüksel Y, Gröschel A, Schäfers H-J, Sybrecht GW, Kirsch CM, Hellwig D. Risk stratification of solitary pulmonary nodules by means of PET using 18 F-fluorodeoxyglucose and SUV quantification. Eur J Nucl Med Mol Imaging 2010;37:1087-1094.
11. Gould MK, Fletcher J, Iannettoni MD, Lynch WR, Midthun DE, Naidich DP, Ost DE; American College of Chest Physicians. Evaluation of patients with pulmonary nodules: when is it lung cancer?: ACCP evidence-based clinical practice guidelines. Chest 2007;132:108-130.
12. Divisi D, Barone M, Bertolaccini L, Rocco G, Solli P, Crisci R; Italian VATS Groupl. Standardized uptake value and radiological density attenuation as predictive and prognostic factors in patients with solitary pulmonary nodules: our experience on 1,592 patients. J Thorac Dis 2017;9:2551-2559.
13. Chen CJ, Lee BF, Yao WJ, Cheng L, Wu PS, Chu CL, Chiu NT. Dual-phase 18F-FDG PET in the diagnosis of pulmonary nodules with an initial standard uptake value less than 2.5. AJR Am J Roentgenol 2008;191:475-479.
14. Erasmus JJ, McAdams HP, Patz EF Jr, Coleman RE, Ahuja V, Goodman PC. Evaluation of primary pulmonary carcinoid tumors using FDG PET. AJR Am J Roentgenol 1998;170:1369-1373.
15. Heyneman LE, Patz EF. PET imaging in patients with bronchioloalveolar cell carcinoma. Lung Cancer 2002;38:261-266.
16. Kapucu LO, Meltzer CC, Townsend DW, Keenan RJ, Luketich JD. Fluorine-18-fluorodeoxyglucose uptake in pneumonia. J Nucl Med 1998;39:1267-1269.
17. Nomori H, Watanabe K, Ohtsuka T, Naruke T, Suemasu K, Uno K. Evaluation of F-18 fluorodeoxyglucose (FDG) PET scanning for pulmonary nodules less than 3 cm in diameter, with special reference to the CT images. Lung Cancer 2004;45:19-27.
18. Ollenberger GP, Knight S, Tauro AJ. False-positive FDG positron emission tomography in pulmonary amyloidosis. Clin Nucl Med 2004;29:657-658.
19. Thie JA. Understanding the standardized uptake value, its methods, and implications for usage. J Nucl Med 2004;45:1431-1434.
20. Kim B, Kim Y, Lee K, Yoon S, Cheon E, Kwon O, Rhee CH, Han J, Shin MH. Localized form of bronchioloalveolar carcinoma: FDG PET findings. AJR Am J Roentgenol 1998;170:935-939.
21. Moon SH, Hyun SH, Choi JY. Prognostic significance of volume-based PET parameters in cancer patients. Korean J Radiol 2013;14:1-12.
22. Orlacchio A, Schillaci O, Antonelli L, D'Urso S, Sergiacomi G, Nicoli P, Simonetti G. Solitary pulmonary nodules: morphological and metabolic characterisation by FDG-PET-MDCT. Radiol Med 2007;112:157-173.
23. Opoka L, Kunikowska J, Podgajny Z, Szołkowska M, Błasińska-Przerwa K, Burakowska B, Oniszh K, Rudziński P, Bestry I, Roszkowski-Śliż K. Accuracy of FDG PET/CT in the evaluation of solitary pulmonary lesions - own experience. Pneumonol Alergol Pol 2014;82:198-205.
24. Deppen S, Putnam JB Jr, Andrade G, Speroff T, Nesbitt JC, Lambright ES, Massion PP, Walker R, Grogan EL. Accuracy of FDG-PET to diagnose lung cancer in a region of endemic granulomatous disease. Ann Thorac Surg 2011;92:428-433.
25. Hou S, Lin X, Wang S, Shen Y, Meng Z, Jia Q, Tan J. Combination of positron emission tomography/computed tomography and chest thin-layer high-resolution computed tomography for evaluation of pulmonary nodules: Correlation with imaging features, maximum standardized uptake value, and pathology. Medicine (Baltimore) 2018;97:e11640.
26. Davidson J, Wong V, Fraser R, Hirsh V. Comparison of primary tumor maximal standardized uptake value (SUVmax) on preoperative (18F) fluorodeoxyglucose positron emission tomography/computed tomography (PET/CT) and histological subtype in patients with non-small cell lung cancer (NSCLC). Journal of Clinical Oncology. 2009;27:7571.
27. Chen HH, Chiu NT, Su WC, Guo HR, Lee BF. Prognostic value of whole-body total lesion glycolysis at pretreatment FDG PET/CT in non-small cell lung cancer. Radiology 2012;264:559-566.
28. Klabatsa A, Chicklore S, Barrington SF, Goh V, Lang-Lazdunski L, Cook GJ. The association of 18 F-FDG PET/CT parameters with survival in malignant pleural mesothelioma. Eur J Nucl Med Mol Imaging 2014;41:276-282.

29. Zhu D, Ma T, Niu Z, Zheng J, Han A, Zhao S, Yu J. Prognostic significance of metabolic parameters measured by 18F-fluorodeoxyglucose positron emission tomography/computed tomography in patients with small cell lung cancer. Lung cancer 2011;73:332-337.
30. Winer-Muram HT. The solitary pulmonary nodule. Radiology 2006;239:34-49.
31. Kim TJ, Park CM, Goo JM, Lee KW. Is there a role for FDG PET in the management of lung cancer manifesting predominantly as ground-glass opacity? AJR Am J Roentgenol 2012;198:83-88.
32. Khalaf M, Abdel-Nabi H, Baker J, Shao Y, Lamonica D, Gona J. Relation between nodule size and 18 F-FDG-PET SUV for malignant and benign pulmonary nodules. J Hematol Oncol 2008;1:13.
33. Zhou J, Li Y, Zhang Y, Liu G, Tan H, Hu Y, Xiao J, Shi H. Solitary ground-glass opacity nodules of stage IA pulmonary adenocarcinoma: combination of 18F-FDG PET/CT and high-resolution computed tomography features to predict invasive adenocarcinoma. Oncotarget 2017;8:23312-23321.
34. Nakamura H, Saji H, Shinmyo T, Tagaya R, Kurimoto N, Koizumi H, Tagagi M. Close association of IASLC/ATS/ERS lung adenocarcinoma subtypes with glucose-uptake in positron emission tomography. Lung Cancer 2015;87:28-33.
35. Chun EJ, Lee HJ, Kang WJ, Kim KG, Goo JM, Park CM, Lee CH. Differentiation between malignancy and inflammation in pulmonary ground-glass nodules: the feasibility of integrated 18F-FDG PET/CT. Lung Cancer 2009;65:180-186.

Interesting Image
Mol Imaging Radionucl Ther 2019;28:120-122 DOI:10.4274/mirt.galenos.2019.09709

Minimal Invasive Radioguided Ectopic Parathyroidectomy in Upper Mediastinum

Üst Mediastinal Paratiroid Adenomunun Gamma Prob ile Minimal İnvaziv Eksizyonu

Zehra Pınar Koç[1], Turgut Karlıdağ[2], Pelin Özcan Kara[1], Abdulvahap Akyiğit[3], Ferda Dağlı[4]
[1]*Mersin University Faculty of Medicine, Department of Nuclear Medicine, Mersin, Turkey*
[2]*Fırat University Faculty of Medicine, Department of Ear Nose and Throat, Elazığ, Turkey*
[3]*Elazığ Training and Research Hospital, Clinic of Ear, Nose and Throat, Elazığ, Turkey*
[4]*Fırat University Faculty of Medicine, Department of Pathology, Elazığ, Turkey*

Abstract

In this study we wanted to present a case with the history of multiple previous neck explorations and persisting upper mediastinal ectopic parathyroid adenoma who underwent a successful operation with radioguided minimal invasive approach.

Keywords: Hyperparathyroidism, adenoma, minimally invasive, radioimmunodetection

Öz

Bu çalışmada çok sayıda boyun operasyonu öyküsü ve kalıntı üst mediastinal ektopik paratiroid adenomu olan ve başarılı bir şekilde radyoişaretli minimal invaziv yaklaşımla opere edilen bir olguyu sunmak istedik.

Anahtar kelimeler: Hiperparatiroidizm, adenom, minimal girişimsel, radyoimmünotespit

Address for Correspondence: Zehra Pınar Koç MD, Mersin University Faculty of Medicine, Department of Nuclear Medicine, Mersin, Turkey
Phone: +90 530 543 05 79 **E-mail:** zehrapinarkoc@gmail.com ORCID ID: orcid.org/0000-0002-3274-5790
Received: 14.03.2016 **Accepted:** 17.03.2019

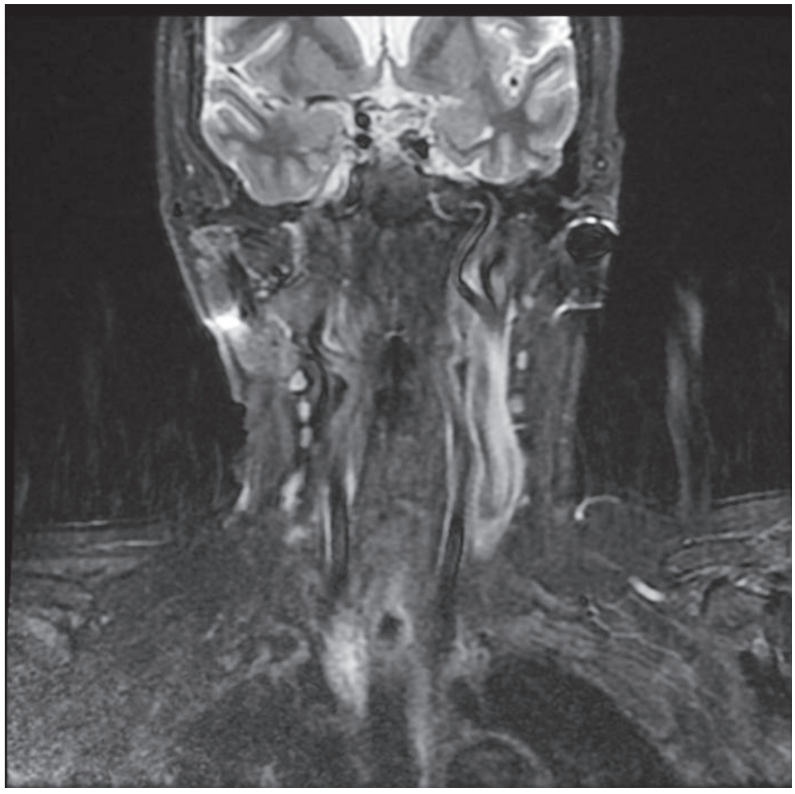

Figure 1. The magnetic resonance images showed remaining upper mediastinal parathyroid adenoma

Figure 2. Anteroposterior early phase Tc-99m MIBI parathyroid planar image including the neck and mediastinum showing right upper mediastinal increased uptake consisted with the ectopic parathyroid adenoma. A 69-year-old female patient with the diagnosis of hyperparathyroidism; hypercalcemia and increased parathyroid hormone (PTH) levels and additional multinodular goiter was referred to our department for labeling for the radioguided surgery. The patient had anamnesis of bilateral total thyroidectomy due to multinodular goiter and an additional failed surgery for the parathyroid adenoma excision due to the ectopic localization of adenoma. She had previous diagnosis of incidental papillary microcarcinoma of the thyroid gland. Persistent hipercalcemia and hyperparathyroidism were observed after the two operative procedures. Parathyroid scintigraphy was performed by intravenous injection of 370 mBq Tc-99m MIBI with low energy high resolution collimator equipped double head SPECT gamma camera prior to the surgery. The clear demonstration of a parathyroid adenoma in planar images obviated the need for SPECT imaging. The patient was

referred to the operation after scintigraphy imaging for radioguided surgery with handheld gamma probe. In the operation room, the background count per minute (cpm) level was 5 from the shoulder and postoperative field count was 200 and the count of the lesion was 1500 cpm. The lesion was between the trachea and esophagus (retroesophageal) and the surgery was performed by a small incision of 2 cm wide. The lesion which was confirmed as a parathyroid adenoma by the pathology result was 2,704 gram in weight and 3 x 1.6 x 0.8 cm in size. Successful removal was confirmed both by postoperative counts and quick PTH analysis (preoperative: 698 pg/mg postoperative: 70.9 pg/mg (normal values: PTH 14-74 pg/mg). No complication was observed during or after the surgery. The patient was normocalcemic after six months of follow up. The definition of minimal invasive parathyroidectomy includes focused surgery planned for the excision of a single enlarged parathyroid gland (1). Routine parathyroid surgery includes inspection and exploration of all the neck, however in recent years the dissemination of imaging methods has contributed to development of this novel surgical approach (minimal invasive surgery) which is a targeted and secure way of successful surgery. Minimally invasive procedures are more comfortable for both the surgeon and the patient due to the cost effectiveness, being safe in terms of complications, and reduced operation, recovery and hospitalization times. Ectopic parathyroid adenoma is a diagnostic challenge which may be located in anywhere between angle of mandibule and mediastinum (2). Approximately 70% of the patients that have failed surgery are due to the ectopic localization of the parathyroid adenoma (3). Most of the upper mediastinal lesions might be excised by a cervical incision (4). However, preoperative localization methods are necessary for successful result (5). Currently the most accurate and reliable method for the localization of the parathyroid adenoma is the parathyroid scintigraphy with additional ultrasonography. Planar parathyroid scintigraphy achieves a sensitivity of 78% and with additional SPECT imaging this ratio increases to 96% according to the previous reports (6). There is limited number of reports of the radioguided surgery for mediastinal lesions. In a previous report, Doğan et al. (7) considered gamma probe as a useful method for ectopic parathyroid adenoma operation. Also in a previous series involving minimal invasive procedures of 102 patients, radioguided surgery was found to be an efficient method, especially in the upper mediastinal lesions (8). The reported patient in this study had a successful surgery and excellent outcome after her third operation without any complications. This case reports shows that minimal invasive radioguided surgery is also possible and required for the patients with history of multiple previous neck explorations and upper mediastinal lesions.

Ethics

Informed Consent: Obtained.

Peer-review: Externally peer-reviewed.

Authorship Contributions

Surgical and Medical Practices: Z.P.K., T.K., A.A., F.D., Concept: Z.P.K., T.K., A.A., Design: Z.P.K., T.K., A.A., Data Collection or Processing: Z.P.K., T.K., A.A., F.D., Analysis or Interpretation: Z.P.K., T.K., A.A., F.D., P.Ö.K., Literature Search: Z.P.K., T.K., A.A., F.D., P.Ö.K., Writing: Z.P.K., T.K., A.A., F.D., P.Ö.K.

Conflict of Interest: No conflict of interest was declared by the authors.

Financial Disclosure: The authors declared that this study received no financial support.

References

1. Noureldine SI, Gooi Z, Tufano RP. Minimally invasive parathyroid surgery. Gland Surg 2015;4:410-419.
2. Wang CA. Parathyroid re-exploration. A clinical and pathological study of 112 cases. Ann Surg 1977;186:140-145.
3. Uludag M, Isgor A, Yetkin G, Atay M, Kebudi A, Akgun I. Supernumerary ectopic parathyroid glands. Persistent hyperparathyroidism due to mediastinal parathyroid adenoma localized by preoperative single photon emission computed tomography and intraoperative gamma probe application. Hormones (Athens) 2009;8:144-149.
4. Medrano C, Hazelrigg SR, Landreneau RJ, Boley TM, Shawgo T, Grasch A. Thoracoscopic resection of ectopic parathyroid glands. Ann Thorac Surg 2000;69:221-223.
5. Wang C, Gaz RD, Moncure AC. Mediastinal parathyroid exploration. A clinical and pathologic study of 47 cases. World J Surg 1986;10:687-695.
6. Harvey A, Bohacek L, Neumann D, Mihaljevic T, Berber E. Robotic thoracoscopic mediastinal parathyroidectomy for persistent hyperparathyroidism: case report and review of the literature. Surg Laparosc Endosc Percutan Tech 2011;21:24-27.
7. Doğan R, Kara M, Yazicioğlu A, Kaynaroğlu V. The use of gamma probe for the intraoperative localization of an ectopic parathyroid adenoma. Tuberk Toraks 2009;57:208-211.
8. Rubello D, Casara D, Giannini S, Piotto A, De Carlo E, Muzzio PC, Pelizzo MR. Importance of radio-guided minimally invasive parathyroidectomy using hand-held gamma probe and low (99m)Tc-MIBI dose. Technical considerations and long-term clinical results. Q J Nucl Med 2003;47:129-138.

Interesting Image
Mol Imaging Radionucl Ther 2019;28:123-125 DOI:10.4274/mirt.galenos.2018.14632

Incidental "Urinoma" in ^{18}F-FDG PET/CT Scan

^{18}F-FDG PET/BT Taramasında Tesadüfi "Ürinoma"

Aziz Gültekin, Olga Yaylalı, Tarık Şengöz, Doğangün Yüksel
Pamukkale University Faculty of Medicine, Department of Nuclear Medicine, Denizli, Turkey

Abstract

^{18}F-FDG PET/CT scanning was performed for the primary staging of a 47-year-old man with urothelial carcinoma. The patient underwent biopsy by ureteroscopy 15 days ago and the PET images revealed ^{18}F-FDG accumulation in the right retroperitenal region, compatible with an "urinoma".

Keywords: Urothelial carcinoma, urinoma, positron emission tomography

Öz

Kırk yedi yaşındaki ürotelyal kanserli erkek hastaya primer evreleme için ^{18}F-FDG PET/BT görüntüleme yapıldı. ^{18}F-FDG PET/BT görüntülemesinden 15 gün önce üreteroskopi ile biyopsi yapılan hastanın sağ retroperitenal bölgesinde "ürinoma" ile uyumlu ^{18}F-FDG birikimi gözlendi.

Anahtar kelimeler: Ürotelyal kanser, ürinom, pozitron emisyon tomografi

Address for Correspondence: Aziz Gültekin MD, Pamukkale University Faculty of Medicine, Department of Nuclear Medicine, Denizli, Turkey
Phone: +90 505 496 93 48 **E-mail:** agultekin@pau.edu.tr ORCID ID: orcid.org/0000-0002-0311-8077
Received: 29.08.2018 **Accepted:** 12.11.2018

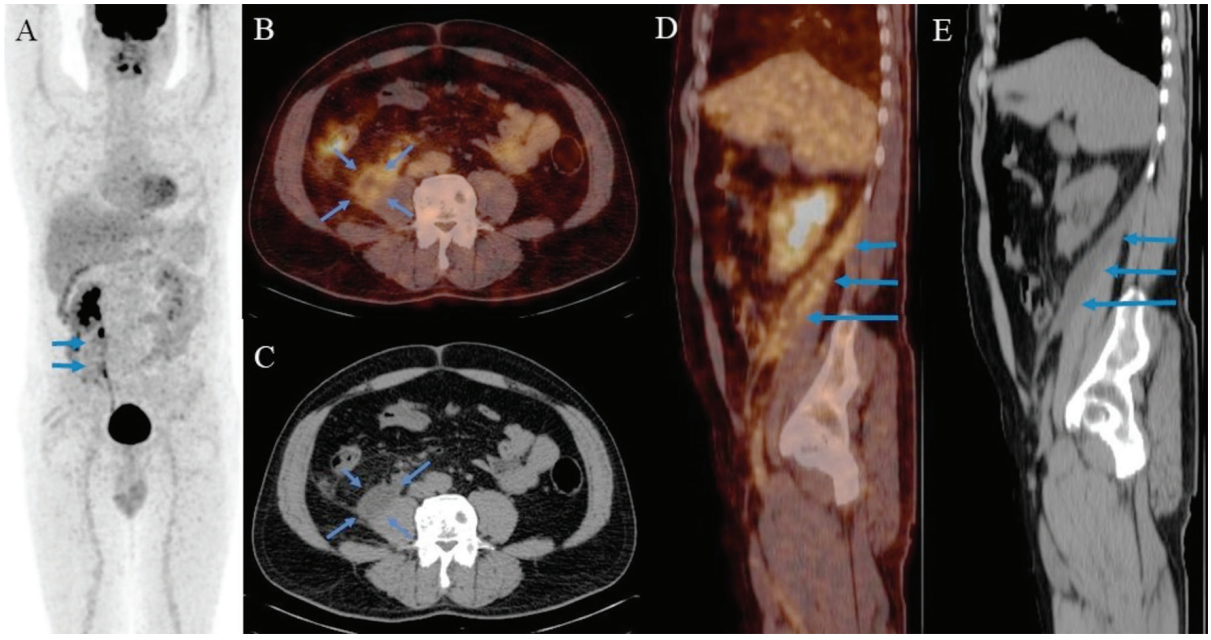

Figure 1. A 47-year-old man with a diagnosis of urothelial carcinoma was referred for primary staging with ^{18}F-FDG PET/CT scan. The ^{18}F-FDG PET/CT scanning was performed 15 days after ureteroscopic biopsy. Imaging was performed 60 minutes after I.V. injection of 395 MBq ^{18}F-FDG, on an integrated 16 slice PET/CT, with scanning from the skull base to the knee. ^{18}F-FDG PET/CT images [(A) MIP; (B) axial fusion; (C) axial CT; (D) sagittal fusion; (E) sagittal CT) showed tracer accumulation in the fluid collection extending to the pelvis along the retroperitoneal area (SUV_{max}: 4.90, mean density; 1 Hounsfield units), associated with the right ureter, in the right iliopsoas region adjacent to the muscle (A-E blue arrows).

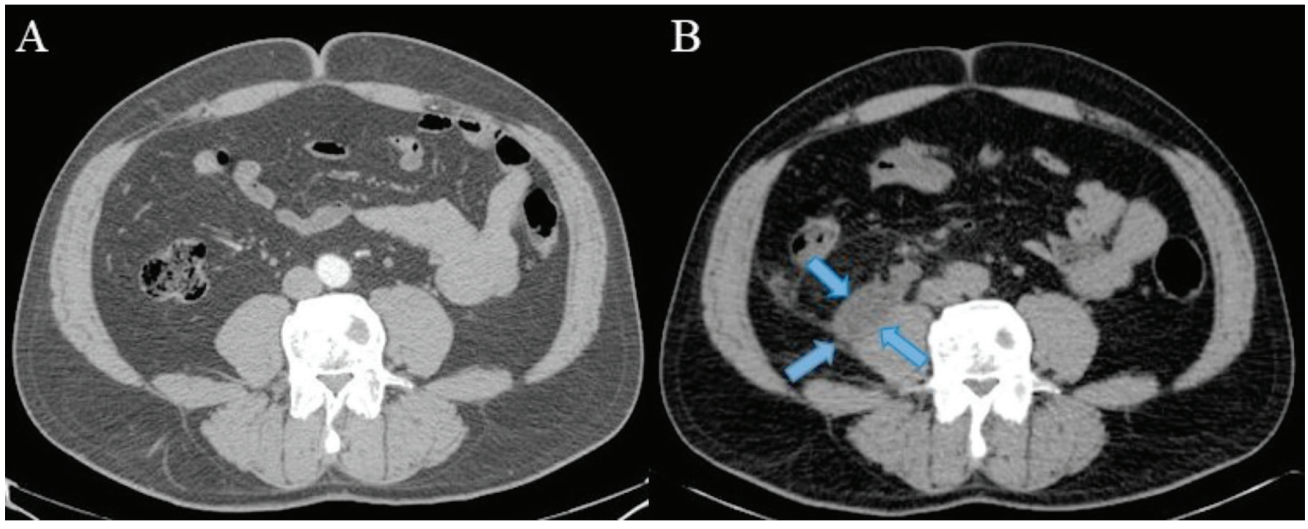

Figure 2. Contrast enhanced CT image before the biopsy (A) and CT image of PET/CT after the biopsy (B). Urinoma was shown (B blue arrows) on the right iliopsoas muscle. CT scanning results of the patient before and after the biopsy procedure were compared and it was recognized that the lesion associated with the right ureter, emerging following the biopsy procedure was a lesion in fluid density consistent with urinoma.

Urinomas may be asymptomatic and occult initially, but may lead to abscess formation and electrolyte imbalances if not diagnosed and managed appropriately (1). Ureteral leaks can result from trauma, ureteral obstruction, tumors or endourologic interventional procedures (2,3,4). The second most common complication of abdominal laparoscopic surgery is ureteral injury (5). Urinomas are rare complications of ureteroscopy. The diagnosis is usually made by ultrasound or CT (2). The incidental discovery of a urinoma by ^{18}F-FDG PET/CT was previously reported (6,7). In our case, urinoma originating from iatrogenic urinary tract injury following endourological biopsy procedure was detected incidentally on PET/CT scan.

Ethics

Informed Consent: Consent form was filled out by the patient.

Peer-review: Externally and internally peer-reviewed.

Authorship Contributions

Concept: A.G., O.Y., Design: A.G., O.Y., Data Collection or Processing: A.G., O.Y., Analysis or Interpretation: A.G., O.Y., T.Ş., D.Y., Literature Search: A.G., Writing: A.G., D.Y.

Conflict of Interest: No conflict of interest was declared by the authors.

Financial Disclosure: The authors declared that this study received no financial support.

References

1. Titton RL, Gervais DA, Hahn PF, Harisinghani MG, Arellano RS, Mueller PR. Urine leaks and urinomas: diagnosis and imaging-guided intervention. Radiographics 2003;23:1133-1147.
2. Gayer G, Zissin R, Apter S, Garniek A, Ramon J, Kots E, Hertz M. Urinomas caused by ureteral injuries: CT appearance. Abdom Imaging 2002;27:88-92.
3. Desai MM, Gill IS, Kaouk JH, Matin SF, Novick AC. Laparoscopic partial nephrectomy with suture repair of the pelvicaliceal system. Urology 2003;61:99-104.
4. Ghali AM, El Malik EM, Ibrahim AI, Ismail G, Rashid M. Ureteric injuries: diagnosis, management, and outcome. J Trauma 1999;46:150-158.
5. Cadeddu JA, Wolfe JS Jr, Nakada S, Chen R, Shalhav A, Bishoff JT, Hamilton B, Schulam PG, Dunn M, Hoenig D, Fabrizio M, Hedican S, Averch TD. Complications of laparoscopic procedures after concentrated training in urological laparoscopy. J Urol 2001;166:2109-2111.
6. Sanchez MJ, Caride VJ. Incidental, early diagnosis of urinoma by F-18 FDG PET/CT. Clin Nucl Med 2005;30:102-104.
7. Dias AH, Ipsen P, Bouchelouche K. Incidental Diagnosis of a Large Retroperitoneal Urine Accumulation (Urinoma) on an 18F-FDG PET/CT Scan Performed for Primary Staging of Urothelial Carcinoma. Clin Nucl Med 2017;42:626-627.

Interesting Image
Mol Imaging Radionucl Ther 2019;28:126-128 DOI:10.4274/mirt.galenos.2018.59251

PET/CT Findings of a Patient with Cardiac Metastasis of Subungual Malign Melanoma

Subungual Malign Melanom Tanılı Hastanın PET/BT Görüntülemesinde Saptanan Kardiyak Metastaz

Özgül Ekmekçioğlu[1], Pelin Arıcan[1], Şermin Meşe[2], Nihal Kaplan[2], Mesut Kafi[1], Duygu Şimşek[1], Mehmet Şükrü Ertürk[3]
[1]Şişli Hamidiye Etfal Training and Research Hospital, Clinic of Nuclear Medicine, İstanbul, Turkey
[2]Şişli Hamidiye Etfal Training and Research Hospital, Clinic of Medical Oncology, İstanbul, Turkey
[3]Şişli Hamidiye Etfal Training and Research Hospital, Clinic of Radiology, İstanbul, Turkey

Abstract

A 58-year old patient with a history of subungual malign melanoma was referred to our department for a ^{18}F-FDG positron emission tomography (PET)/computed tomography (CT) whole body scan. An unexpected ^{18}F-FDG uptake in left ventricule which mimicked either trombus or physiological papillary muscle was detected. Filling defect of intravenous contrast in CT images was also demonstrated in left ventricule cavity. Magnetic resonance imaging scan confirmed cardiac mass with metastatic features of malign melanoma in left ventricule.

Keywords: Malign melanoma, PET/CT, subungual, ^{18}F-FDG

Öz

Subungual malign melanom tanılı 58 yaşında erkek hasta tüm vücut ^{18}F-FDG pozitron emisyon tomografi (PET)/bilgisayarlı tomografi (BT) görüntülemesi için birimimize başvurdu. PET/BT görüntüleri incelendiğinde kardiyak kesitlerde sol ventrikül düzeyinde fizyolojik papiller kas aktivitesine veya trombüse benzer görünümde artmış ^{18}F-FDG tutulumu saptandı. BT kesitlerinde ventriküler kavitede kontrast dolum defekti izlendi. PET/BT sonrasında yapılan manyetik rezonans görüntülemesi ile olguda kardiyak malign melanom metastazı ile uyumlu bulgular saptandı.

Anahtar kelimeler: Malign melanom, PET/BT, subungual, ^{18}F-FDG

Address for Correspondence: Özgül Ekmekçioğlu MD, Şişli Hamidiye Etfal Training and Research Hospital, Clinic of Nuclear Medicine, İstanbul, Turkey
Phone: +90 530 643 54 82 **E-mail:** ozgulek@gmail.com ORCID ID: orcid.org/0000-0002-3313-8087
Received: 17.10.2018 **Accepted:** 26.11.2018

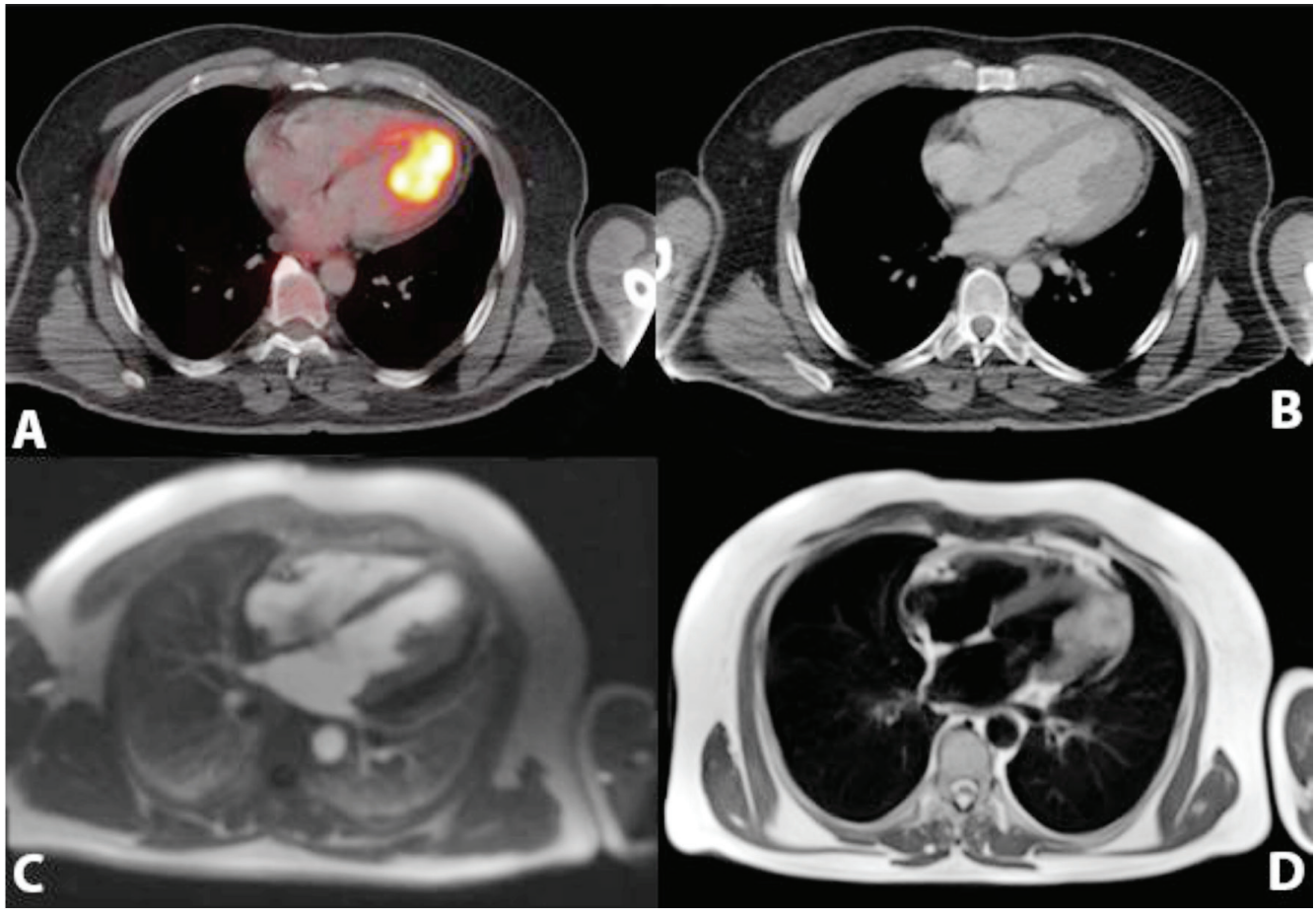

Figure 1. A 58-year old patient with a history of malign melanoma was referred to our PET/CT department for re-staging. Patient was initially diagnosed with excisional biopsy from the nail bed of his first left toe 4 years ago. Inguinal lymph node biopsy revealed negative for metastases at the time of diagnosis. Metastatic lymph nodes were detected in left inguinal region which was confirmed with biopsy 3 years later. Patient was under immunotherapy and had no symptoms either in the control or in the day of scan.
PET/CT scan demonstrated increased cardiac (^{18}F-FDG) 18-fluoro-deoxy-glucose uptake in left ventricule (A). CT images revealed filling defect of the intravenous contrast in left ventricular cavity which was suggestive of a lesion or a benign pathology like papillary muscle hypertrophy (B). MRI scan showed T1 hyperintensity with gadolinium enhancement in late phase of contrast giving process, 4x3 cm sized T2 hypointensity compatible with melanoma metastasis starting from papillary muscle in apical region, infiltrating through myocardium and extending to pericardium (C, D). Biopsy could not be performed from cardiac mass due to high mortality risk of the patient.
Cardiac masses are mostly originated from metastatic spread. Lung cancer, breast cancer and non-hodgkin lymphoma are the most common origins for cardiac metastases (1,2). Malign melanoma has also high potential to metastasize especially to lungs, liver and bones. However, cardiac metastases from melanoma are oftenly detected in autopsy series rather than detected with clinical presentation (3). ^{18}F-FDG uptake could vary in cardiac tissue and it is usually shown to be helpful in differentiating benign lesions from malignancy (4). In addition to this high uptake in myocardium and the left ventricule can be observed physiologically in ^{18}F-FDG PET images (5). Papillary muscle hypertrophy or trombus in ventriculary cavity could show increased ^{18}F-FDG uptake in PET images (6,7). As seen in our case, cardiac uptake should be checked carefully to differentiate physiological uptake which could be normally seen in cardiac tissue. Diversely, intravenous contrast is not routinely used in every PET/CT scan protocol. It has been proven to be helpful in identifying pathologic changes in organs with normal findings in unenhanced CT (8). Our images also demonstrated the usage of intravenous contrast with the filling defect seen in left ventricular cavity.

Ethics

Informed Consent: An explanatory informed consent form is signed and dated both by the doctor and by patient.

Peer-review: Eternally peer-reviewed.

Authorship Contributions

Surgical and Medical Practices: Ş.M., Concept: Ö.E., P.A., Design: N.K., P.A., Data Collection or Processing: M.K., D.Ş., Analysis or Interpretation: M.Ş.E., Literature Search: D.Ş., Writing: Ö.E.

Conflict of Interest: No conflict of interest was declared by the authors.

Financial Disclosure: The authors declared that this study received no financial support.

References

1. Lichtenberger JP, Reynolds DA, Keung J, Keung E, Carter BW. Metastasis to the Heart: A Radiologic Approach to Diagnosis With Pathologic Correlation. AJR Am J Roentgenol 2016;207:764-772.
2. Goldberg AD, Blankstein R, Padera RF. Tumors metastatic to the heart. Circulation 2013;128:1790-1794.
3. Poggi R, Pantaleo MA, Benedetti G, Biasco G. Cardiac metastasis of melanoma. Melanoma Res 2005;15:315-316.
4. Maurer AH, Burshteyn M, Adler LP, Steiner RM. How to Differentiate Benign versus Malignant Cardiac and Paracardiac 18F FDG Uptake at Oncologic PET/CT. Radiographics 2011;31:1287-1305.
5. Fukuchi K, Ohta H, Matsumura K, Ishida Y. Benign variations and incidental abnormalities of myocardial FDG uptake in the fasting state as encountered during routine oncology positron emission tomography studies. Br J Radiol 2007;80:3-11.
6. Lin EC. Isolated papillary muscle uptake on FDG PET/CT. Clin Nucl Med 2007;32:76-78.
7. Chaudhuri KG, Revels JW, Yadwadkar KS, Johnson LS. Intense 18F-FDG Uptake in an Organizing Right Atrial Thrombus Mimicking Malignancy. Radiology Case Rep 2017;12:449-454.
8. Cronin CG, Prakash P, Blake MA. Oral and IV contrast agents for the CT portion of PET/CT. AJR Am J Roentgenol 2010;195:5-13.

Interesting Image
Mol Imaging Radionucl Ther 2019;28:129-131 DOI:10.4274/mirt.galenos.2019.28199

Ileal Neuroendocrin Tumor Metastasis to Breast Diagnosed with Ga-68 DOTATATE PET/CT

Ga-68 DOTATATE PET/BT ile Tespit Edilen İleal Nöroendokrin Tümör Meme Metastazı

Sevda Sağlampınar Karyağar, Osman Güven, Savaş Karyağar
University of Health Sciences, Okmeydanı Training and Research Hospital, Clinic of Nuclear Medicine, İstanbul, Turkey

Abstract

Breast metastasis of the well differentiated neuroendocrin tumor (WDNET) of the ileum is very rare. A case of a 62-year-old woman with ileal WDNET, who underwent restaging with Ga-68 DOTATATE PET/CT due to progression of metastatic lesions under the treatment with somatostatin analog and mammalian target of rapamycin inhibitors. Ga-68 DOTATATE PET/CT demonstrated intense increased uptake in the subsantimetric nodular lesion in the upper outer quadrant of the left breast. The histopathologic findings obtained by tru-cut biopsy revealed WDNET metastasis (Ki-67 proliferation index 1%).

Keywords: Ga-68 DOTATATE PET/CT, well differentiated neuroendocrin tumor, breast metastasis

Öz

İyi diferansiye ileal nöroendokrin tümör (NET) meme metastazı oldukça nadirdir. Altmış iki yaşında iyi diferansiye NET tümör tanılı kadın hastaya, metastatik lezyonlarının somatostatin analoğu ve rapamisinin memeli hedefi inhibitörleri ile tedavi görmekte iken progrese olması nedeniyle yeniden evreleme amacıyla Ga-68 DOTATATE PET/BT görüntüleme yapıldı. Ga-68 DOTATATE PET/BT görüntülemede, sol meme üst dış kadrandaki subsantimetrik nodüler lezyonda yoğun artmış aktivite tutulumu izlendi. Lezyondan yapılan tru-cut biyopsinin histopatolojik incelemesinde iyi diferansiye NET metastazı olduğu tespit edildi (Ki-67 proliferasyon indeksi %1).

Anahtar kelimeler: Ga-68 DOTATATE PET/BT, iyi diferansiye nöroendokrin tümör, meme metastazı

Address for Correspondence: Osman Güven MD, University of Health Sciences, Okmeydanı Training and Research Hospital, Clinic of Nuclear Medicine, İstanbul, Turkey **Phone:** +90 546 260 85 16 **E-mail:** osmngvn@gmail.com ORCID ID: orcid.org/0000-0001-5376-4993
Received: 20.01.2019 **Accepted:** 14.05.2019

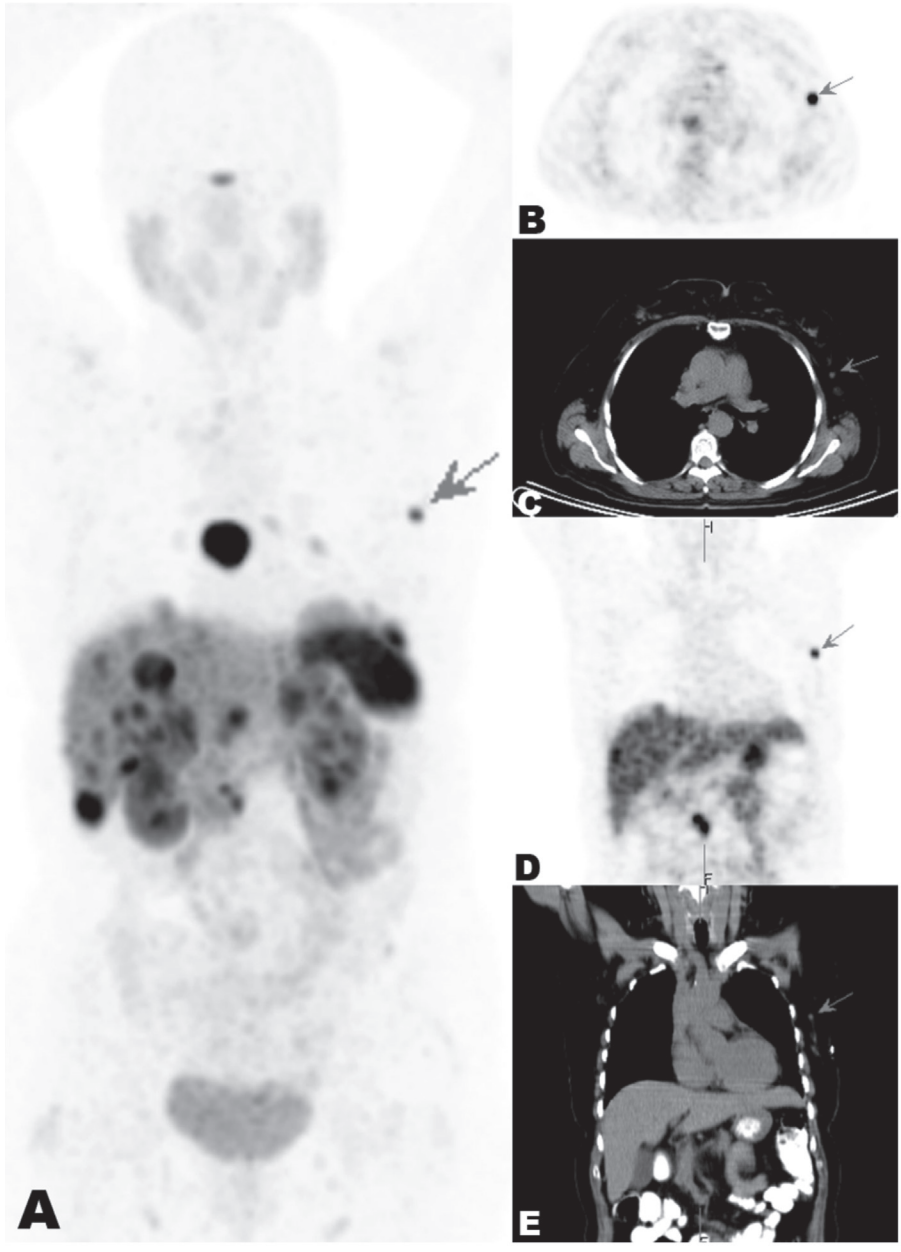

Figure 1. Ga-68 DOTATATE PET/CT images: The whole body coronal image on PET (A), axial images on PET (B) and CT (C) and coronal images on PET (D) and CT (E) at the thoracic level. A 62-year-old woman followed up with well differentiated neuroendocrin tumor (WDNET) of ileum for 6 years was referred for restaging with PET/CT imaging due to progression of metastatic lesions under the treatment with somatostatin analog and mTOR inhibitors. The patient was injected with 5 mCi of Ga-68 DOTATATE intravenously. After 60 minutes of waiting, the patient was imaged from basis of skull to middle of the thigh using an integrated PET/CT scanner which was consisted of a full-ring high resolution PET with lutetium oxy-orthosilicate crystal and a 6-slice CT (Siemens Biograph 6, Chicago, USA). There were multiple hepatic nodular lesions, multiple intense mediastinal (biggest in the subcarinal station) and intraabdominal lymph nodes showing intense somatostatin receptor activity compatible with metastasis. Ga-68 DOTATATE PET/CT images also showed intense increased uptake in the subsantimetric nodular lesion in the upper outer quadrant of the left breast, suggesting metastasis (A, B, C, D and E, arrow). The histopathologic findings obtained by trucut biopsy revealed WDNET metastasis (Ki-67 proliferation index 1%). Ga-68 DOTATATE PET/CT is widely used for initial staging and restaging of WDNET (1). Ileal WDNET usually metastasizes to liver, mesenteric lymph nodes, lung, peritoneum and pancreas (2). Breast metastasis of ileal WDNET is a very rare entity (3,4,5,6). Ga-68 DOTATATE PET/CT can detect metastatic lesions of WDNET in uncommon regions such as breast. Also, diagnosis of breast lesion with Ga-68 DOTATATE uptake on PET/CT lets us distinguish WDNET metastasis from primary breast malignancy without neuroendocrin differentiation. In this case, we report a patient with breast metastasis of ileal WDNET detected with Ga-68 DOTATATE PET/CT.

Ethics

Informed Consent: Consent form was filled out by all participants.

Peer-reviewed: Eternally peer-reviewed.

Authorship Contributions

Surgical and Medical Practices: S.S.K., S.K., O.G., Concept: S.S.K., S.K., O.G., Design: S.S.K., S.K., O.G., Data Collection or Processing: S.S.K., S.K., O.G., Analysis or Interpretation: S.S.K., S.K., O.G., Literature Search: S.S.K., S.K., O.G., Writing: S.S.K.,

Conflict of Interest: No conflict of interest was declared by the authors.

Financial Disclosure: The authors declared that this study received no financial support.

References

1. Subramaniam RM, Bradshaw LM, Lewis K, Pinho D, Shah C, Walker RC. ACR Practice parameter for the performance of Gallium-68 DOTATATE PET/CT for neuroendocrin tumors. Clin Nucl Med 2018;43:899-908.
2. Modlin IM, Lye KD, Kidd M. A 5 decade analysis of 13,715 carcinoid tumors. Cancer 2003;15:934-959.
3. Clark BZ, Bhargava R. Metastatic neuoroendocrin tumors to the breast: Diagnostic pitfall with significant clinical implications. AJSP 2017;22:269-274.
4. Dervishac OA, Renzi AS, Genato R, Xiao PQ, Asarian AP. Neuroendocrin tumor of the breast:is it primary or metastatic? Int J Case Rep Images 2016;7:34-39.
5. Ahn S, Bhagwandin S, Reindl B, Jaffer S, Bickell N, Labow DM, Scmidt H. Metastatic carcinoid tumor presenting as a breast mass: A case report and review of the literature. Arch Surg Oncol 2016;2:1-5.
6. Policeni F, Pakalniskis B, Yang L. Occult primary neuroendocrin tumor metastasis to breast detected on screeniig mammogram. J Clin Imaging Sci 2016;6:41.

2019 Referee Index - 2019 Hakem Dizini

A Tayyar Akpınar
A. Özgür Karaçalıoğlu
Ali Fuat Yapar
Ali Sarıkaya
Angelika Bischof Delaloye
Ayşe Aktaş
Aziz Murat Argon
Bilge Volkan salancı
Billur Çalışkan
Bircan Sönmez
Bülent Turgut
Cengiz Taşçı
Corinna Altini
Çiğdem Soydal
Dogangün Yüksel
Dragana Sobic Saranovic
Emre Demirci
Emre Entok
Fatma Suna Kıraç
Fevziye Canbaz Tosun
Feyza Şen
Fikriye Gül Gümüşer
Francesca Pons
Funda Üstün
Gonca G Bural
Gonca Kara Gedik
Gülay Durmuş Altun
Gülin Vural Uçmak
Hakan Demir
Hamid Amer
Hülya Yalçın
Irena Dimitrova Kostadinova
İlknur Ak Sivrikoz
İnanç Karapolat
Mehmet Reyhan
Meliha Korkmaz
Meryem Kaya
Nalan Alan Selçuk
Nalan Alan Selçuk
Nilüfer Yıldırım
Olga Yaylalı
Özlem Özmen
Pelin Arıcan
Sait Sağer
Serkan İşgören
Seval Erhamamcı
Tamer Atasever
Tanju Yusuf Erdil
Tansel Ansal Balci
Tunç Öneş
Ümit Özgür Akdemir
Yakup Yürekli
Yasemin Şanlı
Zehra Özcan
Zeynep Burak

2019 Subject Index - 2019 Konu Dizini

2019 Subject Index - 2019 Konu Dizini

2019 Author Index - 2019 Yazar Dizini

2019 Author Index - 2019 Yazar Dizini